Design and finite volume evaluation of a counterflow recuperative spiral heat exchanger for additive manufacturing

Bastian Busch

Master in Engineering

2022

Design and finite volume evaluation of a counterflow recuperative spiral heat exchanger for additive manufacturing

Bastian Busch

A thesis submitted to

Auckland University of Technology

in fulfilment of the requirement for the degree of

Master in Engineering (ME)

May 2022

School of Engineering

Under the supervision of:

Professor Sarat Singamneni

Dr Alan Caughley and Dr Neil Glasson of Callaghan Innovation

Attestation of Authorship

I hereby declare that this submission is my own work and that, to the best of my knowledge and belief, it contains no material previously published or written by another person (except that which appears in the citations and acknowledgements). Nor does it contain material which to a substantial extent has been submitted for the award of any other degree or diploma of a university or other institution of higher learning.

Signature of the candidate:

Date: 26/07/2022

Abstract

There is an ever-increasing demand to find alternatives to carbon based fuel sources and move to renewable electric propulsion systems. Recent advances in additive manufacturing have enabled the manufacturing of complex geometries enabling the potential for higher efficiencies for smaller, more compact designs. The aviation sector is a critical aspect of the transition to electrical population and one that cannot be proactively solved with traditional electric motors. To this end, the use of a superconducting electric motor has been proposed to achieve higher efficiencies and make application within aircraft a viable alternative. The investigation of a cryocooling component, specifically, the ability to pump cryogenic fluid through the electrical systems to maintain the superconducting state is critical to determine the viability of such a design.

This research considers the application of a warm pump in combination with a recuperative heat exchanger to fulfil the cryogenic circulation requirement. The utilisation of additive manufacturing to design complex geometries and ANSYS fluent to verify the effectiveness of the design can result in a superior solution. This research proposes the use of homogenised heat transfer within the design to achieve both a room temperature output and a cryogenic output. To achieve this, two critical design requirements were proposed; a low thermally conductive intermediate layer to ensure controlled homogenised heat transfer and fixed temperature inlets, one being room temperature and the other at cryogenic temperature. The high temperature gradient

across the recuperative heat exchanger, in combination with a low thermally conductive intermediate layer allows for an even heat transfer cumulating in the reversal of the inlet temperatures at an efficiency between 95 and 98 percent.

The application of an additively manufactured cryogenic helical recuperate heat exchanger design can yield equivalent efficiencies to a traditional tube in tube design 50% longer along the cross-section. The highest effectiveness for the recuperative heat exchanger can be achieved with the utilisation of very low thermally conductive materials which can result to an up to 20K drop in minimum outlet temperature when compared to the use of stainless steel.

Publication

The following paper has been published in the Cryogenics Journal.

Design and finite volume evaluation of a counterflow recuperative spiral heat exchanger for additive manufacturing

Bastian Bush[1], Alan Caughley[2], Neil Glasson[2], Rod Badcock[3], Hubert Weijers[3], Grant Lumsden[3], Michael Gschwendtner[1], Sangkwon Jeong[4], and Sarat Singamneni[1]

[1]Auckland University of Technology, Auckland New Zealand

[2]Callaghan Innovation, Christchurch, New Zealand

[3]Robinson Institute, Lower Hutt, New Zealand

4Korean Advanced Institute of Science and Technology, Korea

Cryogenics, Volume 127, 2022, 103548, ISSN 0011-2275,

https://doi.org/10.1016/j.cryogenics.2022.103548.

Keywords: Cryogenic; Heat transfer; Additive manufacture; CFD

Acknowledgements

The success of this research work would not have been possible without the generous support and advice from numerous people.

I would like to express my profound gratitude to my primary supervisor, **Professor Sarat Singamneni**, for his valuable support, encouragement, supervision and useful insights throughout the year. His support and continuous guidance enabled me to complete my work successfully. I am also highly thankful to my secondary supervisors **Dr Alan Caughley**, and **Dr Neil Glasson** of Callaghan Innovation, for their valuable suggestions throughout this study. I am also grateful for the AUT Learning Communities team for their ongoing support throughout my time at AUT. The financial support provided by SSIF Project on Electrification of large-scale transportation sector by MBIE New Zealand through a subcontract to AUT from the Robinson Institute is also acknowledged, without which, this project could not have come to life.

I am as ever, especially indebted to my parents, **Sidney** and **Tina Busch** for their love and support. And my brother **Christopher** for both being a great role model and guiding me throughout my time at AUT. Moreover, my sincere thanks go to my friends, for their support and friendship throughout my study.

Table of Contents

Table of Figures

Chapter 1
Introduction

1.1 Background

The demand to reduce noise, carbon and environmental emissions across all sectors including aviation has led to an increased reliance on new electric propulsion systems. Aviation especially, has great challenges to overcome due to the critical high power density requirement for light weight efficient solutions. There is increasing demand for solutions including superconducting electric motors to meet this requirement. An efficient cryogenic cooling system is an essential part for a superconducting motor and imposed a great challenge to develop. Heat exchangers are critical components that contribute to the effective thermal management in systems using thermodynamic processes. Traditionally, heat exchangers are either in the form of intricate networks of tubes or multi-dimensional fins. These relatively simple forms of the essential components of the heat exchanger systems are the result of the limitations of the traditional manufacturing processes. With the advent of additive manufacturing technologies, there is no need to be restrained by the limitations of traditional methods. The freedom to fabricate more complex forms and three-dimensional shapes with free-

form surfaces and intricate re-entrant sections based on the additive manufacturing methods opens up a plethora of new design opportunities for heat exchangers.

1.2 Additive manufacturing

From 3D printing to additive manufacturing, the additive material consolidation methods have grown rapidly, acquiring both material and process enhancements. With around half a dozen techniques withstanding the tests of time and reaching the necessary quality assurance levels, additive manufacturing is finding wider application in areas where the added design freedom and the ability to achieve more complexity in the fabricated forms are of importance. Industrial tooling, automotive, aerospace, and medical application areas are noteworthy. While numerous examples of outstanding applications and new product concepts have been reported quite extensively in all these fields, the ability to push the boundaries of the freedom for free-form fabrication drew particular attention in the applications for heat exchangers, for obvious reasons that geometrical complexity is an inherent requirement for efficient heat transfer.

1.3 Objectives

The application that has driven this heat exchanger design is the aim of a high effectiveness counterflow recuperative heat exchanger for cryogenic coolant

circulation systems where it is desirable to have a warm circulation pump and a heat exchanger that takes the coolant (nominally gaseous helium) from very low temperatures (around 20 K) up to ambient for pumping then cooling it down again. The trade-off being the energy losses and expense associated with a cryogenic pump vs the pressure drops and temperature difference associated with a heat exchanger. It is hypothesised that additive manufacture may be able to allow previously unmanufacturable geometries that can result in a compact and highly efficient heat exchanger. This work aims to fully utilise the freedom to additive manufacturing to design and manufacture a geometrically complex recuperative heat exchanger. Additive manufacturing, although significantly extending the manufacturing capability has its own set of limitations which must be overcome.

The primary challenges involve the support structures that are required to support the structure during the additive manufacturing process and the potential for defects to occurring during the manufacturing. Avoiding internal support structure within the manufacturable geometry is critical, both to minimise performance losses in the heat exchanger and the ability to validate the model with computation fluid dynamic tools. A core focus of the heat exchanger geometry was to include no internal support structures while maintaining a stable, reliable, and repeatable manufacture process. The proposed solution to meet this requirement was to ensure that all inclined surfaces maintain a minimum 45-degree inclined plane to ensure that every manufactured layer during the manufacturing process has sufficient support and does not collapse during the print. The risk of a print failing was significant due to not only the long duration manufacturing process being at risk, but simultaneously any additional parts that were started alongside the proposed heat exchanger geometry would also be likely to fail.

The second primary limitation was the risk of defects during the manufacturing process to create small gaps in the geometry, increasing the risk for leaks to occur within the printed geometry. To mitigate this risk, the minimum wall thickness between adjacent fluid was set to 1mm. This allows tolerance for the multiple successive defects to not lead to a heat exchanger vulnerable to fluid leaks. Additionally, the limited construction area and cost associated with additive manufacturing limited the size of the geometry to a maximum 200mm height.

The overarching aim of this research is to develop a high performance cryogenic recuperative counter flow heat exchanger utilising the advantages of additive manufacturing. The following objectives were set as part of this research:

- Evaluation of the possibility to develop high-performance cryogenic heat exchanger designs by means of additive manufacturing
- Design and develop various CAD recuperative heat exchanger models, utilising complex geometries to enhance performance.
- To utilise the additive manufacturing benefits and developing a geometry that outperforms traditional heat exchanger designs.
- Numerical evaluation and validation of the heat exchanger design for thermal performance
- Investigate the feasibility of using traditional additive manufacturing materials for the design of the recuperative heat exchanger.

Chapter 2

Literature Review

2.1 Typical additive manufacturing techniques

Additive Manufacturing, also known as 3d printing, is a process that successively adds materials in a layer-by-layer fashion build three-dimensional objects from a computer-aided design model. There are various additive manufacturing techniques that are commercially viable, of which the relevant ones are reviewed here.

Fused deposition modelling (FDM) is the most common additive manufacturing method, and is based on the melting, extrusion, and deposition of thermoplastic polymers [1]. The thermoplastic polymer, which is the building material, is heated to its melting point, at which point it becomes ductile and can be shaped as desired. For FDM printing, the thermoplastic polymers are modified to reduce their shrinkage or to improve layer bonding, making the manufactured object less prone to delamination.

FDM has several key advantages detailed below:

- FDM 3D printers are relatively simple to design and corresponding relatively inexpensive to purchase as well as requiring minimal maintenance
- FDM is a safe process for everyday use
- There are a wide range of thermoplastic polymers available at low prices, which significantly reduces to cost of manufacturing prototypes

Selective laser melting (SLM) is a powder-bed-fusion additive manufacturing process. SLM uses a high-density laser beam to selectively scan the powder bed, where the solidified layers are stacked upon each other to produce the three-dimension object [2]. Selective laser sintering (SLS) is very similar to SLM but uses partial melting or sintering for binding powder particles rather than fully melting.

SLM has several key advantages detailed below:

- SLM has a wide range of materials can be used including stainless steels, Al alloys, Ni super alloys, Ti, and its alloys as well as precious metals
- A small powder particle size between 10 and 45 micrometres
- A small typical layer thickness between 20 and 50 micrometres

2.2 The current status of the application of AM for heat exchangers

The ability to produce more complex forms and the added design freedom with the advent of the additive technologies naturally attracted significant research attention in revisiting the design of heat exchangers. A polymer composite heat exchanger designed and fabricated by fused deposition modelling [3], innovative manifold microchannel design evaluated considering additive manufacturing methods [4], a high-performance counterflow heat exchanger evaluated by means of selective laser melting [5], compact manifold-microchannel heat exchangers manufactured by direct metal laser sintering technique [6] are a few examples. Two successfully manufactured heat exchangers are depicted in Fig 2.1 and Fig 2.2. Fig 2.1 utilises 1mm*1mm fluid flow channels, with a maximum channel separation of 3mm. A

minimum wall thickness of 1mm was used to reduce the risk of fluid leakage due to potential ruptures in the walls. Fig 2.2 shows a cut section of a manifold microchannel heat exchanger which show manufactured fins as small as 0.110mm. Both these solutions successfully utilise additive manufacturing to achieve smaller fluid flow channels.

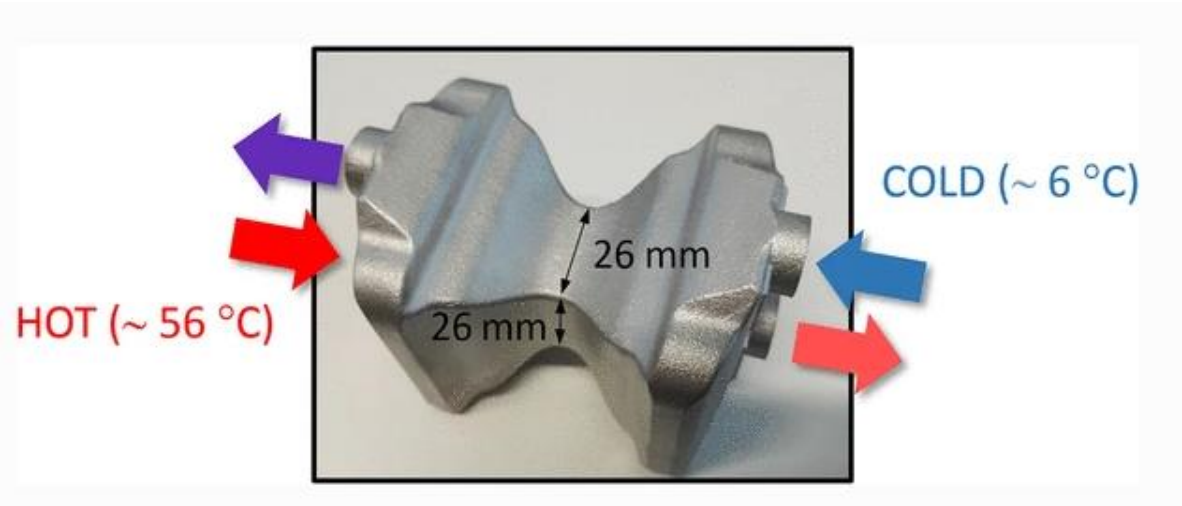

Figure. 2.1 Shell and Tube Heat Exchanger, Obtained from [4]

Figure. 2.2 Cut view of a Manifold-Microchannel Heat Exchanger, Obtained from [6]

Considering the complex fluid and thermodynamics conditions that often arise along with the geometrical optimisation, numerical and analytical simulations [7, 8, 9] and topology optimisation [7, 10] schemes are commonly associated with the evaluation of heat exchanger designs based on the additive manufacturing applications. Considering these new technological advances and their possible applications in the design of efficient heat exchanger systems, the current paper is focussed on the design of counterflow heat exchangers that can benefit from the use of the additive technologies. Given the constraints of length and the thermal load levels, spiral heat exchangers were proven to outperform other arrangements [11]. Fig 2.3 represents a micro double tube helical heat exchanger that was used to compare various pitch, turn numbers and height with 12 separate configurations. The helical double tube heat

exchange configuration showed a up to 45% enhancement when compared to a straight double tube heat exchanger. It was also shown that the length of the helical coil becomes the most effective geometric parameter influencing the performance of the heat exchanger [12]. Fig 2.4 shows the schematic for the triple helix ground heat exchanger that was used to conclude that as the helical diameter increase the effectiveness and thermal performance of the heat exchanger decreased. Furthermore, the effectiveness of the heat exchanger was considerably impacted by the distance between the centres of the inner and outer helical branches. These conclusions encourage the use of additive manufacturing to produce very small fluid flow channels along with a helical arrangement to enhance the effectiveness of the heat exchanger.

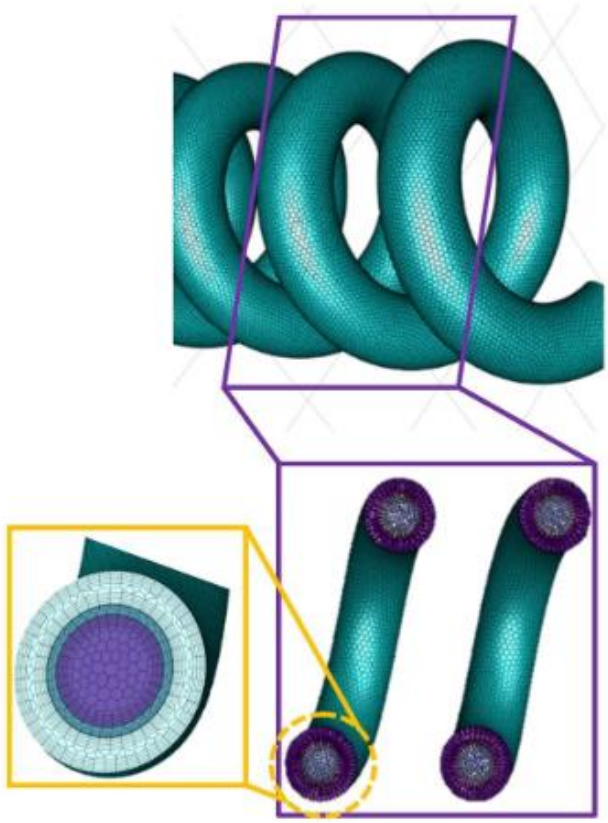

Figure. 2.3 Meshes of a micro helical double tube heat exchanger, Obtained from [11]

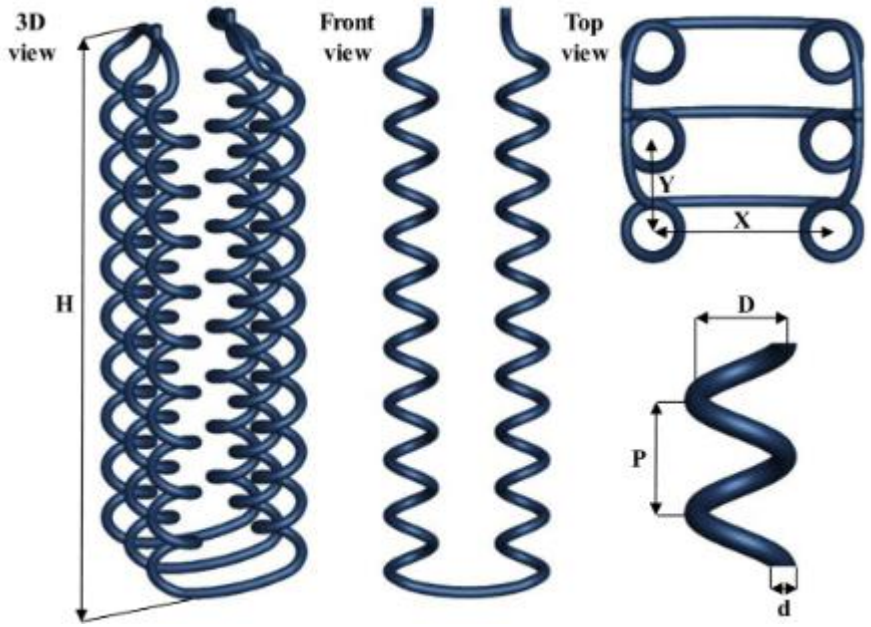

Figure. 2.4 schematic of a triple helix ground heat exchanger, Obtained from [12]

2.3 Recuperative Heat Exchangers

Recuperative heat exchangers have been used in the past with many aspects including the use with a Stirling engine [13] which date back decades. In this case helium or hydrogen was used as working fluid for the Stirling engine with small dimeter tubes in the range of 3.0mm to 6.0mm constructed as part of the heat exchanger. Two incoming and two outgoing streams describe the stationary operation of any recuperative heat exchangers [14]. The various calculation methods for recuperative heat exchangers with two incoming and two outgoing streams include LMTD and NTU [15]. The preferred calculation method for recuperative heat exchangers is NTU due to the lack of the iterative requirement in the calculation. The process for the geometric

optimisation of a heat exchanger can be quantified with the use of controllability matrix [16]. This resulted in the minimisation of this matrix with respect to the tube aspect ratio and the fluid mass flow rate. However, it is possible to calculate any recuperative heat exchanger without know the operating characteristics [17], specifically when the mean temperature difference is approximately 1. A critical factor in the effectiveness of a recuperative heat exchange includes the pressure drop characteristics [18, 19]. The use of recuperative heat exchangers applies to a wide range of cases which include improving the efficiency of aviation turbofan engines [20], within a regenerative gas turbine cycle [21] and a MR J-T cryocooler [22, 23]. Theoretical models include a Purge ventilation system [24] as well as the investigation of the use of wavy plates within recuperative heat exchangers [25]. To achieve certain design requirements in steady state, the transient response of the heat exchanger must also be known [26].

2.4 Existing Heat Exchanger Systems

Past research on gas-to-gas heat exchange systems have highlighted the use of traditional standard single and dual channel spiral arrangements [27] which presented high flow rate fluids passing through thin inner tubes shown in Fig 2.5. The study concluded with an additional observation that heat transfer increases as fluid velocity is reduced, however a pressure drop is experienced at the same rate. The initial designs in this work were based on these standard forms, while also considering the application of other standard forms such as the shell and tube heat exchanger arrangements [28]. The shell in tube heat exchanger depicted in Fig 2.6, show a segmented baffled design each inclined at 90 degrees and resulted in a large pressure

drop at each baffle. The addition of a helical baffle in a shell and tube heat exchanger [29] was also considered for this work.

Figure. 2.5 Single Channel Spiral Arrangement, Obtained from [27]

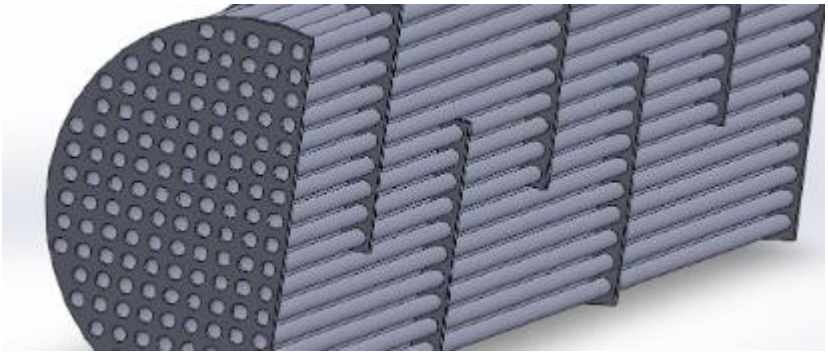

Figure. 2.5 Shell and Tube Heat Exchanger, Obtained from [28]

Combining the two concepts and the critical benefits of both together, the final design concept converged on a shell and spiral tube heat exchanger arrangement. This design also allows the use of multiple parallel tubular cavities running in parallel along the helical pathways around the central axis of the tubular heat exchanger. The use of the multi-tubular helical arrangement is in accordance with the observations made by [30], that incorporating a helix improves heat transfer which incorporated the design presented in Fig 2.7 and also showed a performance improvement with fluid flow rate. Further, [31] concludes that elliptical cross sections perform better than circular sections and so also is the case with rectangular shapes against square shapes for

the cross sections of the tubular passages. This led to the incorporation of a non-uniform sections within the design to aid with heat exchanger performance.

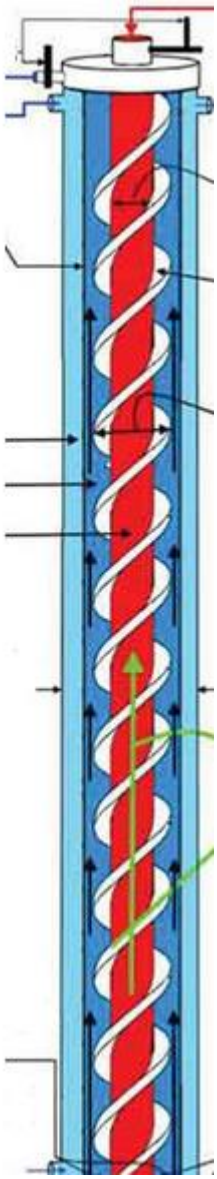

Figure. 2.6 Spiral Helical Fin Arrangement, Obtained from [30]

2.5 Objectives and methods

This work sets to establish the foundations of a counterflow recuperative heat exchanger design, set to be used within a cryogenic helium circuit. To fully utilise the advantages of a warm pump, set to operate at close to ambient temperature, the recuperative heat exchanger is aimed to provide a highly efficient separation from the warm and cold parts of the circuit. Avoiding the complexities of 2 phase flow, this work incorporates the use of helium as a convenient heat exchange fluid. With a target application range between 50K – 20K and ambient temperature, helium will remain gaseous over the entire temperature range. The recuperative component of the heat exchanger is set with the function of providing the separating between the warm and code parts of the circuit. This fixes the volume flow of both inlets and outlets to be approximately equal.

Additive Manufacturing is set are the core manufacturing process to produce highly complex geometries, capable of achieving the required high efficiencies. Conventional manufacturing techniques are limited significantly and are unsuitable for this design. Designed for incorporation within an aircraft system, the low weight of the design is partially critical. Large heat transfer areas, good flow characteristics and good heat transfer between the fluid and solid surfaces are key to achieve the required high effectiveness. No leakage between the flow channels as well as low conduction along the length of the heat exchanger are essential for the successful design of a counterflow recuperative heat exchanger for this application. Fig 2.7 lists the key objectives planned to be carried out as part of this research, which include geometric design and modelling, finite volume discretisation and evaluation and additive manufacturing.

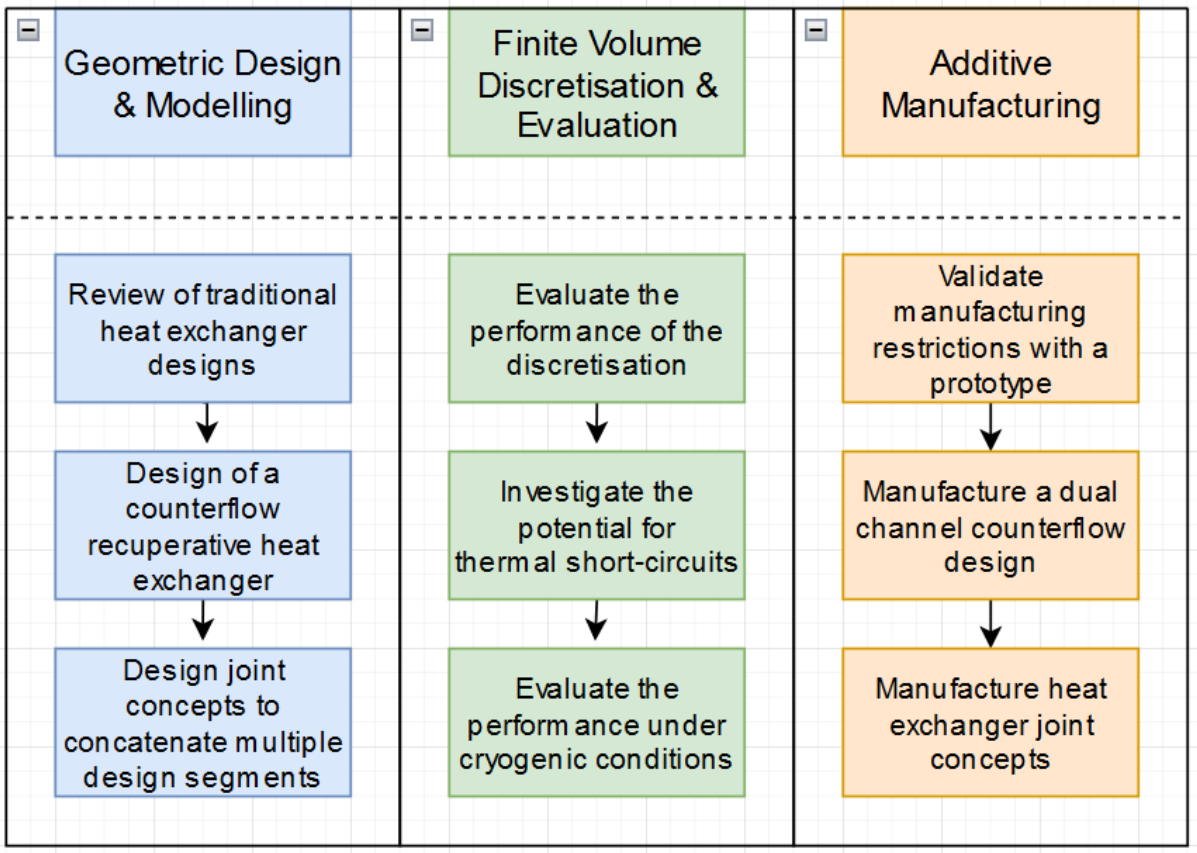

Figure. 2.7 The Research Plan

Chapter 3
Design of the Recuperative Helical Spiral Heat Exchanger

3.1 Design path for an Additively Manufactured Heat Exchanger

There are two key requirements for the successful design of an additively manufactured recuperative spiral heat exchanger. These are both the high-performance capability of the heat exchanger, as well as the feasibility of a successful manufacturing process. The limitations placed on the design by the manufacturing process are detail in this chapter. These include the limited manufacturing space for an additively manufactured design as well as the tolerances required to remove all internal support structures, without sacrificing build stability. The primary software tool which was used to generate all the presented model concepts and designs was ANSYS Design Modeller. This specific tool allowed for the continued progression of the design, without having to redesign the complete model, through the use of a modifiable linear design history.

Traditional heat exchangers such as a shell and tube heat exchanger as well as heat exchange systems with a spiral arrangement have been used successfully for decades. These traditional designs have been used to design a heat exchanger depicted in Fig 3.1, which combines both a high-density pipe arrangement of a shell and tube heat exchanger as well as the advantages shown with the use of a spiral

configuration. This heat exchanger design, closely resembling existing heat exchangers satisfies the key requirements of a heat exchanger. These include a high surface area for efficient heat transfer, and that the design is simple to manufacture using traditional manufacturing techniques. However, the additional of the spiral arrangement complicates the manufacturing process. Furthermore, optimising the geometry to further improve heats exchanger performance would make the heat exchanger infeasible for traditional manufacturing techniques. This is where additive manufacturing has shown promising results to fabricate complex geometries, rapidly and at significantly lower cost. Metal 3D printing methods such as selective laser melting (SLM) can be of use to some extent. However, based on the initial trials, the geometry was found to be unsuitable for fabrication by even SLM due to the need for inserting multiple internal support structures that cannot be removed after printing. After a careful consideration of the possibilities with SLM, it was observed that a minimum helix angle of 45° can conveniently avoid the need for using the unwanted support structures in and around the helical tubular structures. Using this as an opportunity a multi-tubular helical spiral heat exchanger model is designed with a 45° helix angle as shown in Fig. 3.2 (a). From the considerations of the SLM build restrictions, this geometry is amenable for printing without the use of any internal or external support structures, with a vertical build orientation on the base plate.

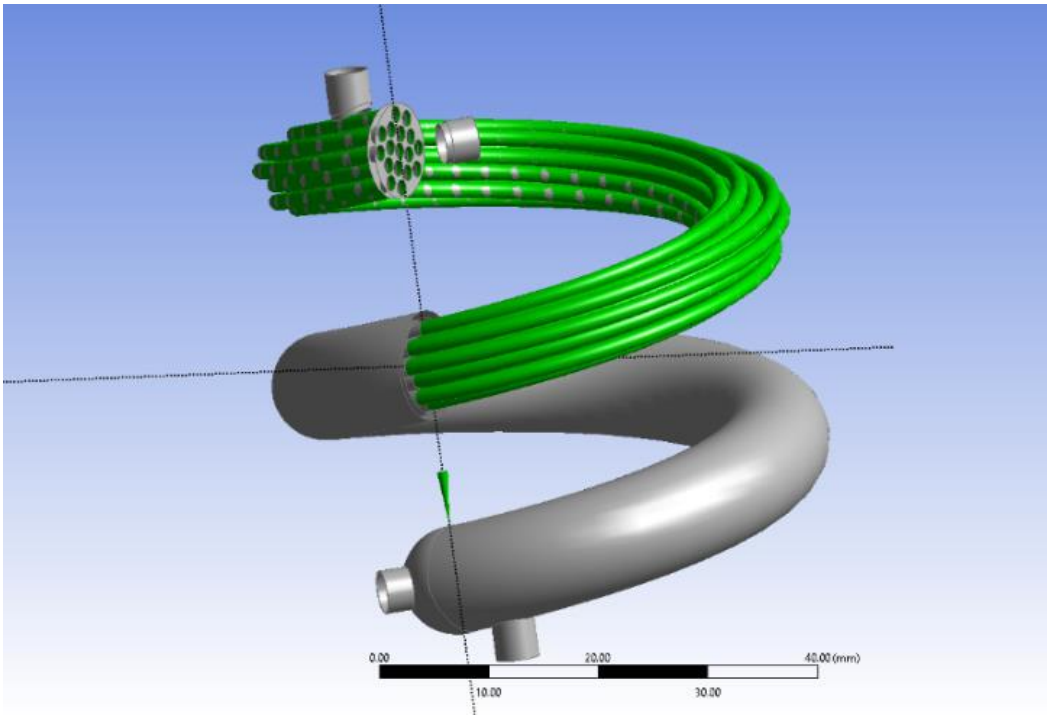

Figure. 3.1 Combined shell and tube helical spiral heat exchanger model

To overcome the difficulties of the manufacturing stated above, the form as shown in Fig 3.2 (a) has been designed. This multi-channel helical heat exchanger aims to maximise both the external surface area for the heat exchange and the volumes of the columns for the fluid transportation. However, there was yet another limitation arising out of the laser melting process. Typically, the minimum thickness of the tube cross sections for the convenient manufacturing of complex shapes by SLM cannot be less than 1 mm. In specific cases thicknesses lower than this can be attained but considering the complexity of the geometry and based on past experiences, the 1 mm limit was set for the current heat exchanger design. However, the 1 mm limitation in the wall thickness did not allow to incorporate the traditional shell and tube design within this model. Consequently, an alternative design with two overlapping rings was

employed, the CAD model of which is presented in Fig. 3.2 (b). Two separate dedicated helical spiral flow paths for the two fluids is a suitable configuration for additive manufacturing and having a single flow channel instead of several parallel flow channels (or tubes) is a better way for effective cryogenic heat exchange. It is well known that flow-maldistribution is a problem for achieving high effectiveness value in most heat exchangers as well as cryogenic heat exchangers. This is a novel combination of the tube-in-a-tube counterflow heat exchanger together with the helical spiral flow paths for the two fluids.

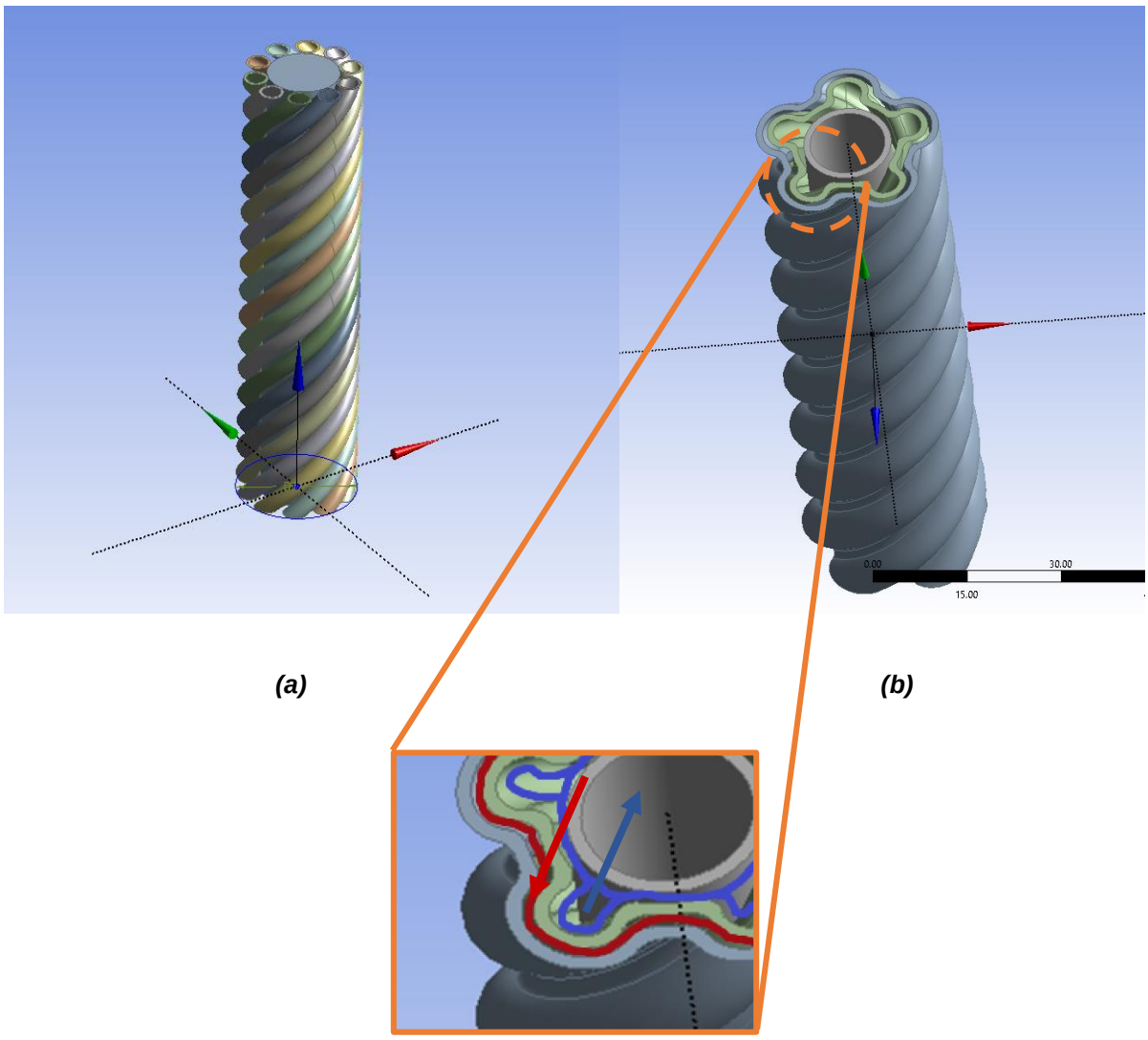

Figure 3.2 Design of a counter-flow heat exchanger for additive manufacturing (a) the spiral multi-channelled heat exchanger design concept and (b) the novel tube-in-a-tube spiral helical counterflow design

The multi-channel helical heat exchanger shown in Fig. 3.2 (b) has two spiral rings around the central cylinder which are configured for two counterflow fluids one the inlet, and the other the outlet. In the idea case the two fluids would be at the same temperature at end of the heat exchanger. This design however has a critical problem. The inner fluids can flow longitudinally along the axial direction, instead of following the specifically helical pathways, due to the connection between the five semi-circular rings. This has the potential to negatively affect heat exchanger performance. In the next design iteration, the fluid connection between the five semi-circular rings were replaced with solid regions, leaving only the tubular helical pathways for the two counterflow fluids to flow through.

The ANSYS ® Design Modeller module was used to create the CAD models of the designed heat exchanger. In order to create the geometry of the spiral tubes, the two sketches shown in Fig 3.3 were used as the basis. Fig 3.3 (a) is the 2D cross-sectional sketch of the solid volumes and Fig 3.3 (b) is that of the liquid pathways defining one pathway of each of the two fluids. Five such sketches were repeated around the central longitudinal axis of the tubular structure and a sweep extrusion action around the helical pathway was used to create the spiral helical geometry shown in Fig 3.3 (c).

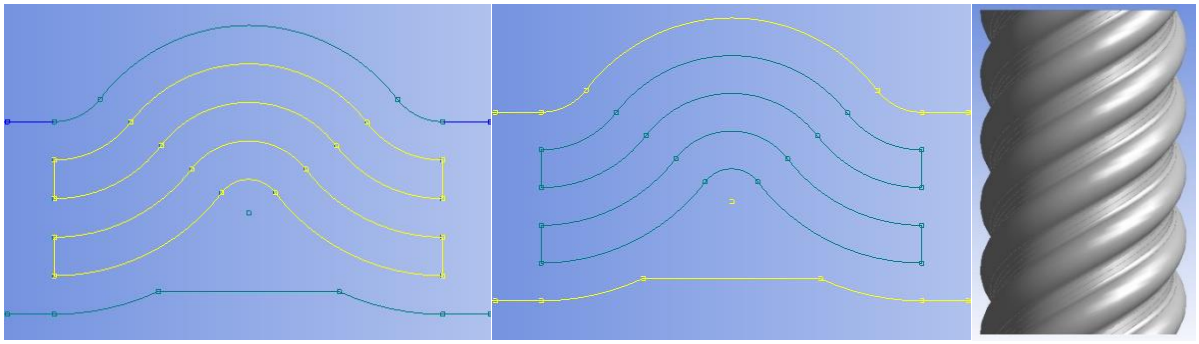

(a) ***(b)*** ***(c)***

Figure 3.3 2D Swept Surface for the Counterflow Helical Heat Exchanger (a) the 2D surface to generate solid body and (b) the 2D surface to extrude the fluid volumes and (c) the spiral helical geometry

As a result, five separate helical tubular pathways were created around the central axis for each fluid to flow through, as shown in Fig 3.4 (a). The critical next step was to converge the 10 separate fluid pathways into two distinct volumes, that was used to build the single inlet and outlet for each of the fluid pathways at the ends of the tubular heat exchanger. The skin function was used to connect the fluid regions into two distinct annular spaces, as depicted in Fig 3.4 (b), where the shaded areas are the cross-sections of the three annular solid spaces that form the two annular fluid spaces in between. The shaded cross-sectional areas were used to create the conical cylindrical extensions by extrusion, as shown in Fig. 3.4 (c) and Fig 3.4 (d), which were later converted into the inlet and outlet pipes for connecting the hoses at the two ends of the cylindrical heat exchanger.

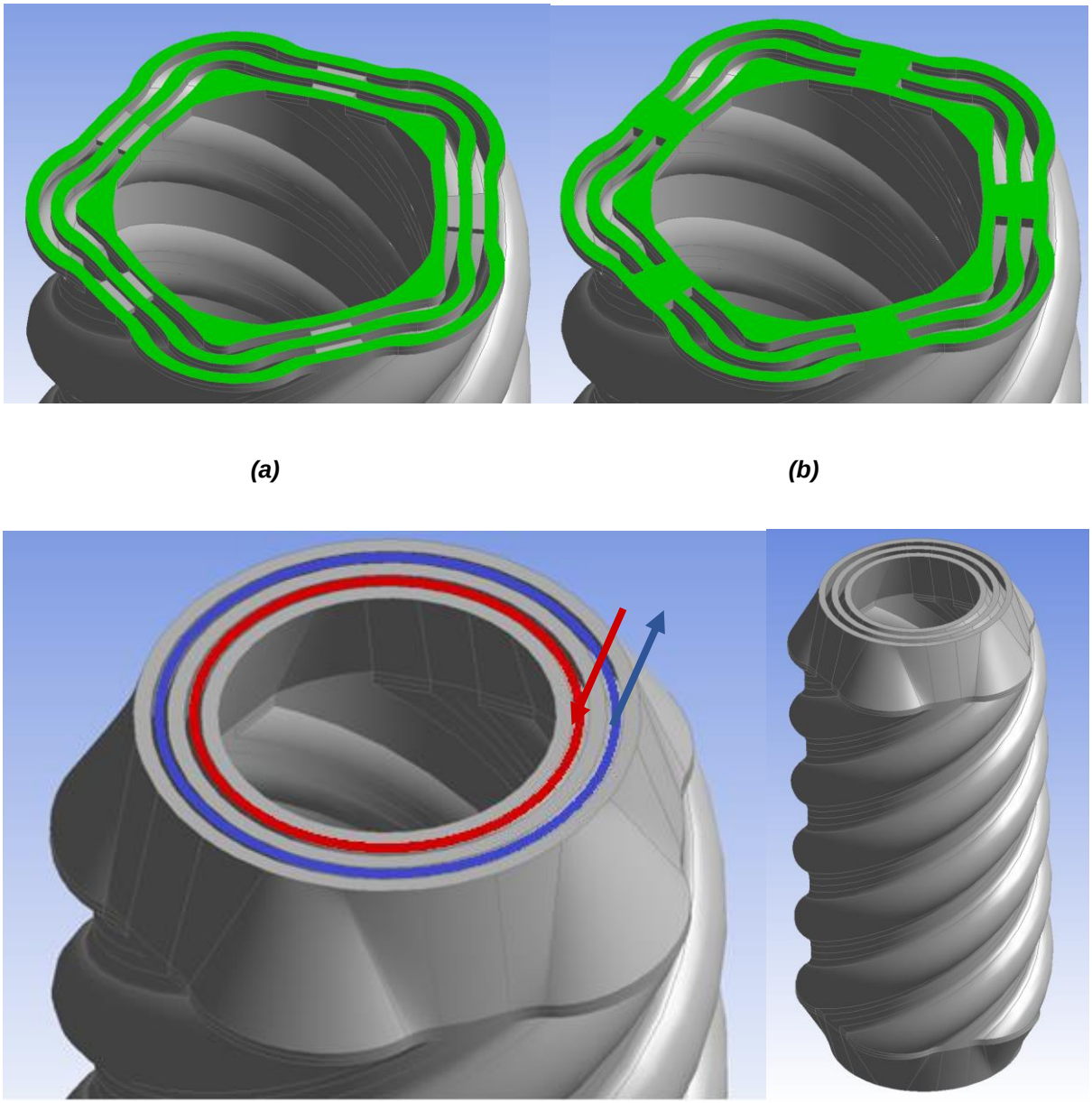

(a) *(b)*

(c) *(d)*

Figure 3.4 Design of the inlet and outlet for a counter-flow heat exchanger for additive manufacturing (a) the five separate helical tubular pathways and (b) the merged fluid inlet and outlet pathways and (c) the merged fluid inlet and outlet and (d) connection the spiral multi-channelled heat exchanger design concept

A core design concept requirement for the recuperative heat exchanger, compared to traditional heat exchanger systems was the core purpose to complete a warm pump loop. This required cryogenic fluid to we warmed to room temperature, which could then be pumped efficiency and finally return to a cryogenic state. The two fluid streams, one from cryogenic to room temperature and the other from room to cryogenic temperature could be adjacently placed to efficiently complete this cycle with minimal additional energy input. For this requirement to be satisfied the room temperature fluid must transfer heat into the cryogenic fluid raising the temperature to room conditional while itself being cooled to cryogenic temperatures.

Several key requirements were identified for this successful design and manufacturing of the proposed recuperative heat exchanger:

1. The flow rate of the two fluids must be closely aligned to ensure the overall closed loop system can be satisfied
2. To produce an efficient recuperative heat exchanger within geometric constraints
3. The design must require no internal support structures to additively manufacture the design.
4. The design must be able to be manufactured successfully, with minimal risk of fluid leakage due to manufacturing defects.
5. The fluid inlets and outlets must follow a generic geometry to match typical connection to the overall system
6. The fixed volume of the additive manufacturing method used cannot hinder the lengthening of the design to improve heat exchanger efficiency.

3.2 Base Design of the Recuperative Helical Spiral Heat Exchanger

Three fundamental design choices were combined to generate the foundations for a recuperative heat exchanger. First, two adjacent fluid regions of near equal volume are required to transfer heat between the two fluids, in consideration for the first stated requirement. These regions were required to have a large joining area for which to transfer heat. The second design decision was to use a spiral design, which increases the length the fluid travels along the heat exchanger while reducing the total length of the design, seeking to satisfy the second requirement. The third, was a design limitation placed by the manufacturing process, specified in the third requirement, which limited the wall thickness to at least 1mm and required a minimum inclined slope at 45 degrees to ensure that no internal support structures were required during the print. To maintain a small design an remain within the design constraints the wall between the two fluid was a constant thickness of 1mm, to ensure that there was no fluid leakage due to imperfections in the manufacturing process, stated in the fourth requirement. Within these constraints a design was made to increase the perimeter of the fluid regions per unit area while maintaining a constant 1mm gap between the two fluids. And the 45-degree incline was the key restriction for a spiral design concept.

The next major design decision was related to the overall size of the design. Due to the limited printable volume of the printer as well as cost considerations for each print, the limitations for a maximum width of 40mm was placed. Due to the 40mm restriction as a 45-degree max spiral incline, the total heigh for 1 full spiral rotation was 62.832mm, exactly pi*r. Unlike traditional spiral heat exchangers that used a low degree incline to increase the length of the fluid region, for a given height of the heat exchanger a different approach was taken. Rather than having two fluid regions along

the heat exchanger, which leave large areas of the spiral empty. Each fluid region was separated into 5 concurrent fluid regions, totalling 10 fluid regions along the recuperative heat exchanger. This design fully utilised the available area along the outside the recuperative heat exchanger.

3.2.1 Profile of the of the Recuperative Heat Exchanger

The design of the 2d profile originated with the sketch of one of the five sections regions to form the desired 10 fluid regions. Following the spiral design, the sketch includes concentric rings each with a set 1mm tolerance between them for both the fluid and solid regions. These rings formed the fundamental design of the profile depicted in Fig 3.5 (a). The tolerances surrounding the concentric also include the same 1mm gap between the start of the next section. This generated a profile where all perpendicular distances are set at 1mm with the exception of the ends of the heat exchanger where the concentric rings merge to a point. This aspect is enlarged to include a greater than 1mm tolerance at all points. The 1mm design tolerance allowed for a consistent design across the entire section. The core limitations placed on the entire profile which can been seen in Fig 3.5 (b) shown the 62.832mm length tolerance for the profile, with a 45-degree incline and a height limitation of 10mm with the closest section of the profile positioned 10mm from the central axis of the geometry. This restricts each of the five sections within the full profile to a length of 12.566mm.

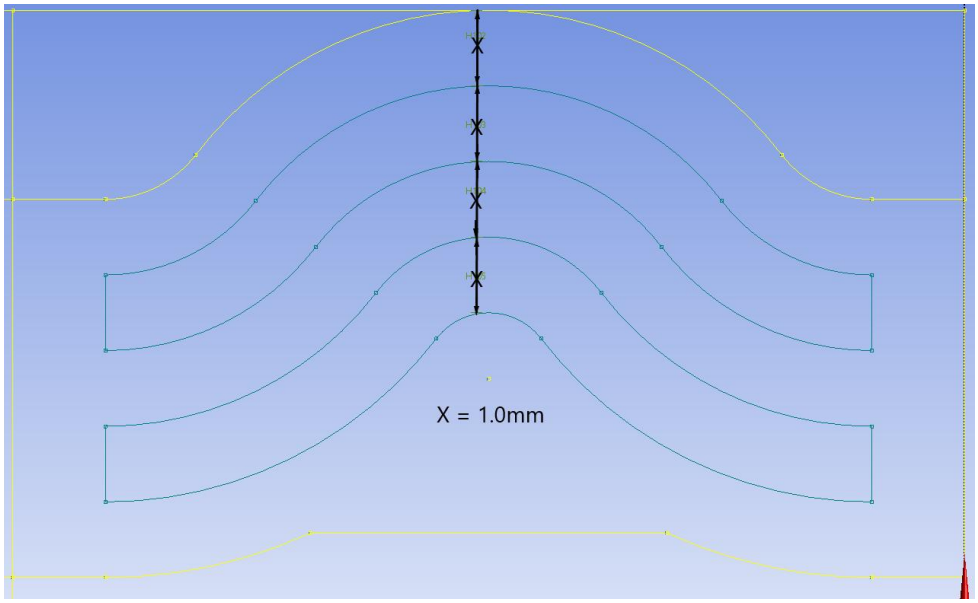

(a)

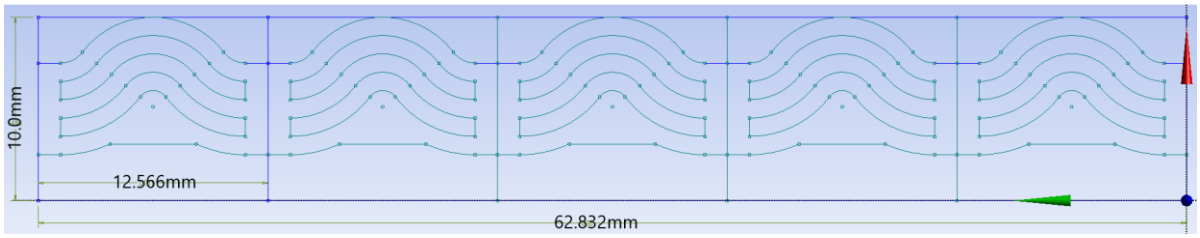

(b)

Figure 3.5 Recuperative Counterflow Helical Heat Exchanger Profile (a) a single section of the swept profile and (b) the full 2D profile of the swept surface

Each section of the full profile was split into two distinct sections. Rather than generation the entire geometry within a single sweep function, which incorporated additional complexities due to the 45-degree sweep function, the profile was split into a solid and a fluid region. This is displayed in Fig 3.2.2, where Fig 3.6 (a) highlights the solid region of the heat exchanger and Fig 3.6 (b) depicting the two fluid regions contained within each segment of the full 2d profile.

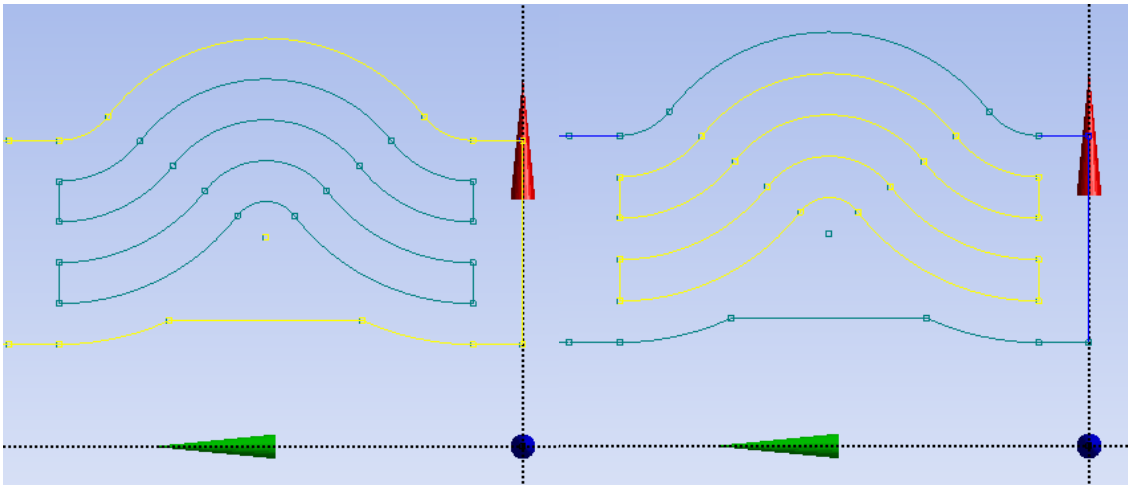

(a) ***(b)***

Figure 3.6 Core of the Recuperative Counterflow Helical Heat Exchanger Profile (a) the profile to generate the exterior layer of the complete counterflow heat exchanger and (b) the profile to generate the two fluid regions for the complete counterflow heat exchanger

3.2.2 Swept Design of the Recuperative Heat Exchanger

The generation of the 2d geometry for the heat exchanger originated with the sweep of the solid region of the recuperative heat exchanger profile. The sweep function precisely configured at a set pitch of the exact length of the profile, 62.832mm, generates a revolving profile. This revolving profile loops back where the lower end of the profile coincides with the upper end of the profile after one complete rotation at a 45-degree incline. This generates a section where rather than a simple spiral design being generated, the centre of this geometry includes a cylindrical section. This cylindrical section is ideal for the design of the recuperative heat exchanger due to the consistent being and end of the design. Fig 3.7 shows the start of the spiral geometry formed from the solid profile. This geometry is extended up to three times the desired length of the heat exchanger.

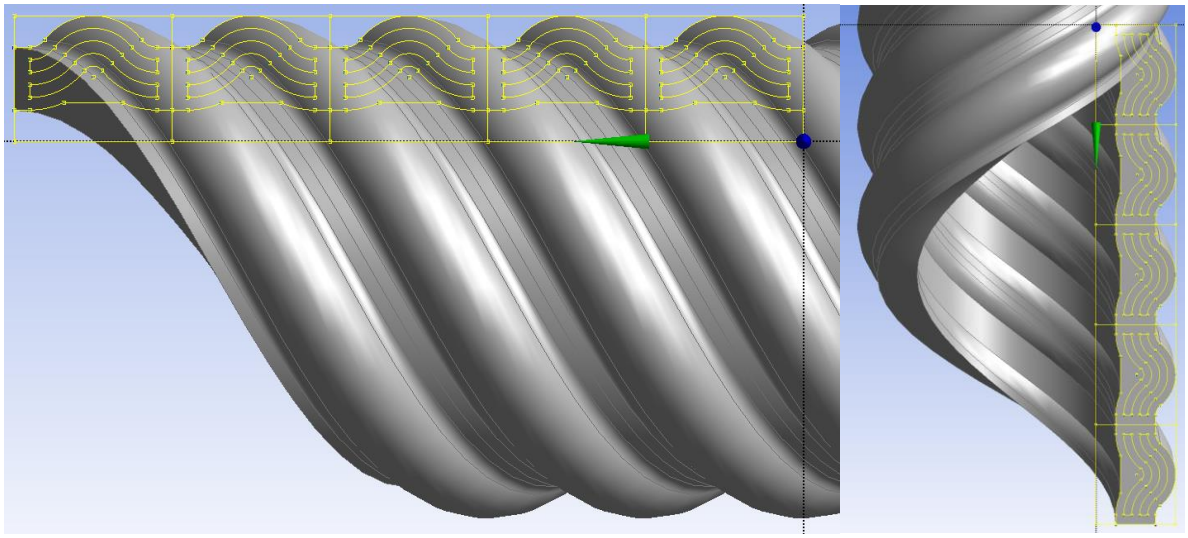

Figure 3.7 2D Swept Solid Geometry for the Counterflow Helical Heat Exchanger

To create a cylinder of height 62.832mm from this swept screw surface. The top and the bottom of the screw is removed with the extrusion function, leaving a full cylinder with the specified length of 62.832mm. Fig 3.8 (a) shows the central section of the solid body of the heat exchanger which forms the core of the heat exchanger design, which Fig 3.8 (b) depicting the cut lower section of the solid body. No including the fluid paths in this step greatly improved the reliability of the sweep process and hence was separated into two distinct stages. Due to the behaviour of removing surfaces and regions within Design Modeller, there is no limitation or restriction with the order of removing surface and regions from a solid. This allows for greater flexibility with the design process. Which promotes the use of removing sections and geometries from a core design rather than building new geometries on top of previous designs.

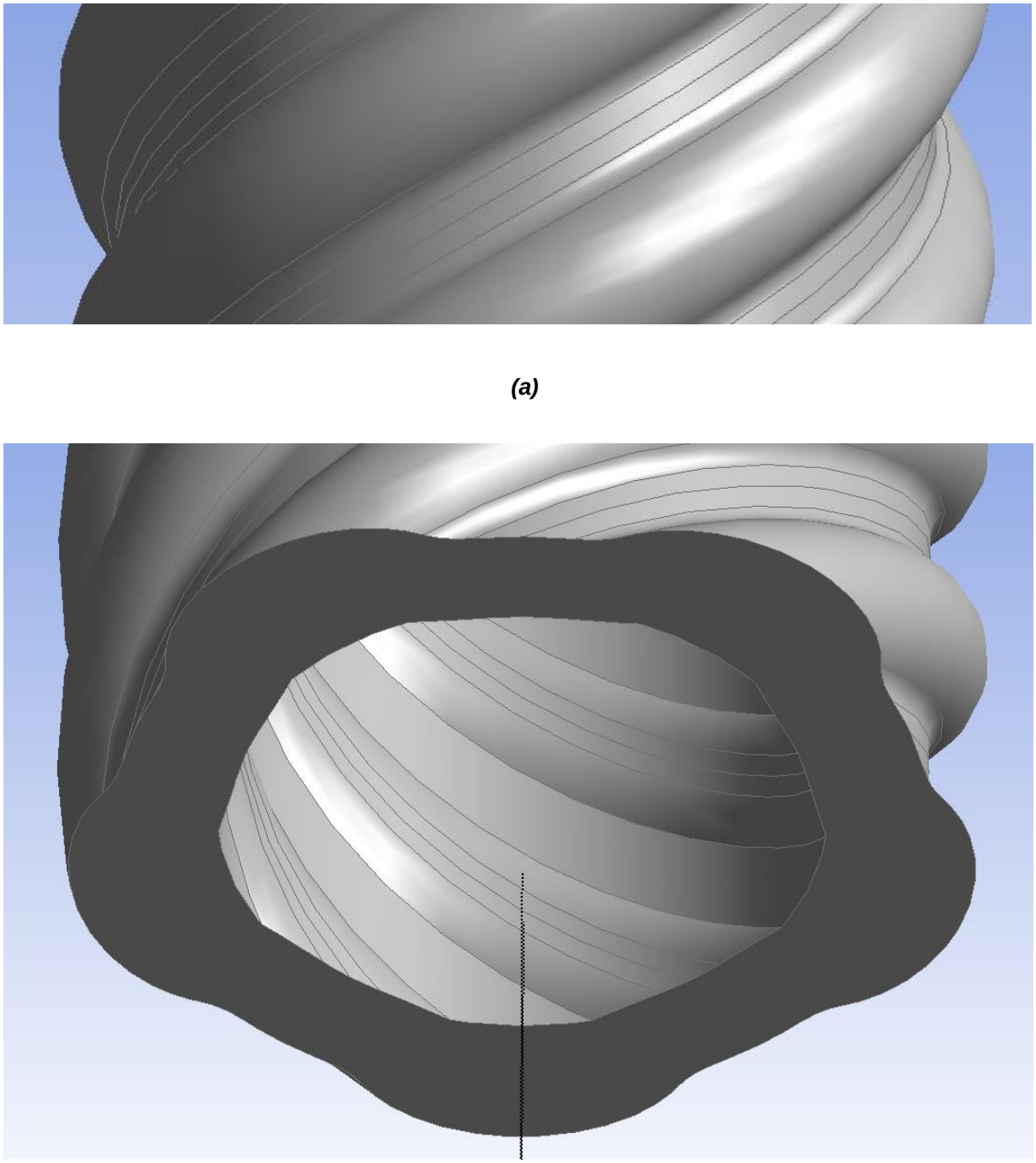

(a)

(b)

Figure 3.8 2D Swept Solid Geometry for the Counterflow Helical Heat Exchanger (a) the central section of solid body and (b) the cut lower section of the solid body

The final stage of designing solid region of the recuperative heat exchanger, was to trim the upper and lower surfaces of the swept design to produce a completed spiral cylinder. This trim of the heat exchanger was executed before the generation of the

fluid region, due to the performance implications of the swept cut process. As the length for which the swept design was removed was reduced, this accelerated the overall generation of the design. The second stage of designing the recuperative heat exchanger was to cut the fluid regions into the solid structure. This involved repeating the exact steps that were taken with the solid profile but substituting the fluid region profile. This generated 10 fluid regions with the solid bold. The top and bottom sections of the heat exchanger including the fluid regions can be seen in Fig 3.9 (a) and Fig 3.9 (b) respectively.

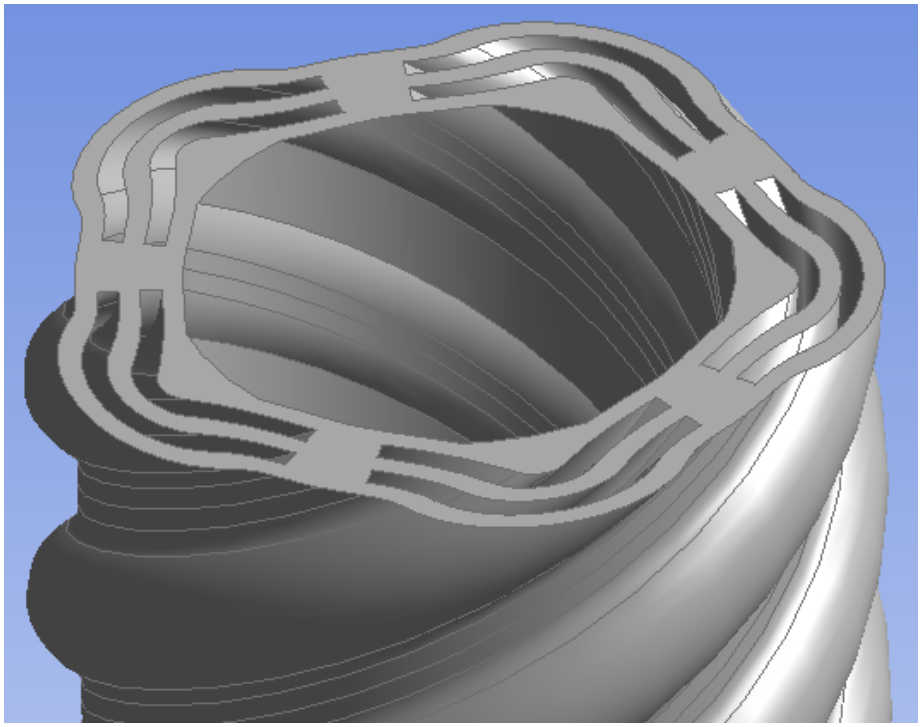

(a)

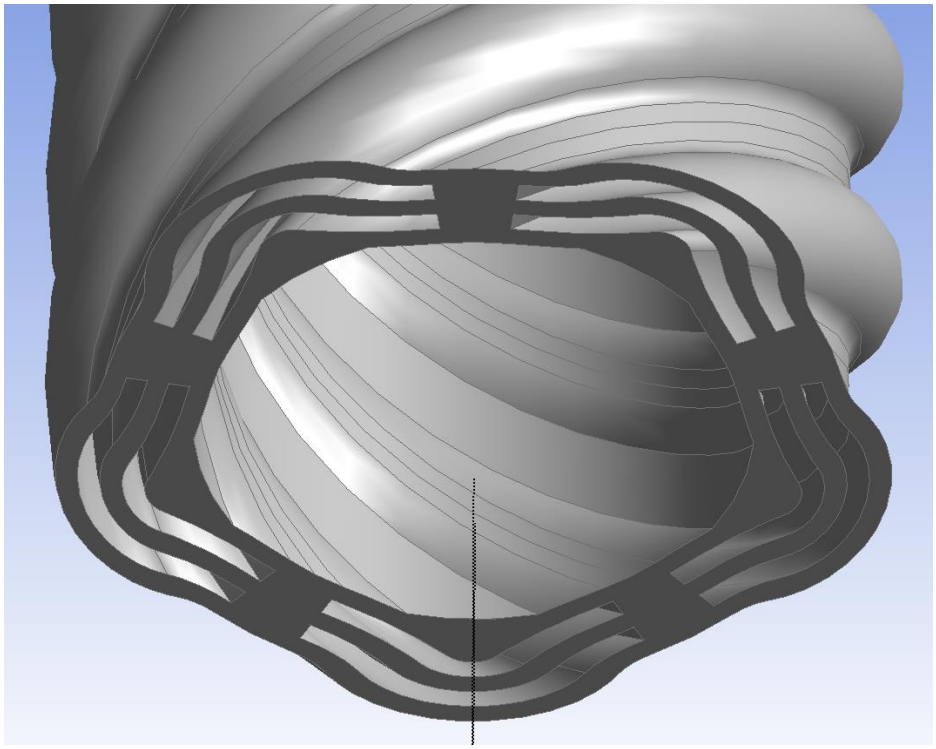

(b)

Figure 3.9 Solid and Fluid region geometry for the Counterflow Helical Heat Exchanger (a) the top section of the heat exchanger and (b) the bottom section of the heat exchanger

3.2.3 Inlet and Outlet Design

The next stage of the design process was to join the 10 separate fluid regions on each end of the recuperative heat exchanger to meet the fifth requirement specified for the design. Ensuring the 10 separate fluid regions were joined into two fluid regions that can be used as a simple inlet and outlet for the heat exchanger, while reducing the impact on fluid flow. To join these volumes together several steps needed to be combined to generate this complex non uniform geometry. The key feature that was considered was the skin process which enabled the generation of a surface through the selection of two lines rather than two areas. This allows for the desired outlet and the 10 fluid regions to be fluidly joined together, without the restriction of a fixed geometry.

The first step in this process was to generate two separate linear extruded surfaces each 0.5mm in height from each end of the heat exchanger. This was done to allow for the selection of a distinct region exactly 0.5mm along this extrusion. Fig 3.10 (a) shows the top surface of the heat exchanger before the dual extrusion with Fig 3.10 (b) depicting the dual extruded top section. On each of the four newly upper extruded surfaces to the adjacent fluid regions, a rectangle was sketched on a plane. This is presented in Fig 3.11 (a). The two pairs for each fluid regions were then selected with the skin function which removed the volume between the two adjacent fluid regions joining them along the upper extruded surface. This generated a connection region with a height of 0.5mm which can be seen in Fig 3.11 (b). These steps were repeated for the remaining four fluid boundaries. This resulted in the joining of the five separate fluid volumes into a single volume for each of the two fluids regions depicted in Fig 3.12.

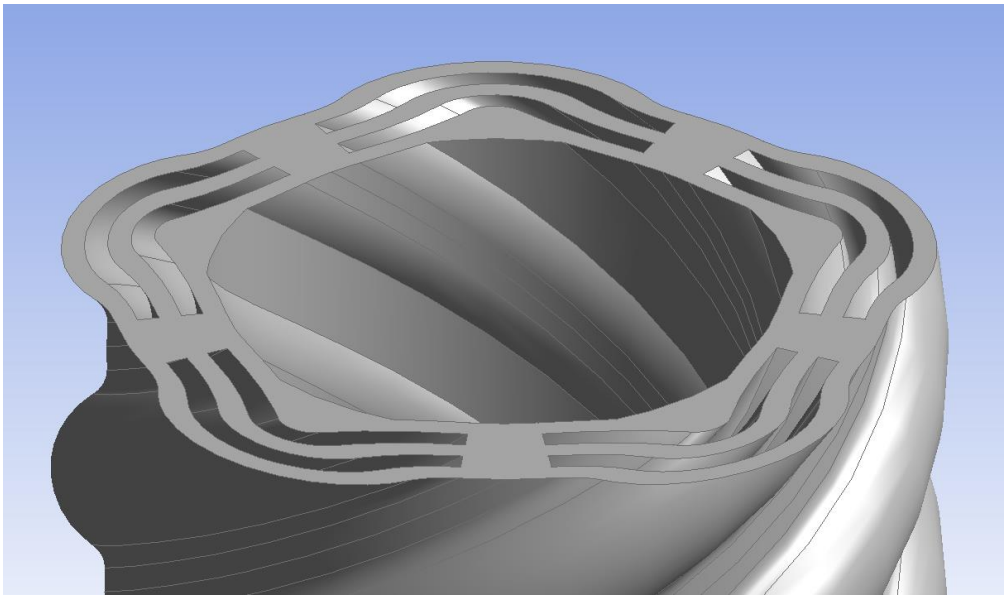

(a)

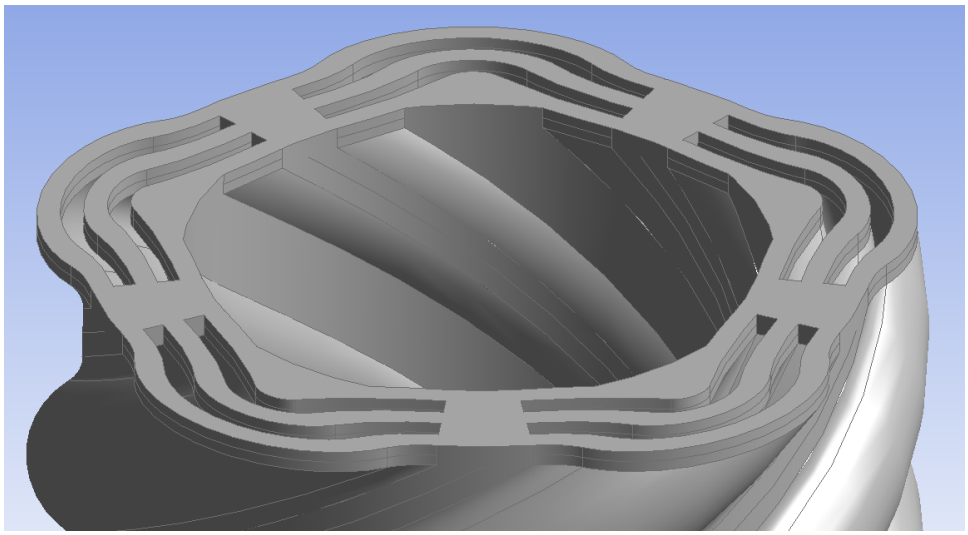

(b)

Figure 3.10 Top Surface for the Counterflow Helical Heat Exchanger (a) base top surface of the heat exchanger and (b) the dual extruded surface of the heat exchanger

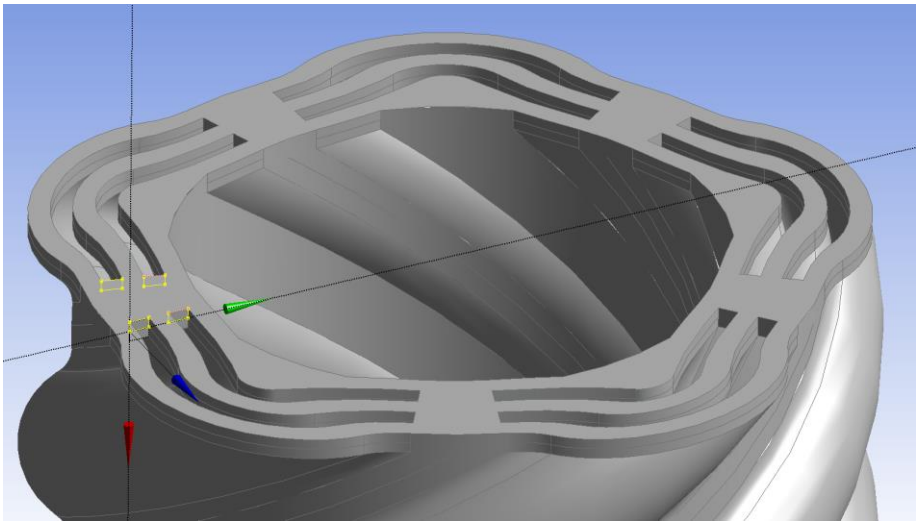

(a)

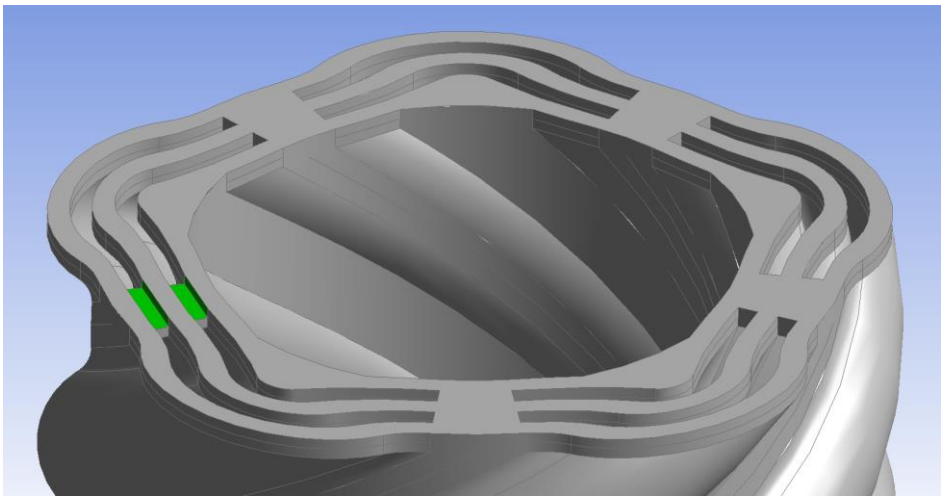

(b)

Figure 3.11 Extruded Top Surface for the Counterflow Helical Heat Exchanger (a) the 4 rectangles to the two adjacent fluid regions and (b) the cut section between the two adjacent fluid regions

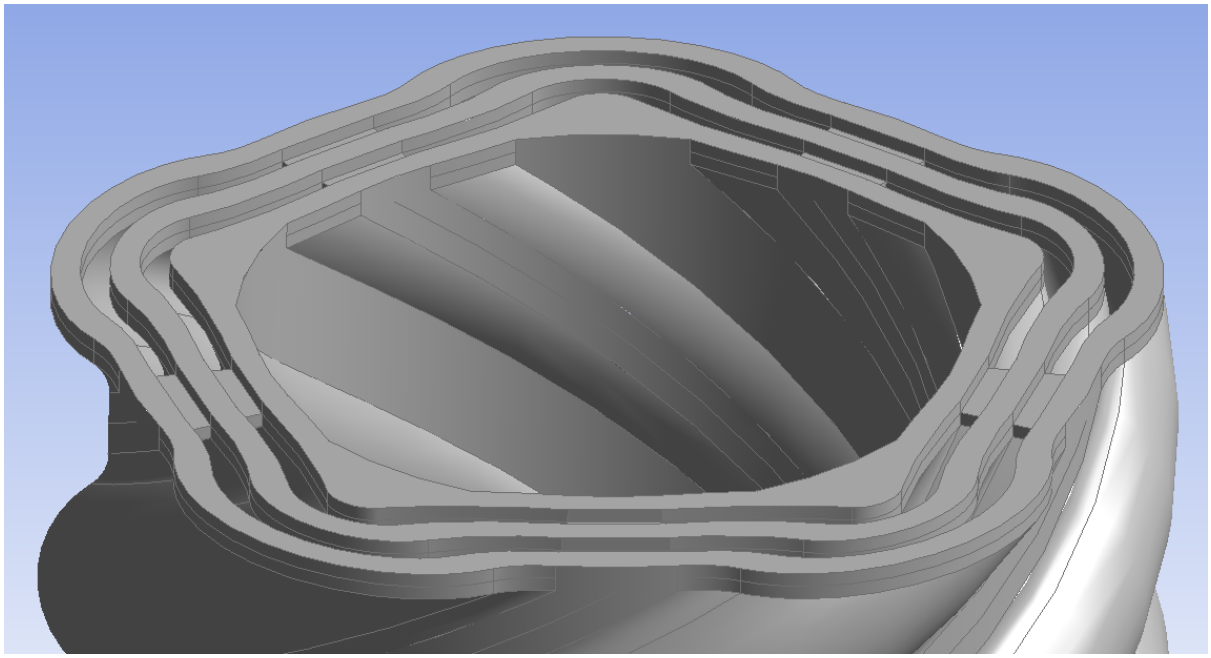

Figure 3.12 2D Extruded Top Surface for the Counterflow Helical Heat Exchanger with fully connected fluid regions

With the 10 separate fluid paths, successfully connected into two fluid regions, the next steps could be taken to join the complex perimeters of the fluid regions into circular sections. This was again achieved with the use of the skin function where each of the six perimeters of the connected fluid regions, were successively joined together with the corresponding circular perimeter generated for the purpose of a fluid inlet and outlet. The circular perimeter used for the inlet and outlet was designed on a plane 10mm above the end of the heat exchanger shown in Fig 3.2.9. This allowed for sufficient vertical clearance for the skin function to smoothly connect the surfaces. A second requirement for the skin function was that each of the two selected profiles had an identical number of subsections within the profile. The helical spiral geometry generated 20 distinct subsections for the extruded top and bottom surfaces of the heat exchanger. To match the requirements of the skin, function all the circular perimeters used for the opposite end of the skin function also required 20 distant subsections.

This involved manually dividing the circular perimeter into 20 equal length subsections. The first pair of circular perimeters shown in Fig 3.13 (a) is used to generate the outer solid region where the second presented in Fig 3.13 (b) generate the solid region between the two fluids. The third pair highlighted in Fig 3.13 (c) generated the final region for the inner wall of the fluid boundary. Overall, these six perimeters were used to create two annular fluid regions.

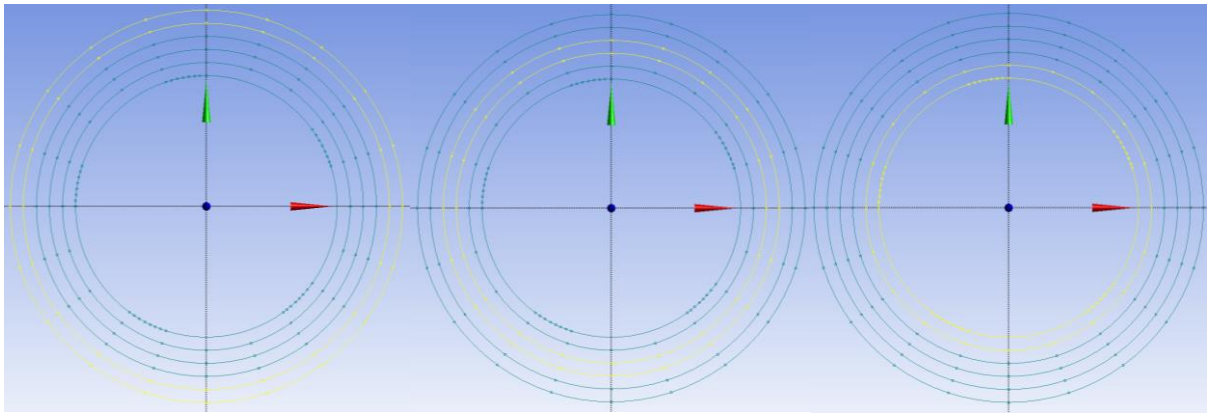

(a) ***(b)*** ***(c)***

Figure 3.13 Circular Perimeter for the Inlet and Outlet Connection of the Counterflow Helical Heat Exchanger (a) the two profiles used to generate the outer wall of the outer fluid and (b) the two profiles used to generate the wall between the two fluid boundaries and (c) the two profiles used to generate the inner wall of the inner fluid

The last and most critical requirement to complete the inlet and outlet connections was the order for which these surfaces were generated. Due to each of the six circular perimeters being generated separately from another, each use of the skin function had the potential to affect the previous iterations of the skin function. Fig 3.14 (a) depicts how the skin function on the outer most region of the heat exchanger, generated a volume complete encompassing the top surface of the heat exchanger. This results in the deduction that use the cut skin function will remove the entire volume within. In this

case any generate volumes within the cut region will be completely removed. To overcome this complication the generation of surfaces was required to be commenced from the outer most to inner most profiles. Fig 3.14 (b) shows the completed cut skin function of the outer most solid boundary surface. This process moving from the outer to inner profiles was repeated to generate the outer fluid region presented in Fig 3.15 (a) and the start of inner fluid regions and the solid boundary between the two fluid regions depicted in Fig 3.15 (b). The final iteration of this process resulted in Fig 3.16 (a) which shows the complete inner fluid region and Fig 3.16 (b) which represents the complete inlet and outlet connection for one end of the heat exchanger.

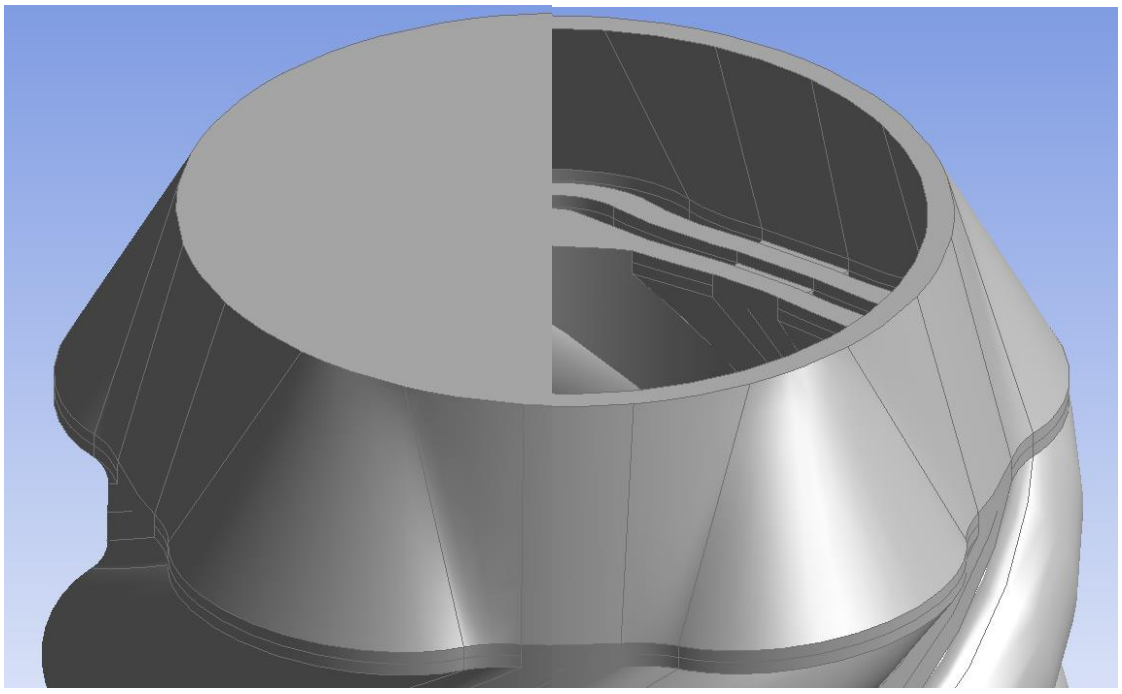

(a) ***(b)***

Figure 3.14 Inlet and Outlet Connection for the Counterflow Helical Heat Exchanger (a) the volume following the outer external region of the heat exchanger and (b) the cut volume following the outer ring of the outer fluid region

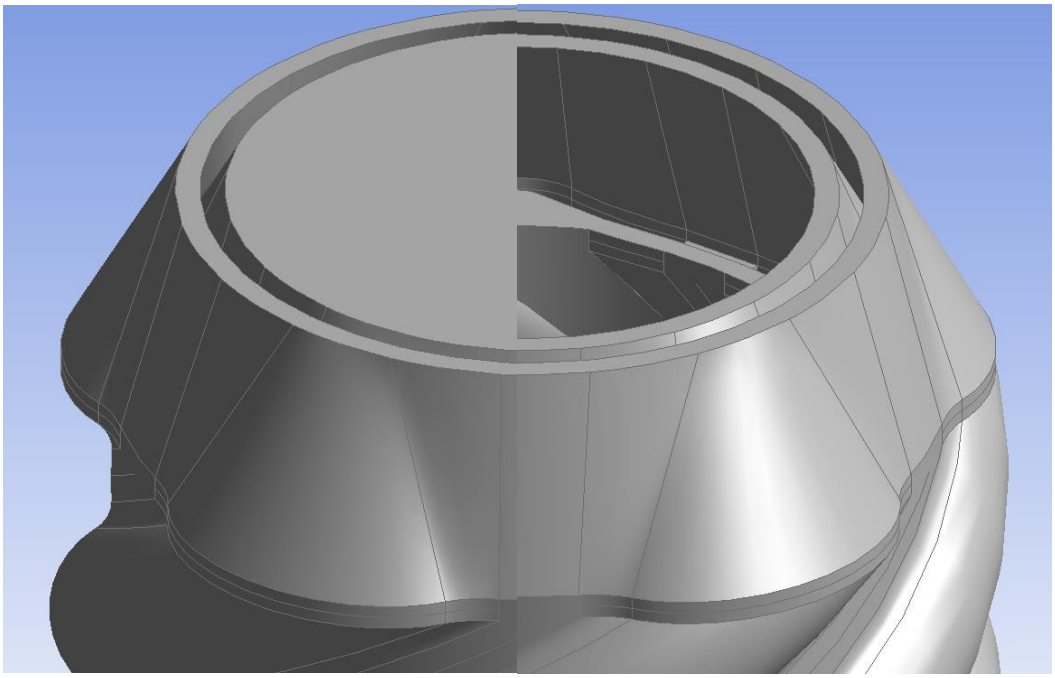

(a) ***(b)***

Figure 3.15 Inlet and Outlet Connection for the Counterflow Helical Heat Exchanger (a) the volume following the inner ring of the outer fluid region and (b) the cut volume following the outer ring of the inner fluid region

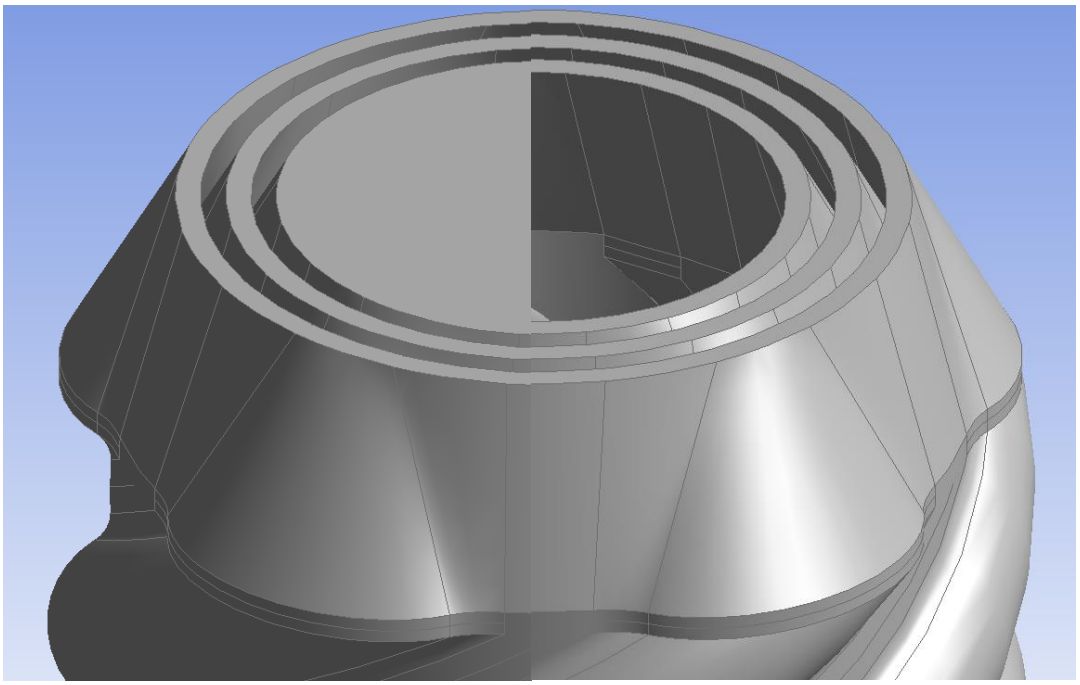

(a) ***(b)***

Figure 3.16 Inlet and Outlet Connection for the Counterflow Helical Heat Exchanger (a) the volume following the inner ring of the inner fluid region and (b) the cut volume following the inner external surface on the heat exchanger

After duplicating this process on the other end of the recuperative heat exchanger a complete geometry was formed. Entirely comprising of surfaces inclined and a minium of 45-degrees and walls with a thickness of 1mm the geometry statisfied all the requirements for an additively manufactured geomety. To reduce the cost of manufacturing while reducing the time requirement half of the geomtry was used for an initial test print, to establish foundations for both the reliablility of the process and the 45-degree geometry. Fig 3.17 depicts the complete heat exhcanger design with a single fluid inlet and outlet at each end of the heat exchanger. Completing the counterflow requirement, the inlets to the heat exchanger were at opposite ends.

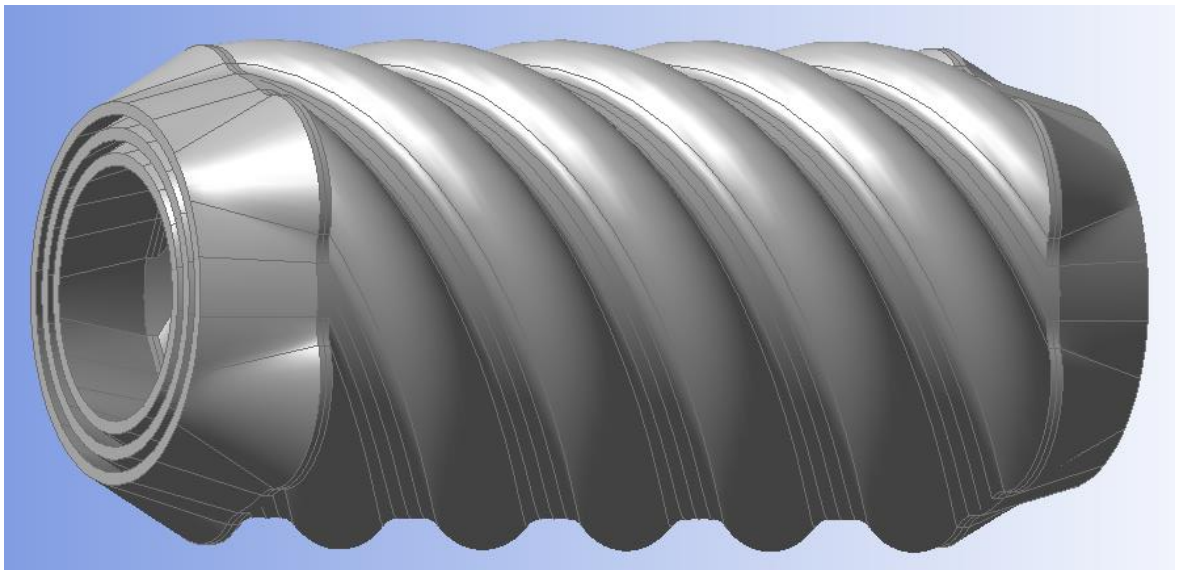

Figure 3.17 Complete Recuperative Counterflow Helical Heat Exchanger with two Inlet and two Outlets.

3.2.4 Thermal Short Circuit Recuperative Heat Exchanger Design

The solid body of the sprial heat exchanger promted concerns with potential thermal short cirucits parallel to the crossection of the cylinder. Thermal short circuits is an risk with traditional spiral heat exchangers, which lead to a second design which resolved these concerns. The core design change was to remove the solid section linking the five sections of the heat exchanger removing the direct veritcal conduction path through the addition of an air gap. The adjusted profiles for a single section is shown in Fig 3.18 (a) with the entire section presented in Fig 3.18 (b). The section higlighted in Fig 3.19 (a) represents the modified solid profile of a body with a constant 1mm gap between each of the five sections. While the fluid region presented in Fig 3.19 (b) remains identical to enure that the fluid flow paramters remain the same.

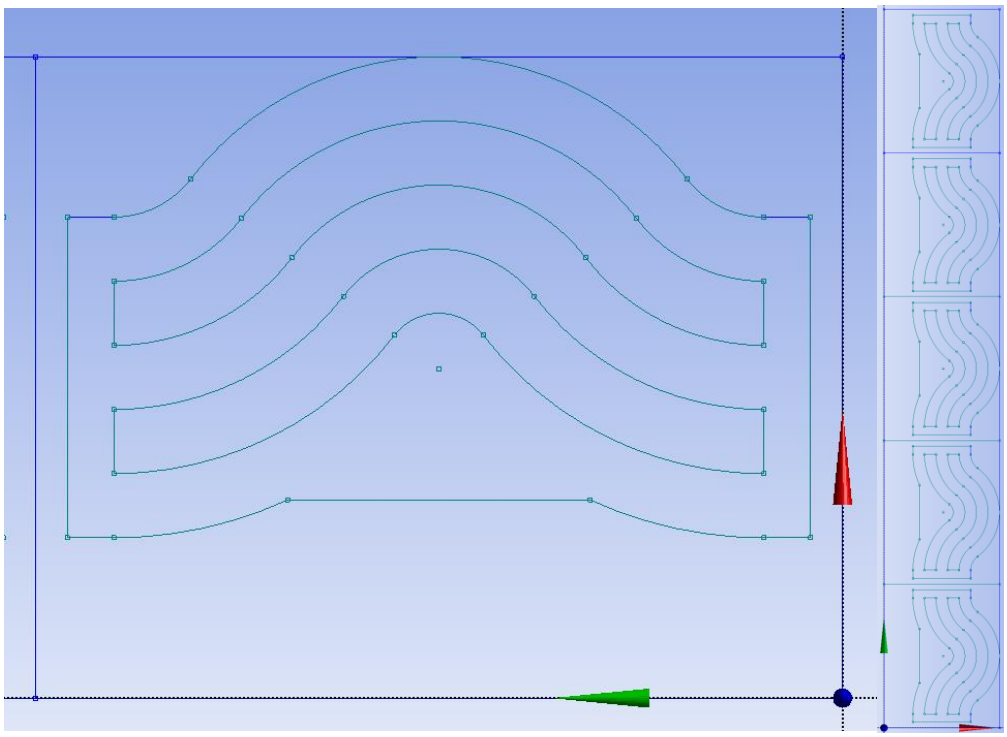

(a) ***(b)***

Figure 3.18 non-thermal short circuit Recuperative Counterflow Helical Heat Exchanger Profile (a) a single section of the swept profile and (b) the full 2D profile of the swept surface

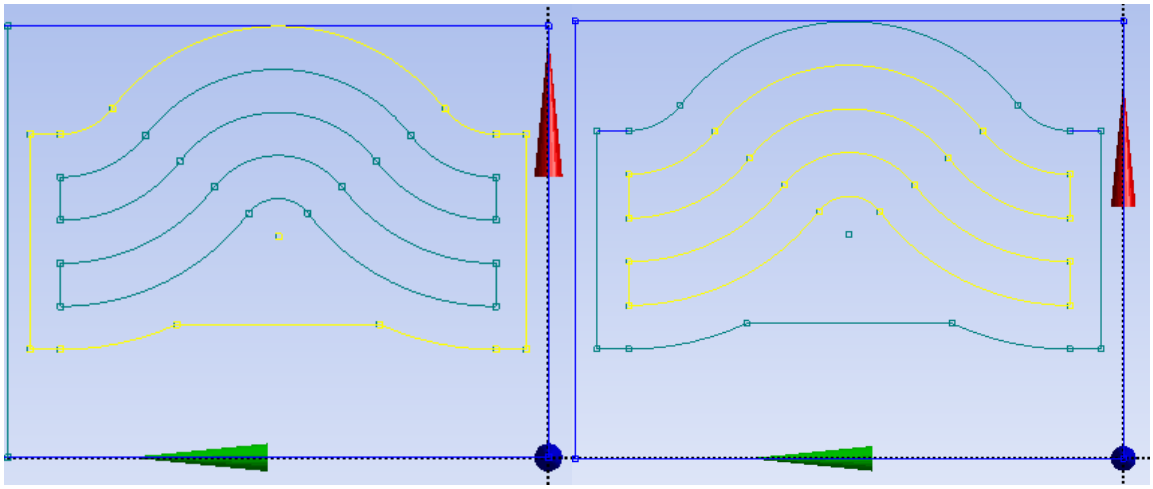

(a) ***(b)***

Figure 3.19 Core of the non-thermally short circuited Recuperative Counterflow Helical Heat Exchanger Profile (a) the profile to generate the exterior layer of the complete counterflow heat exchanger and (b) the profile to generate the two fluid regions for the complete counterflow heat exchanger

As a direct consequence of the linear constrution design within DesignModeller which maintains a record of all the steps used to geneate the geomtry edits can be made to the profiles at the beging of the generation process which influence the rest of the design. This enables the change of the solid regions to be immediately implemented with the rest of the steps remaining identical. The only complication with this generation was the connection of the inlet and outlet regions as due to the additonal gap between the five sections an additional subsection was generated on the end of the heat exchanger. This lead to a total of 25 subsections on both ends of the heat exchanger which created a critcal error in the skin function. To remedy this, each ciruclar perimeter was redivided into 25 equal subsections instead of 20. With this update to the inlet and outlet design the complete geometry presented in Fig 3.20 was produced. The slight gap between each of the five rings urrondg the heat excahnger represent the air gap in the design, resolving the potential thermal short circuits in the design.

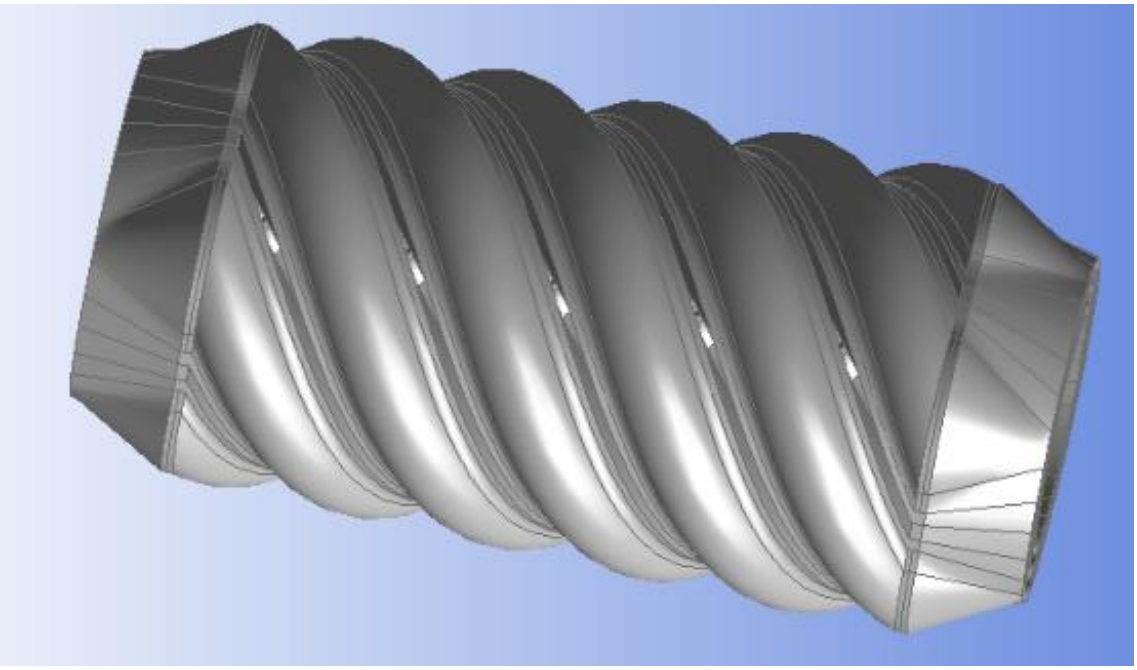

Figure 3.20 Complete Recuperative non-thermal short circuit Counterflow Helical Heat Exchanger with two Inlet and two Outlets

3.3 Design of the connection between multiple Recuperative Heat Exchangers

On account of the height limitation of the 3d printer set at 200mm, in order to produce a larger design, multiple separately printed parts needed to be combined as specified in the sixth requirement. Three key objectives were set with this requirement. The first that the fluid flow must be minimally impacted by the joint, with the second minimising the crossflow between the two fluids. The third ensured that the structural integrity of the heat exchanger was not reduced significantly during the construction of the connection. To ensure the two ends of the recuperative spiral heat exchanger could be connected precisely, the inherent spiral in the design was continued to form a screw concept. This involved two parts of the recuperative heat exchanger could be screwed

together, ensuring a precise connection point, while supporting the connection with a rigid structure directly connected to the core of heat exchanger body.

3.3.1 Profiles of the Recuperative Heat Exchanger Connection Joint

The design of this screw within the current design, required a fundamentally new approach to the generation of the recuperative heat exchanger. Due to the use of the swept function, to generate a cylinder, a sweep of at least two additional rotations of the spiral is required to produce a complete cylinder. This complicates the design of additional swept areas, as they all must be generated in a very specific order. All swept designs must be generated such that none of the subsequent sweeps or the extrusions required to form a cylinder would be in conflict. This required the screw concept to be produced first, with the rest of the previously generated recuperative heat exchanger to be repeated at the end. A single section of the newly generated profile can be seen in Fig 3.21 (a) where Fig 3.21 (b) shows the entire profile. The new profile consists of an addition two components. The first being the core screw construction highlighted in Fig 3.22 (a) while an associated 0.2mm tolerance was used, presented in Fig 3.22 (b). This 0.2mm tolerance was to ensure that the two ends of the screw connection could join without the risk of printing defects influencing the connection as a whole. The other two aspects of the profile while include both the solid body shown in Fig 3.23 (a) as well as the dual fluid region present in Fig 3.23 (b) remain the same.

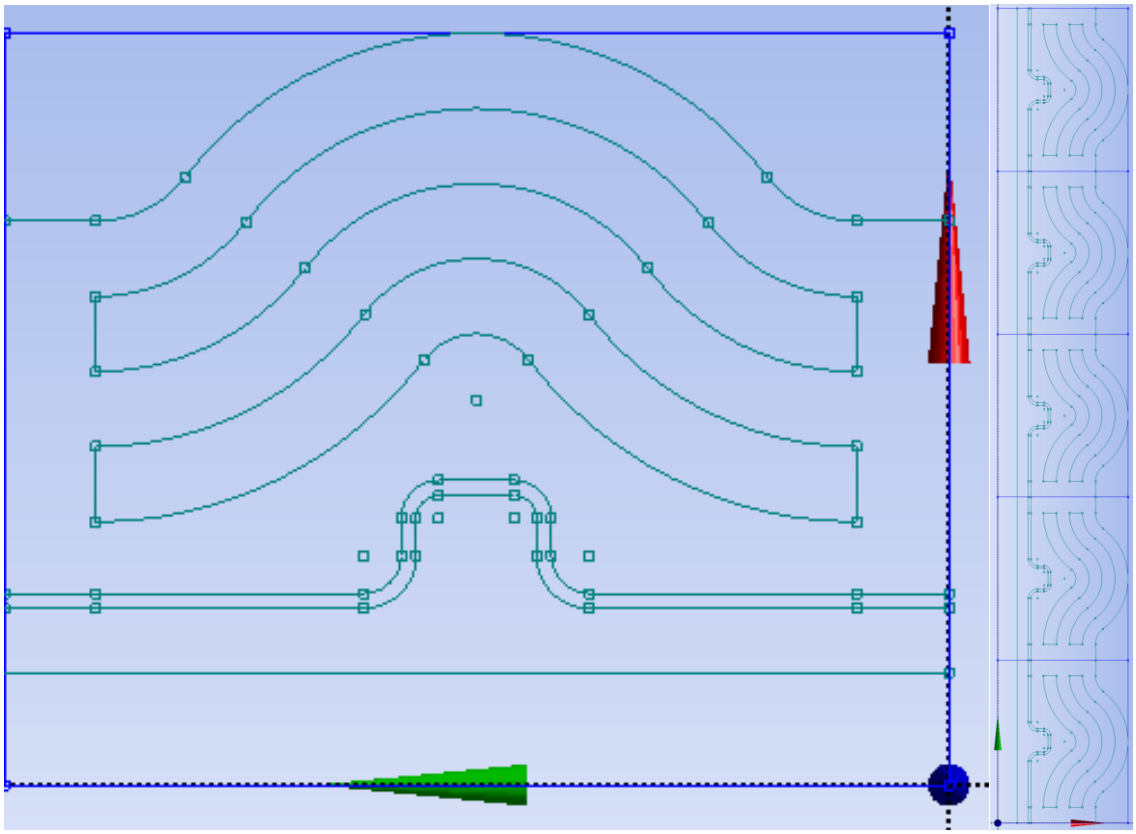

(a) *(b)*

Figure 3.21 Screw Connection Profile of the Recuperative Counterflow Helical Heat Exchanger (a) a single section of the swept profile and (b) the full 2D profile of the swept surface

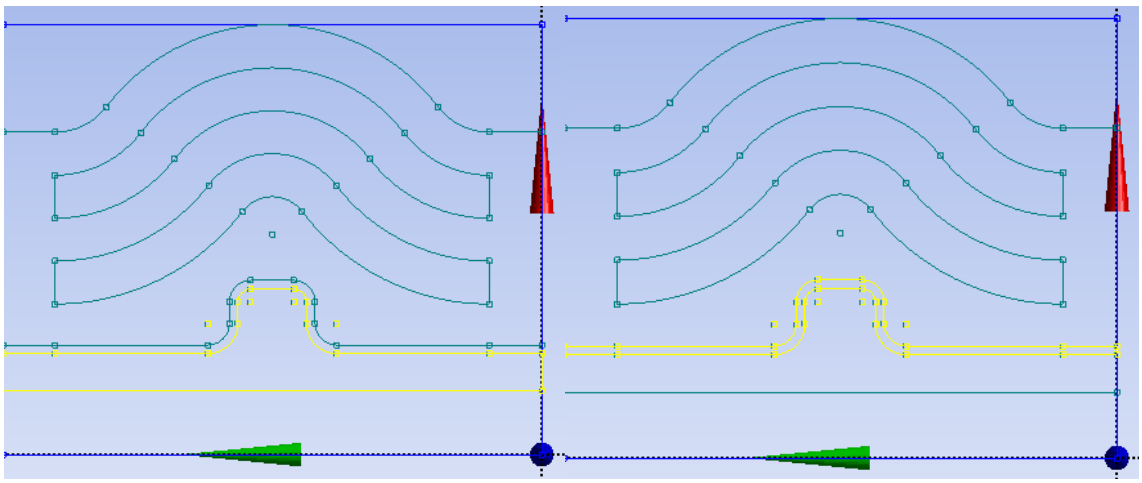

(a) *(b)*

Figure 3.22 Central Screw Joint of the Screw Connected Recuperative Counterflow Helical Heat Exchanger Profile (a) the profile to external surface and (b) the profile to generate the tolerance between the external and internal surface of the helical screw joint

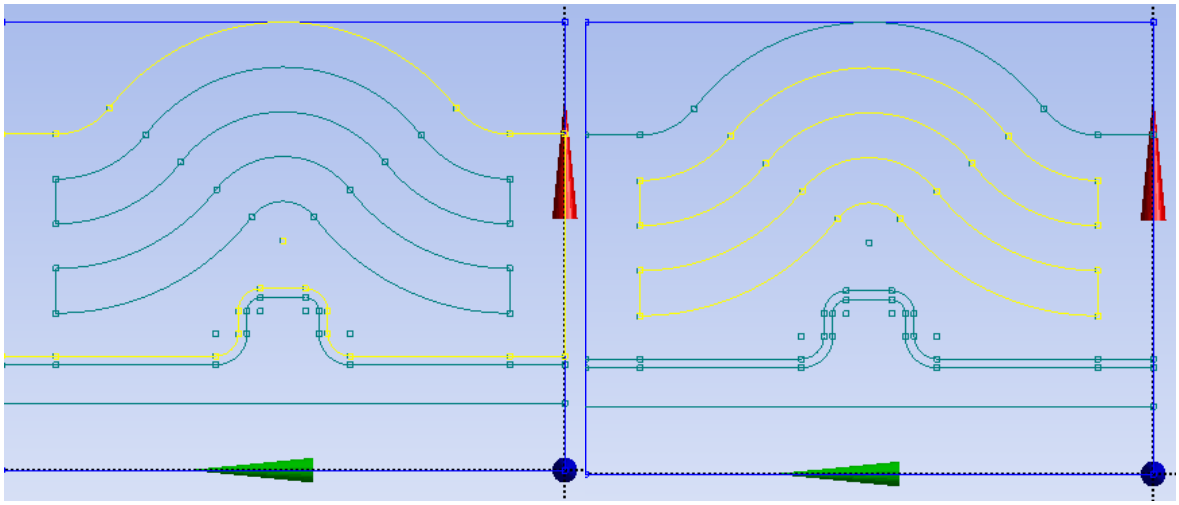

(a) ***(b)***

Figure 3.23 Core Layer of the Screw Connected Recuperative Counterflow Helical Heat Exchanger Profile (a) the profile to generate the exterior layer of the complete counterflow heat exchanger and (b) the profile to generate the two fluid regions for the complete counterflow heat exchanger

3.3.2 Swept Design of the Recuperative Heat Exchanger Connection Joint

To generate the male connection of the screw design, the tolerance of 0.2mm profile was generated first, shown in Fig 3.24 (a). This was due to the screw thread sweep extending further than the tolerance gap sweep, which would interfere with the extruded cut if a different generation order was taken. Fig 3.24 (b) presented the extruded cut of the screw connection, leaving a very thin cylindrical surface. The screw thread profile was then swept following Fig 3.25 (a), which then followed an additional extruded cut 5cm further along the recuperative heat exchanger. The second cylindrical surface formed from the second extruded cut can be seen in Fig 3.25 (b).

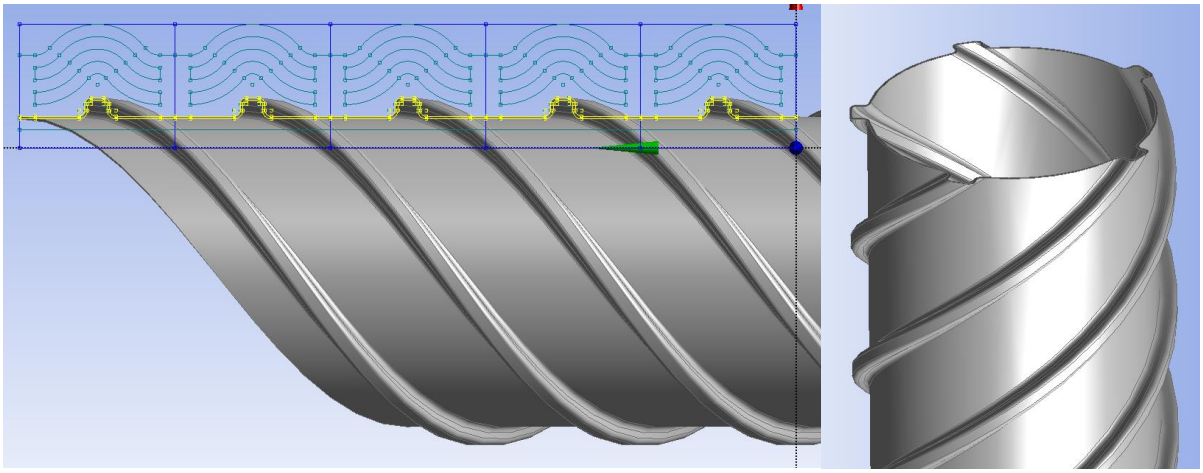

(a) ***(b)***

Figure 3.24 Swept Surface generated from the 0.2mm tolerance between the screw joint and the solid recuperative heat exchanger profile (a) the full helical profile of the sweep function and (b) the cut cylindrical surface matching heat exchanger connection junction

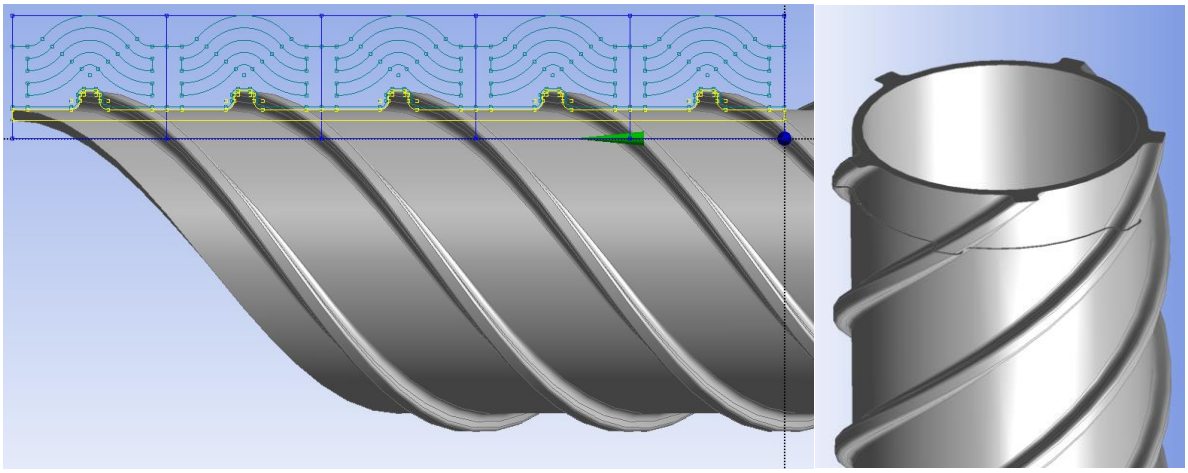

(a) ***(b)***

Figure 3.25 Swept Surface generated from the screw joint of the recuperative heat exchanger profile (a) the full helical profile of the sweep function and (b) the cut cylindrical surface matching heat exchanger connection junction

10cm along the opposite end of the screw connection joint a third extruded cut was performed, leaving the completed threaded geometry of the screw presented in Fig 3.26 (a). This geometry formed the internal thread of the screw as was then required to be connected to the subsequent sections of the heat exchanger. The final stage of the screw connection involved using a fillet function to round the opposite end of the screw connection. Shown in Fig 3.26 (b), this produced a smooth connection between the screw connection and the counterflow heat exchanger.

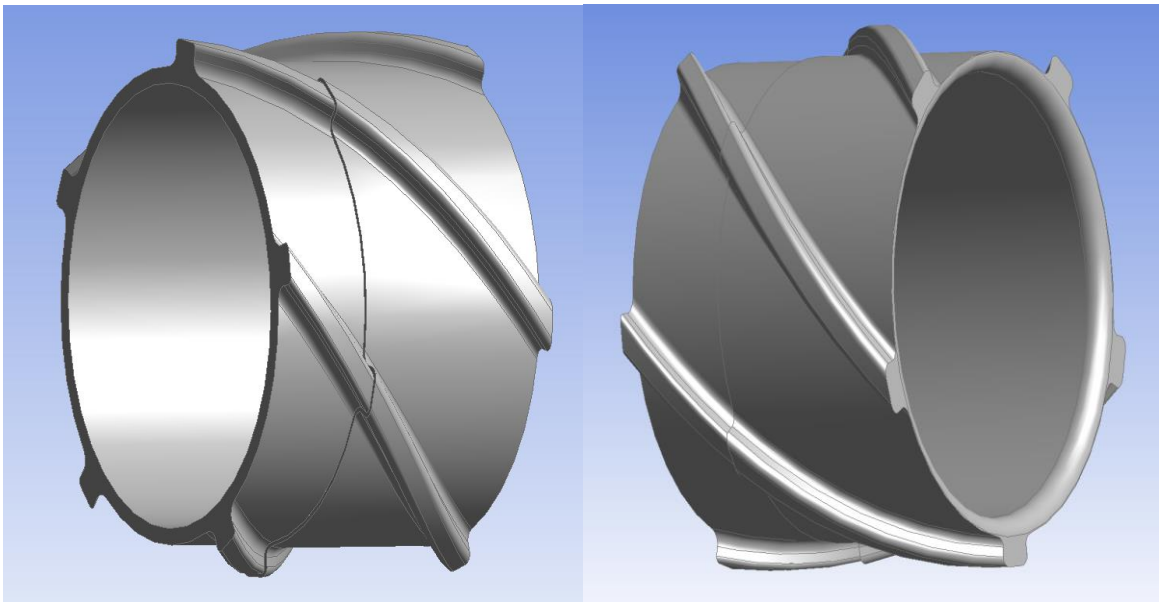

(a) ***(b)***

Figure 3.26 Screw connection joint for the Counterflow Helical Heat Exchanger (a) the male connection joint and (b) the connection of the screw joint to the rest of the heat exchanger

The final two profiles, which comprised of the solid and fluid region, were then used to produce the recuperative heat exchanger design. Initially the solid profile applied the sweep function which produced a spiral surface beyond the threaded screw design which is depicted in Fig 3.27 (a). However, unlike the previous extruded cuts that were used to trim the top and bottom surfaces of the screw thread feature, to avoid also cutting the screw thread a swept cut function was applied. To produce the geometry depicted in Fig 3.27 (b), a new cylindrical profile of the screw highlighted in Fig 3.28 was used. This new profile in combination with the swept cut function cut the solid region of the heat exchanger while leaving the screw connection untouched. The final step to produce the full counterflow heat exchanger geometry was to sweep the fluid regions into the geometry. Owing to the application of the swept cut with the fluid profile, no additional steps were required to produce the Fig 3.3.9.

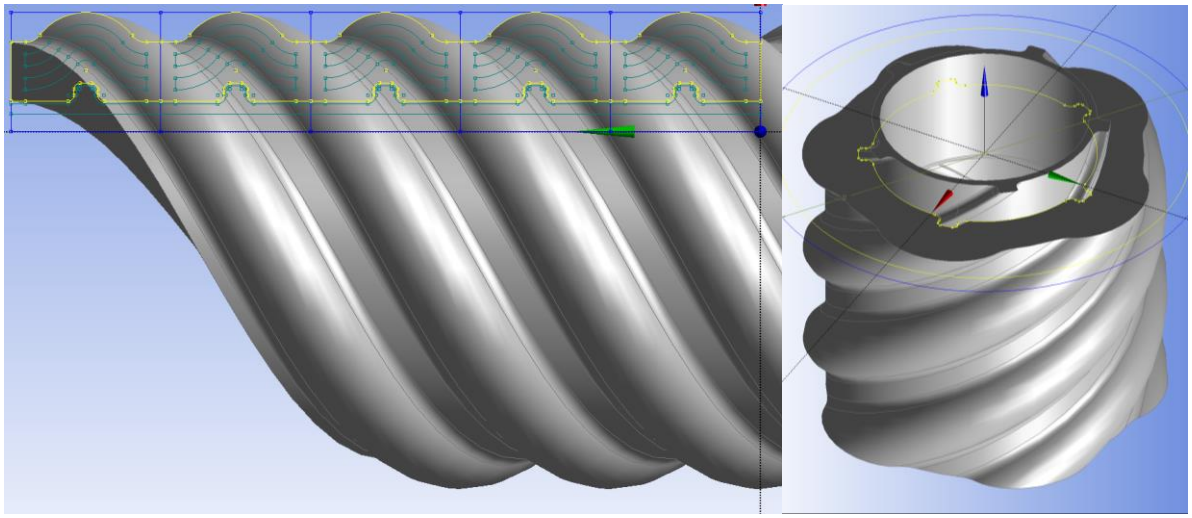

(a) *(b)*

Figure 3.27 Swept Surface generated from the solid profile of the recuperative heat exchanger (a) the full helical profile of the sweep function and (b) the cut cylindrical surface matching heat exchanger connection junction

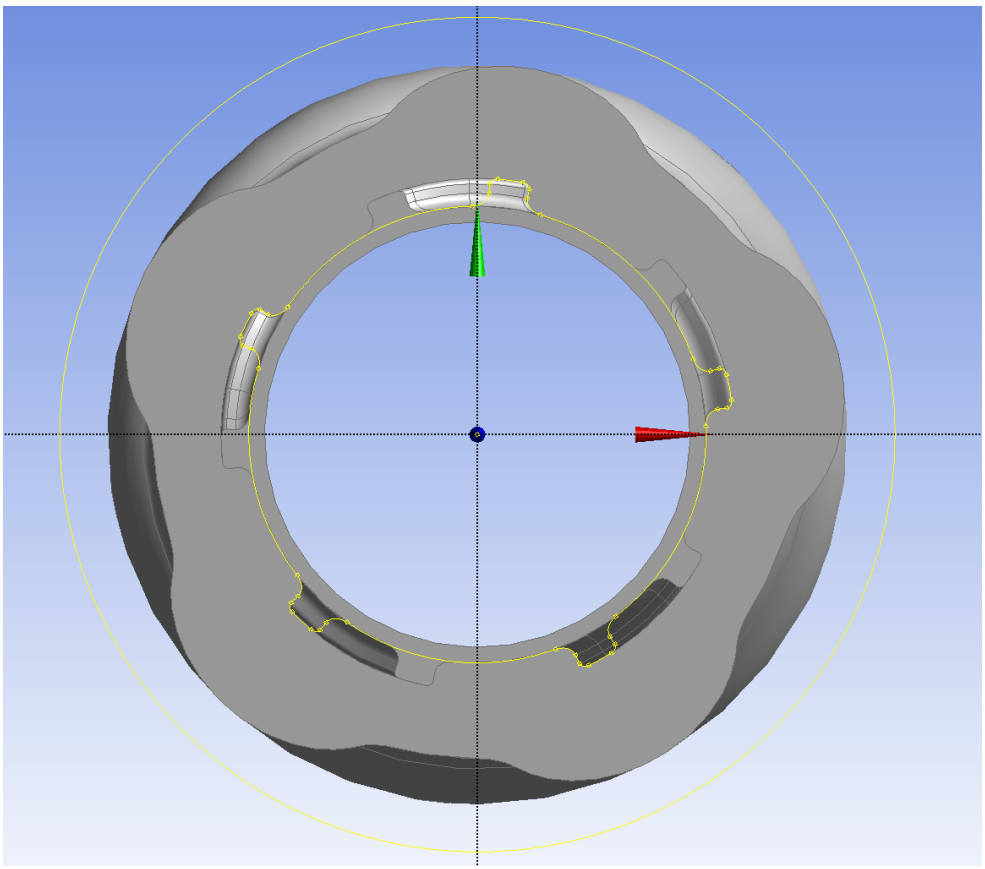

Figure 3.28 2D Profile to extrude cut the solid region while maintaining the screw connection joint of the counterflow heat exchanger

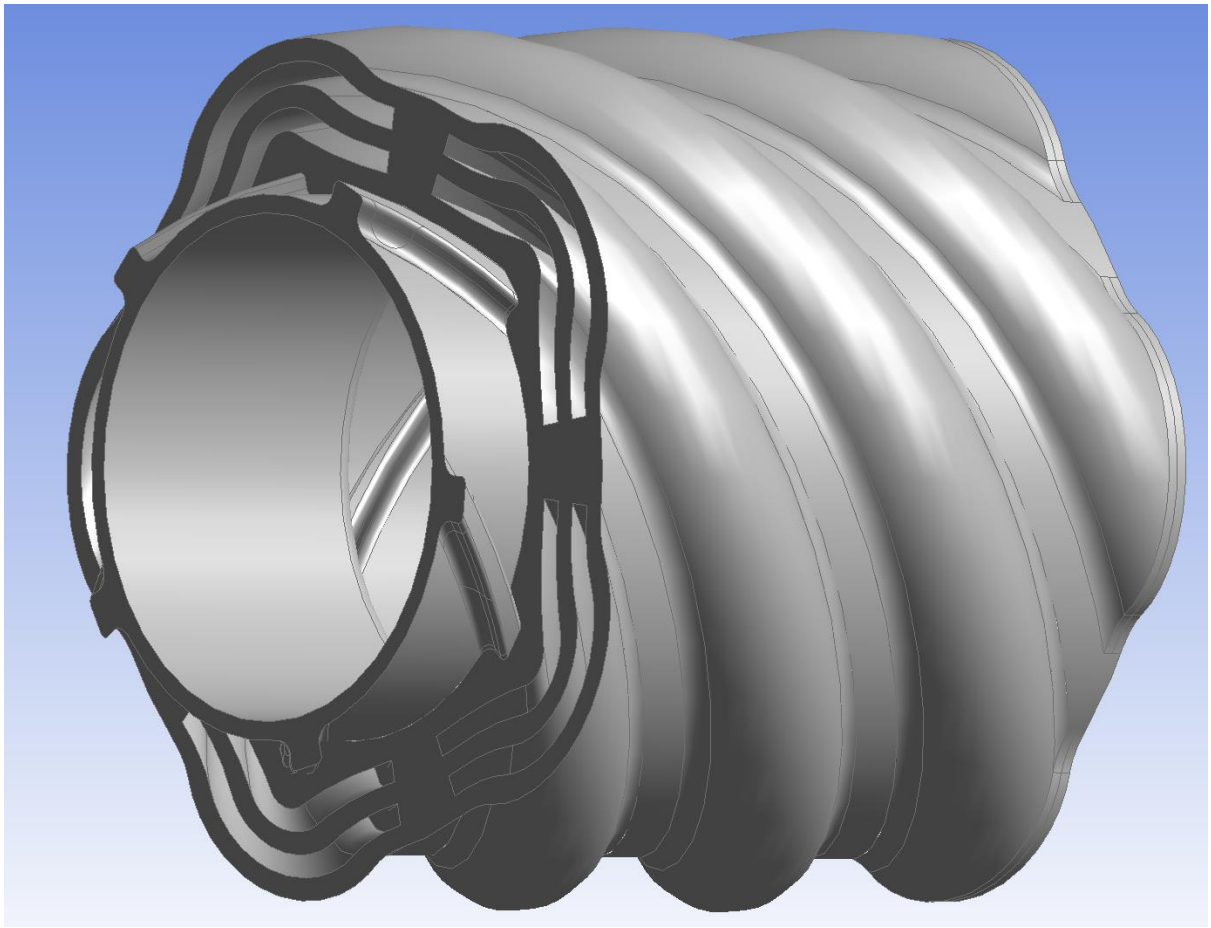

Figure 3.29 Solid and Fluid region geometry for the Screw Connection Joint of the Counterflow Helical Heat Exchanger

3.3.3 Male and Female Recuperative Heat Exchanger Connection Joints

The generation of the female connection joint was simpler due to the careful selection of the profiles. The lower region of the previously generate male connection joint perfectly matches the female connection. This allows multiple geometries following the male screw connection design to be concatenated to form a long helical recuperative heat exchanger. However, for the final piece of this geometry a single female thread was produce. This final piece can be seen in Fig 3.30 which exclusively incorporates the female screw joint.

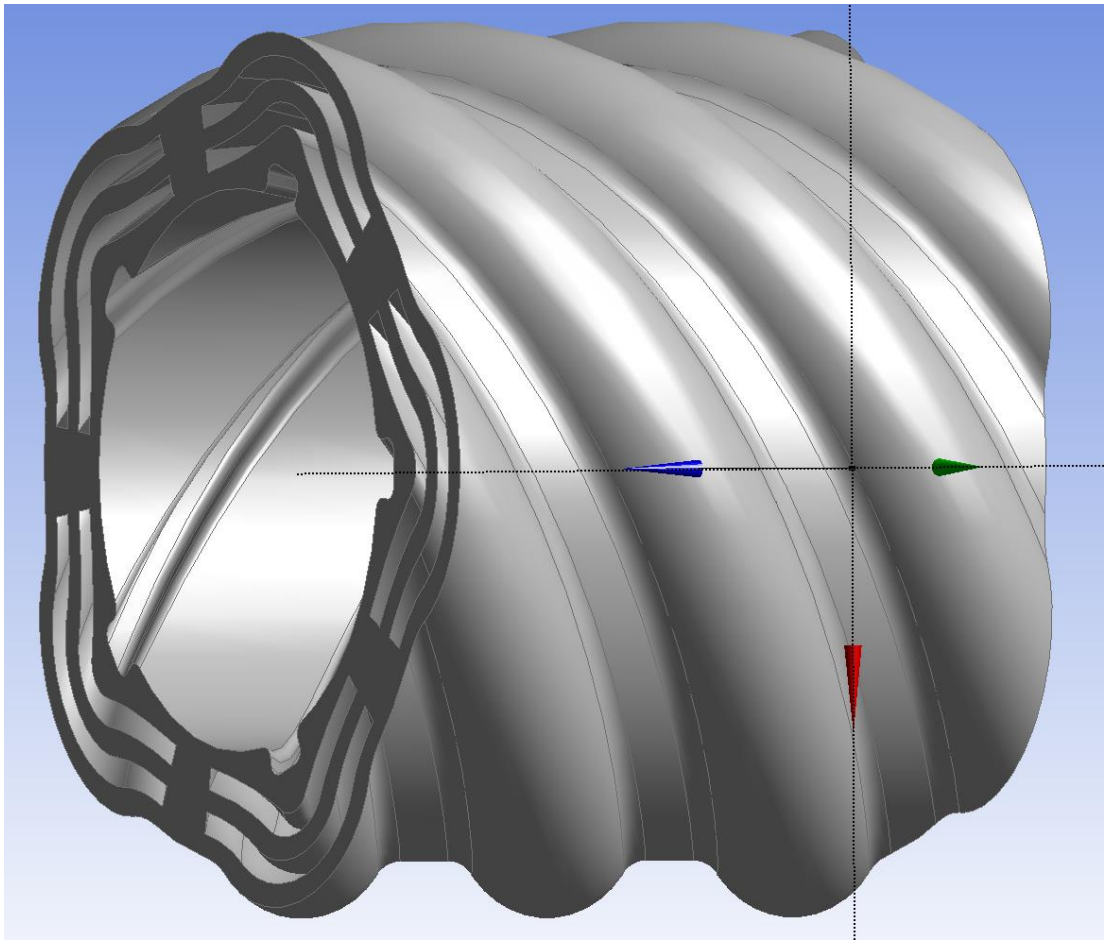

Figure 3.30 The complete female screw connection for the Counterflow Helical Heat Exchanger

In order to achieve the same inlet and outlet connections as the original heat exchanger designs, the 5 separate fluid regions for both the inner and outer fluids were again combined into two inlet and outlet regions. This followed an identical process as the previous design as the opposite end of the screw connection fundamentally remained the same. Fig 3.31 (a) shows the thread screw on the top in combination with the merged inlet and outlets on the bottom. Fig 3.31 (b) represents a flipped version of this geometry highlighting an identical inlet and outlet configuration.

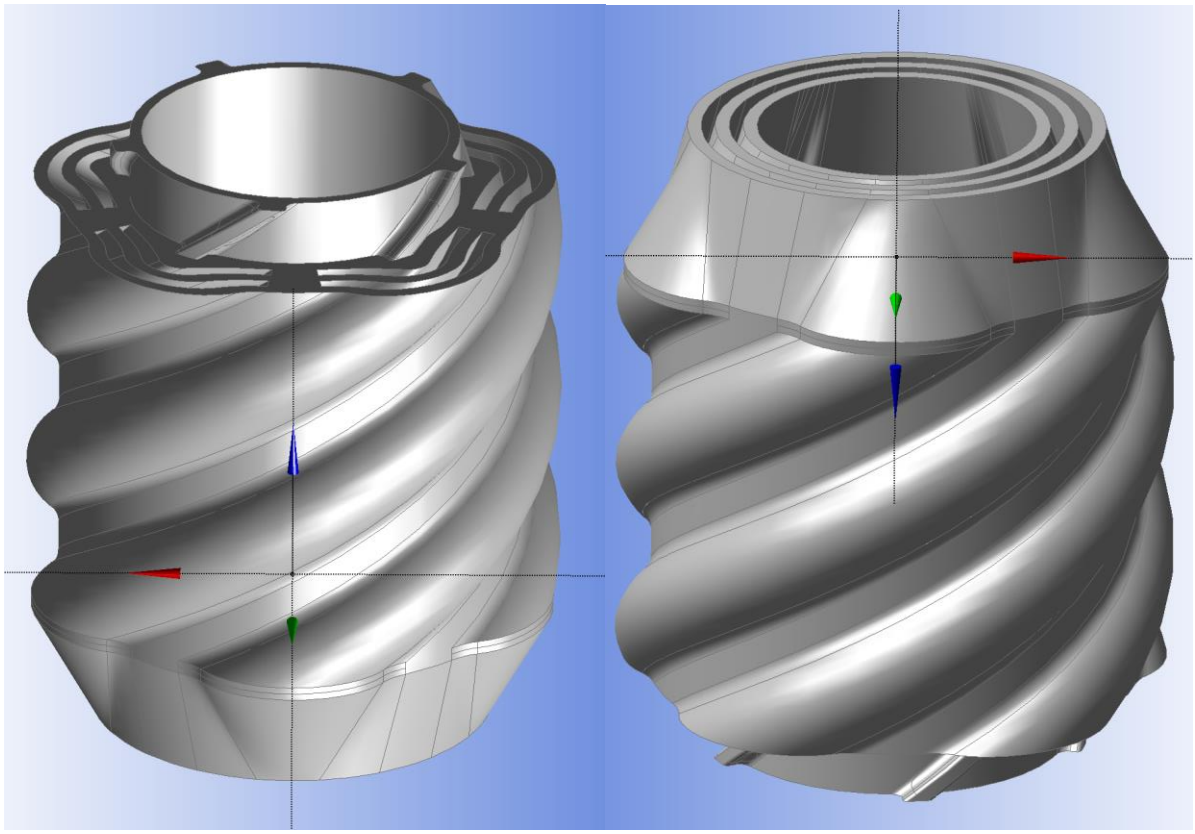

(a) ***(b)***

Figure 3.31 The complete male screw connection for the Counterflow Helical Heat Exchanger (a) the top section of the heat exchanger including the screw connection and (b) the bottom section of the heat exchanger including the merged inlet and outlet connection

3.4 Design of the leak resistant connection for the Recuperative Heat Exchanger

Due to the concerns of fluid leakage along the connection of the heat exchanger a new design aspect was considered. This design continued the core concept of the helical screw joint, while also implementing the concept of creating a more resilient seal through the joining of two angled surfaces. This has the potential to improve the seal between two fluid regions and the exterior of the recuperative counterflow heat exchanger while allowing tolerances for potential inaccuracies for the printed surface. Due to the successful print of the previous screw design with a tolerance between 0.1 and 0.2mm, this requirement was continued for the next iteration of the helical screw joint.

The profile shown in Fig 3.32 (a) shows one of the five sections of the recuperative counterflow heat exchanger profile. One key improvement to the design can be seen with the addition of six additional surfaces surrounding both the fluid regions as well as the external surfaces of the design. The second improvement incorporates the concept of sealing two angled surfaces by including a two-degree incline to each of the concentrically design screw profiles. Fig 3.32 (b) depicts the entire five section recuperative counterflow heat exchanger profile used to sweep the complete design. This follows the same design principles as the previous iterations of the heat exchanger.

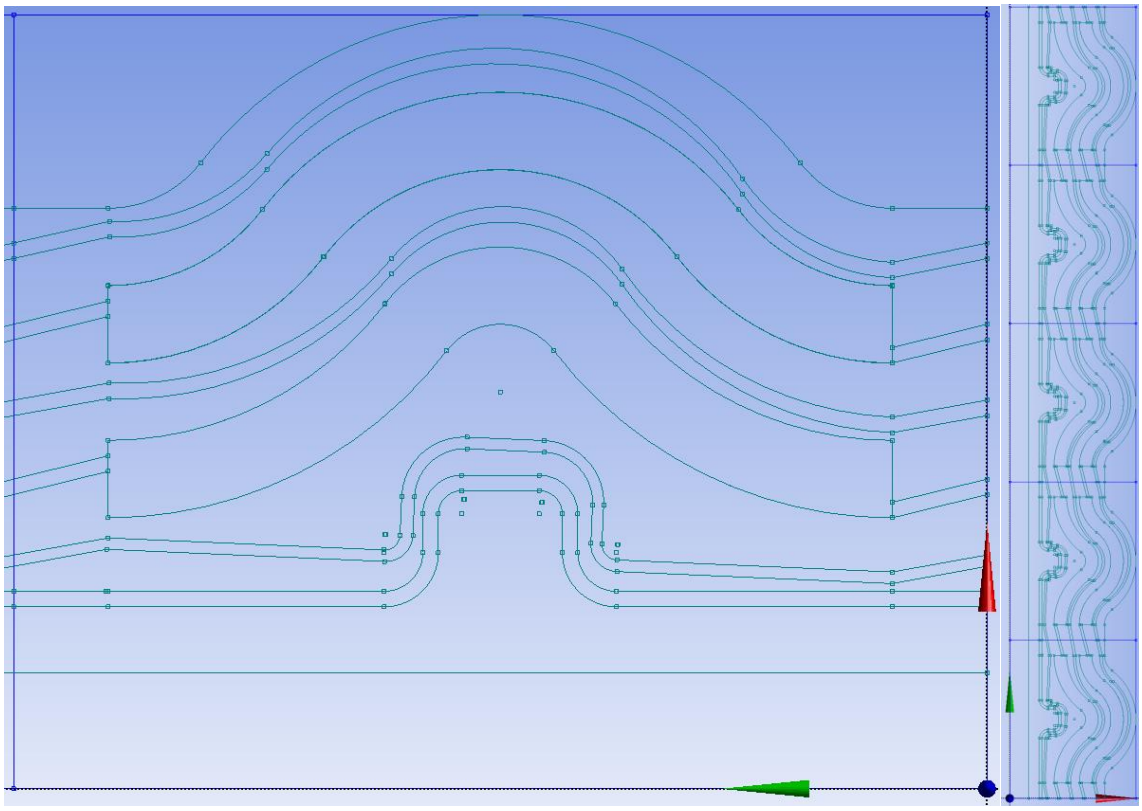

(a) *(b)*

Figure 3.32 Leak Resistant Recuperative Counterflow Helical Heat Exchanger Profile (a) a single section of the swept profile and (b) the full 2D profile of the swept surface

3.4.1 Profiles of the Leak Resistant Recuperative Heat Exchanger Connection Joint

To generate the six additional surfaces required to reduce the risk of fluid leakage, six separate profiles were designed. These separate each of the three existing solid boundaries of the recuperative heat exchanger, two for the external surface of the heat exchanger and one for the intermediate surface between the two fluid regions, into two distinct surfaces. Each pair of surfaces includes a tolerance set between 0.1 and 0.2mm and follows a two-degree inline and aim to seal the fluid regions along the screw connection. These pairs of surfaces are highlighted in each of the figures below. Fig 3.33 shows the outer pair of surfaces, used to restrict the flow of the outer fluid region and the external surface of the heat exchanger. Fig 3.33 (a) is the external

surface, aligning with the exterior of the cylinder with Fig 3.33 (b) highlighting the surface connecting to the outer fluid region. Each of the two surfaces will join separately to either the male or female connection piece.

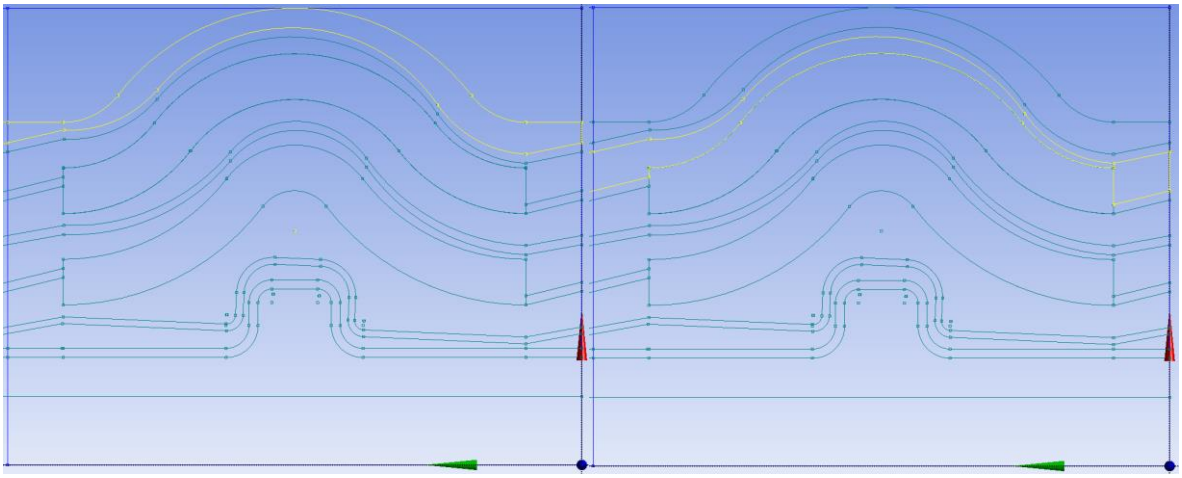

(a) ***(b)***

Figure 3.33 Outer Layer of the Leak Resistant Recuperative Counterflow Helical Heat Exchanger Profile (a) the profile to generate the external surface and (b) the profile to generate the outer surface of the outer fluid region

The next pair of surfaces depicted in Fig 3.34 are designed to reduce the flow between the two fluids, ensuring to separate each of the fluid entirely. Although both fluids are the same, due to the difference in temperate, flow between the two should be restricted. Fig 3.34 (a) accompanies the outer fluid region while Fig 3.34 (b) connects to the inner fluid region, following the same concentrically designed profile at a two-degree incline to the existing fluid region profile.

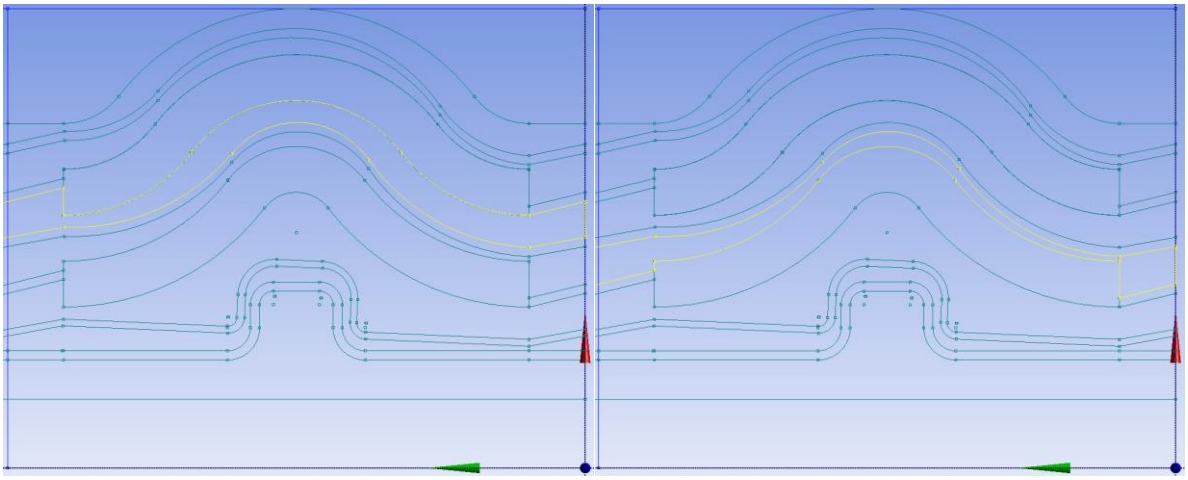

(a) ***(b)***

Figure 3.34 Internal Layer of the Leak Resistant Recuperative Counterflow Helical Heat Exchanger Profile (a) the profile to generate the inner surface of the outer fluid region and (b) the profile to generate the inner surface of the inner fluid region

The final pair of surfaces are shown in Fig 3.35 which separate the inner fluid region from the core screw connection. These surfaces are designed to reduce the risk of inner fluid leakage through the screw connection. Fig 3.35 (a) connects to the inner fluid region with Fig 3.34 (b) connecting to the screw joint. Due to the screw joint also being additively manufactured there is also a tolerance of 0.1 – 0.2 mm between the second profile and the screw joint profile.

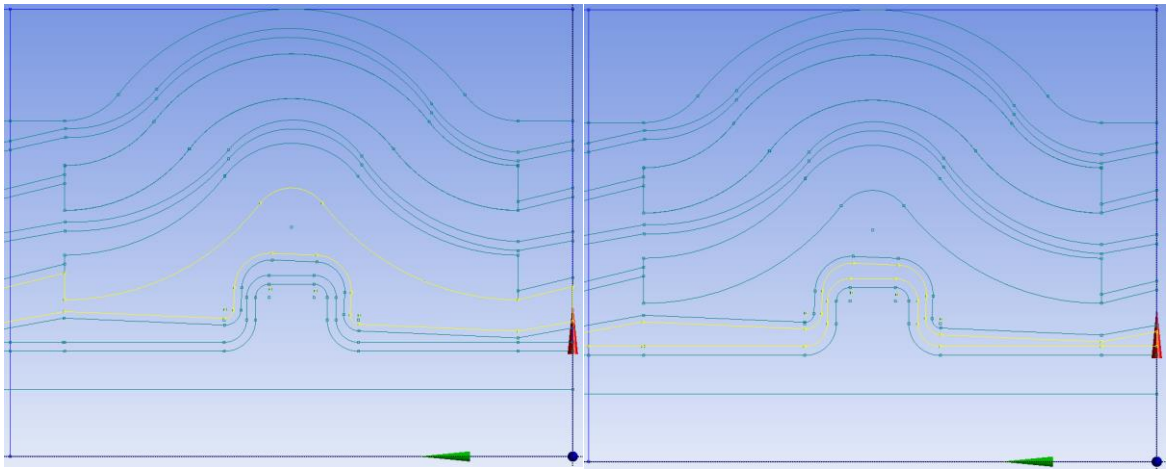

(a) ***(b)***

Figure 3.35 Inner Layer of the Leak Resistant Recuperative Counterflow Helical Heat Exchanger Profile (a) the profile to generate the outer surface of the inner fluid region and (b) the profile to generate the inner surface of the central helical screw joint

The external surface of the recuperative heat exchanger as well as the fluid regions shown in Fig 3.36 (a) and Fig 3.36 (b) respectively follow the same profile as previous iterations of both the heat exchanger and screw connection design. There is no tolerance between the fluid regions and their respective bounding pair of surfaces as the generated surface follows the fluid regions precisely. This also applies to the generation external surface as well the connection to the core screw design. Fig 3.37 (a) highlights the core screw connection, continued form the previous screw design iteration as well the 0.2mm boundary tolerance depicted in Fig 3.37 (b).

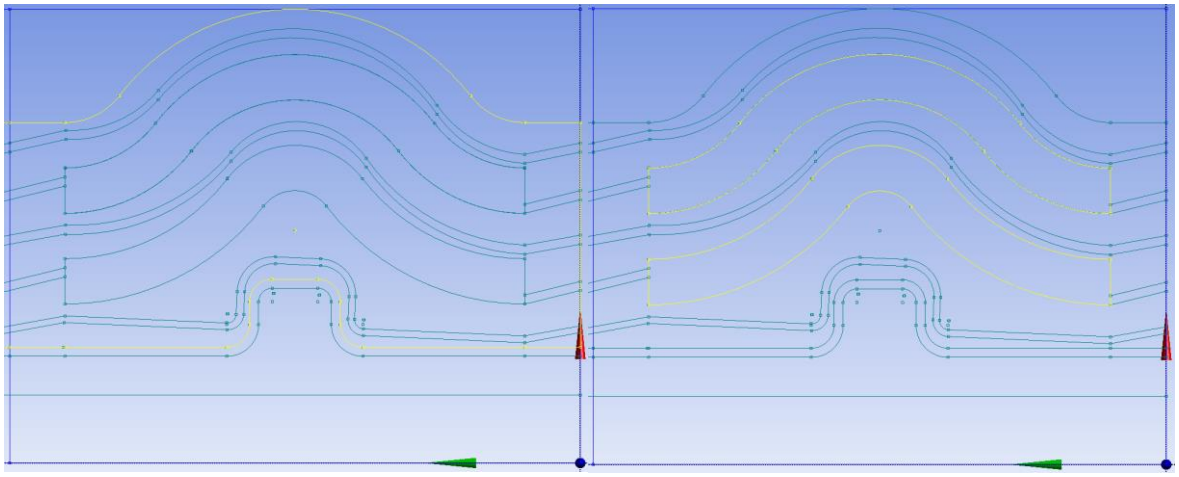

(a) *(b)*

Figure 3.36 Core Layer of the Leak Resistant Recuperative Counterflow Helical Heat Exchanger Profile (a) the profile to generate the exterior layer of the complete counterflow heat exchanger and (b) the profile to generate the two fluid regions for the complete counterflow heat exchanger

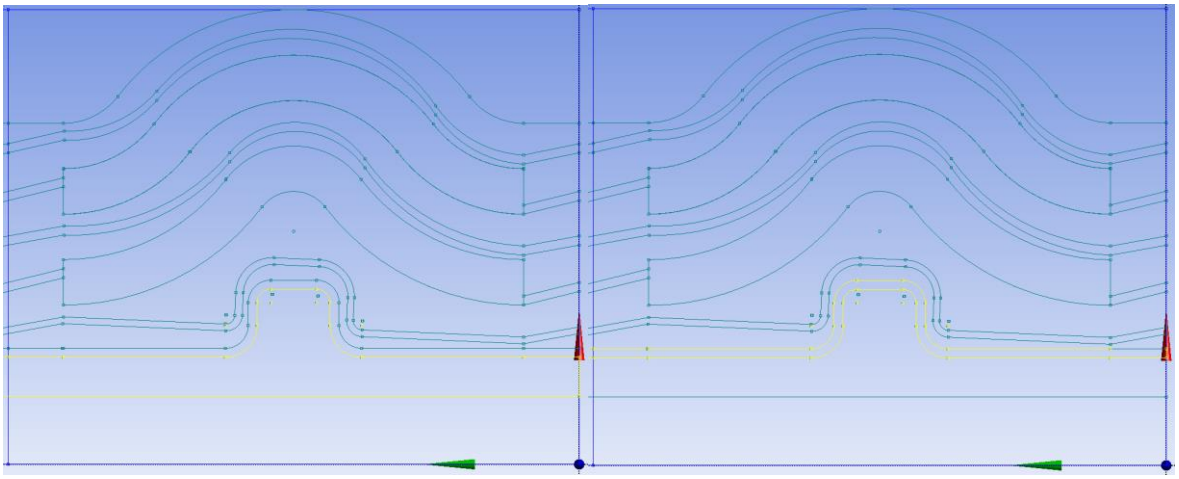

(a) *(b)*

Figure 3.37 Central Screw Joint of the Leak Resistant Recuperative Counterflow Helical Heat Exchanger Profile (a) the profile to external surface and (b) the profile to generate the tolerance between the external and internal surface of the helical screw joint

3.4.2 Swept Design of the Leak Resistant Recuperative Heat Exchanger

The generation of the additional six profiles into the final swept design follows a more involved process due to the layered extrusion process required to create cylindrical surfaces from a 2d profile swept along a central axis at a 45-degree angle. To achieve the desired screw joint generated at the top of the heat exchanger design a new approach was taken. Instead of immediately generating the required surface from the 2d profile as intermediate step is required, while includes generating a second 2d profile which can be used to immediately form a cylindrical surface without the extrusion requirement. This allows a more direct approach to be taken with the design of the six additional bounding surfaces, which is critical to reduce the risk of generation errors due to overlapping surfaces. Fig 3.38 shows the three swept surfaces corresponding to the female section of the screw. Fig 3.38 (a), Fig 3.38 (b) and 3.38 (c) are generated from the swept profiles of Fig 3.33 (a), 3.34 (a) and 3.35 (a) respectively. Following the same design Fig 3.39 depicts the swept surfaces corresponding to the male section of the screw with Fig 3.39 (a), Fig 3.39 (b) and 3.39 (c) are generated from the swept profiles of Fig 3.33 (b), 3.34 (b) and 3.35 (b) respectively. To ensure that all six surfaces align correctly with the desired tolerances and inclined surfaces, they are all generated together which is shown in Fig 3.4.9. Fig 3.40 (a) highlights that their tolerances set at 0.1-0.2 mm between the six surfaces are maintained while Fig 3.40 (b) shows the inclined plane from the swept profiles. Both figures are combined to form Fig 3.40 (c) which confirms that there are no overlapping surfaces and that all the tolerance requirements are satisfied.

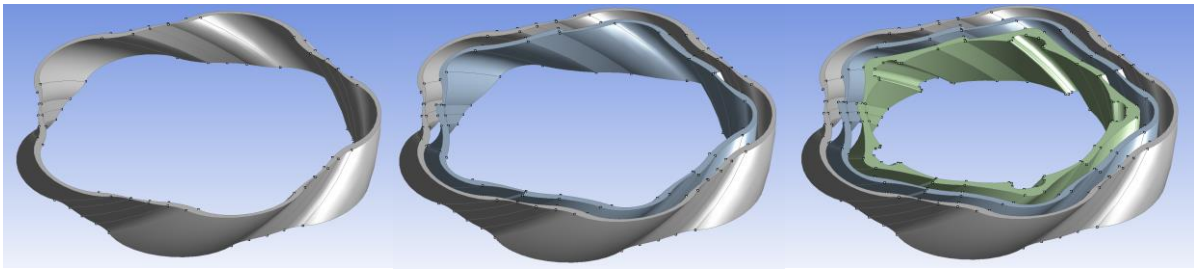

(a) *(b)* *(c)*

Figure 3.38 2D Swept Surface for the Female Screw Design (a) the swept surface corresponding to the external surface of the heat exchanger (b) the swept surface corresponding to the outer surface of the outer fluid region and (c) the swept surface corresponding to the outer surface of the inner fluid region

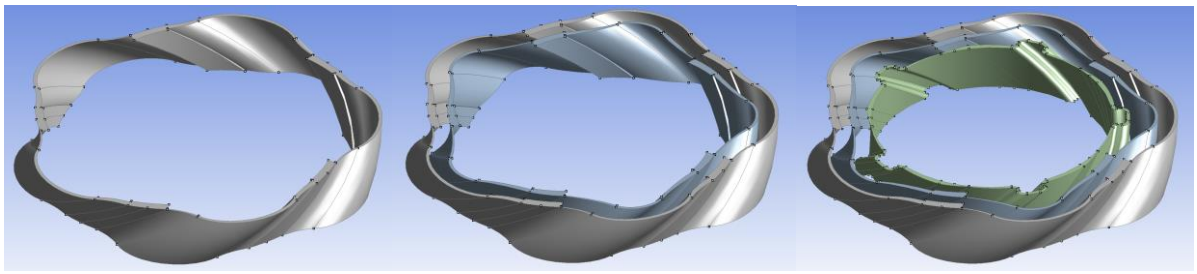

(a) *(b)* *(c)*

Figure 3.39 2D Swept Surface for the Male Screw Design (a) the swept surface corresponding to the inner surface of the outer fluid region (b) the swept surface corresponding to the inner surface of the inner fluid region and (c) the swept surface corresponding to the inner surface of the core screw joint

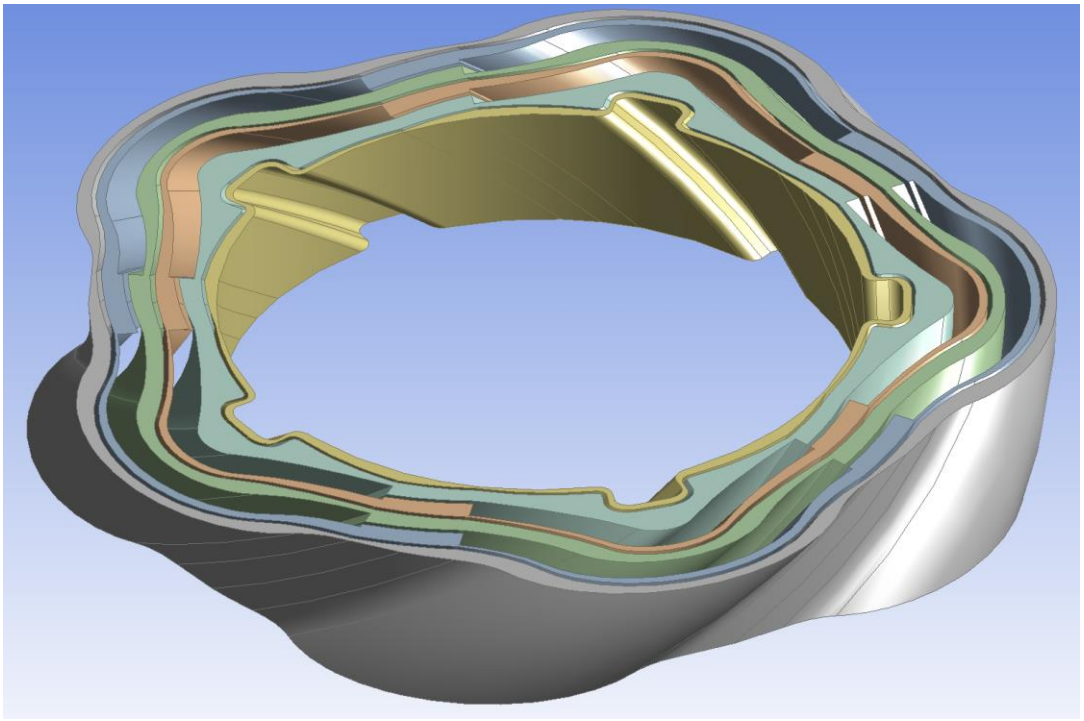

(a)

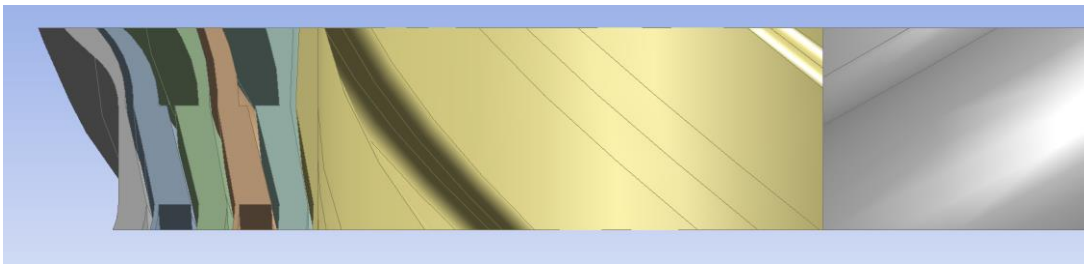

(b)

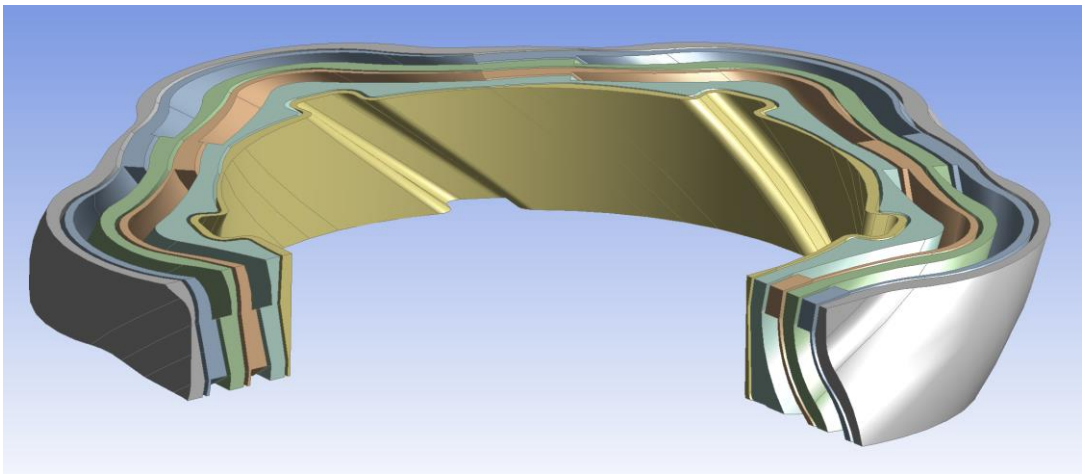

(c)

Figure 3.40 2D Swept Surface for the entire Leak Resistant Screw design (a) an isometric view of the six swept surfaces and (b) the sectioned view of the six profiles along the vertical axis and (c) the section isometric view of the six swept surfaces

3.4.3 Male and Female Recuperative Heat Exchanger Leak Resistant Connection

The six generate swept designs can now be used to generate the second set of 2d profiles required to form the screw connection on the heat exchanger design. The key concept that is utilised for the generation of the complex screw joint was that cutting geometries is more reliable than generating a new surface. This allows more complex geometries to be generated more reliably by building a base geometry first and the cutting certain sections from the base geometry to from the desired design. Following this the six 2d sections that were generated from the initial 2d swept deigns are used to cut sections from the base recuperative heat exchanger design. Fig 3.41 (a) shows the three profiles corresponding to the male screw section with Fig 3.41 (b) highlighting the three profiles associate with the female leak resistant screw. These sections are combined to cut the sections from the base design. Within DesignModeller, multiple sections can be cut simultaneously with the cut section being between the two outermost profiles. The next section is then not cut and this repeats itself for the number of given profiles. This allows the complete cut of multiple profiles to be executed simultaneously within a single function.

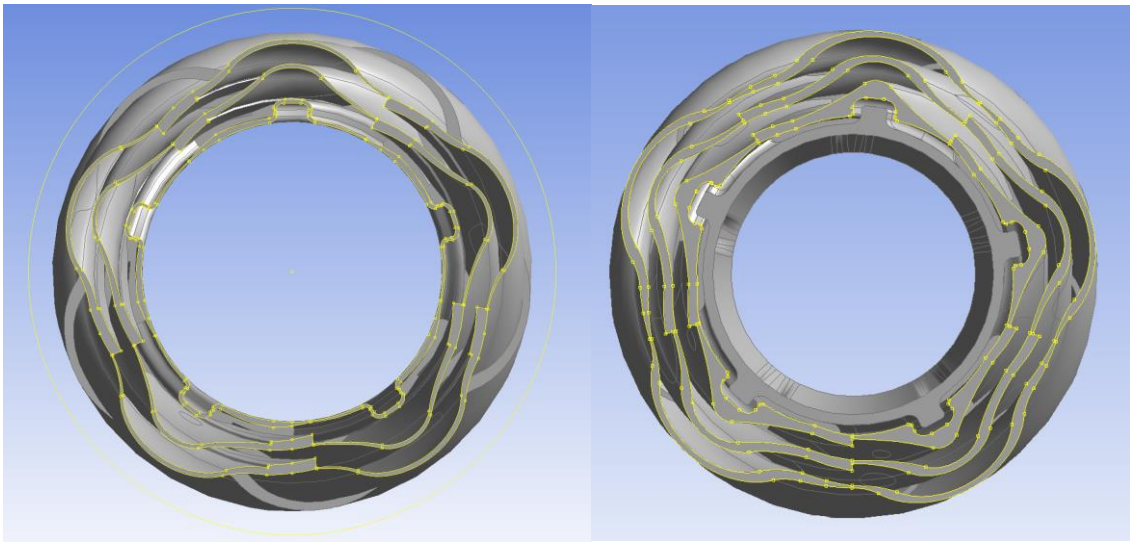

(a) ***(b)***

Figure 3.41 Leak Resistant Screw Section for the Counterflow Helical Heat Exchanger (a) the male screw connection and (b) the female screw connection including the core screw design

Applying the same generation methods as previously used in the generation of both the recuperative counterflow heat exchanger and the core screw design, the new leak resistant screw results in the geometries shown in Fig 3.4.11. The male section is depicted in Fig 3.42 (a) with Fig 3.42 (b) corresponding to the female section. The completed geometry with the corresponding fluid inlet and outlet connection at one end of the heat exchanger is shown in Fig 3.4.12. The male section depicted in Fig 3.43 (a) is used to screw on to the female section shown in Fig 3.43 (b). The opposite sides of the recuperative counterflow heat exchanger are shown Fig 3.44 with Fig 3.44 (a) showing the bottom section of the male geometry with Fig 3.44 (b) representing the merged fluid inlet and outlet junction.

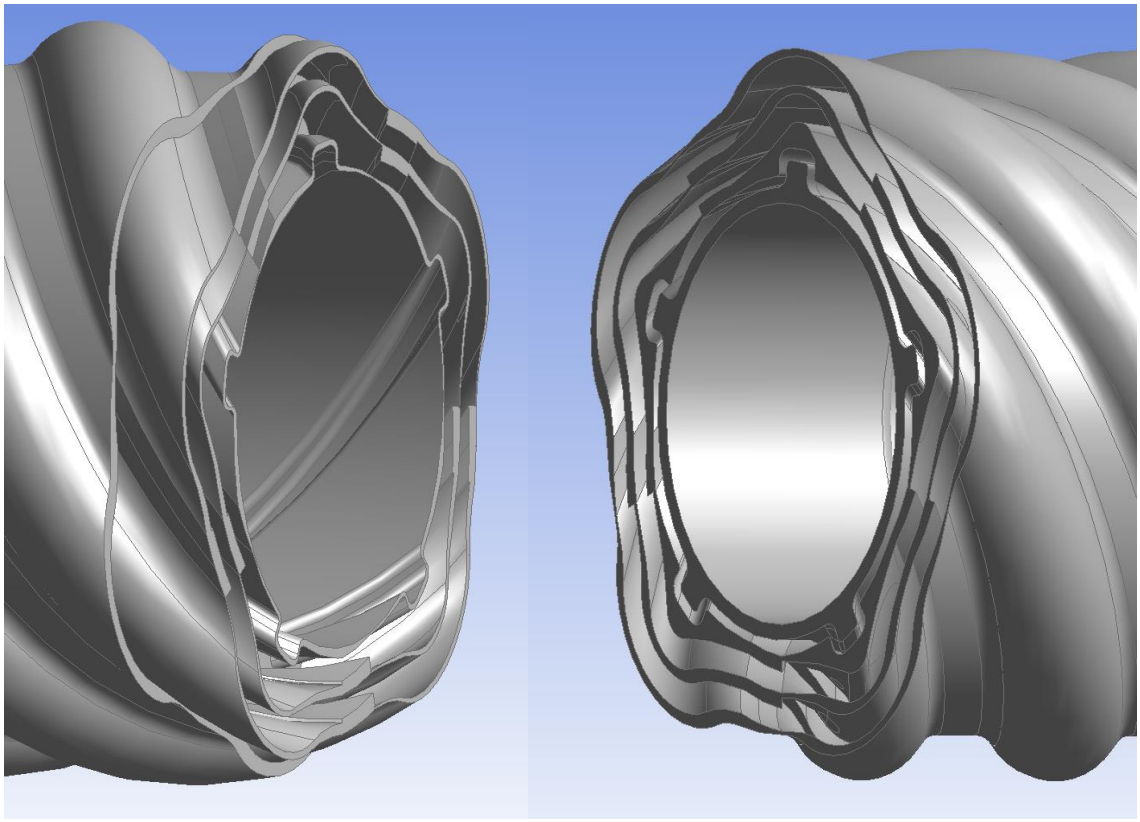

(a) *(b)*

Figure 3.42 Leak Resistant Screw for the Counterflow Helical Heat Exchanger (a) the male screw connection and (b) the female screw connection including the core screw design

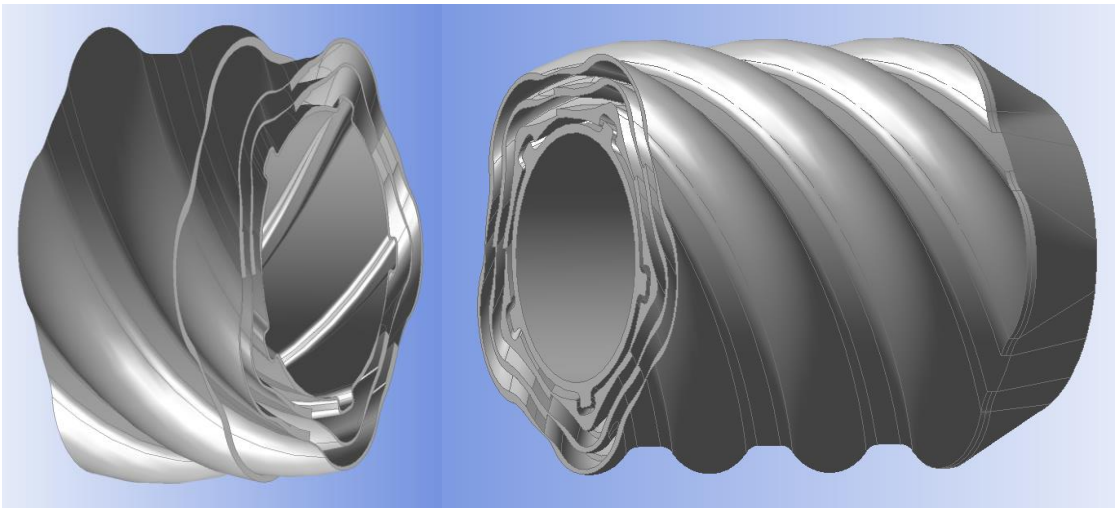

(a) *(b)*

Figure 3.43 Complete Leak Resistant Screw for the Counterflow Helical Heat Exchanger (a) the male screw connection and (b) the female screw connection including the core screw design

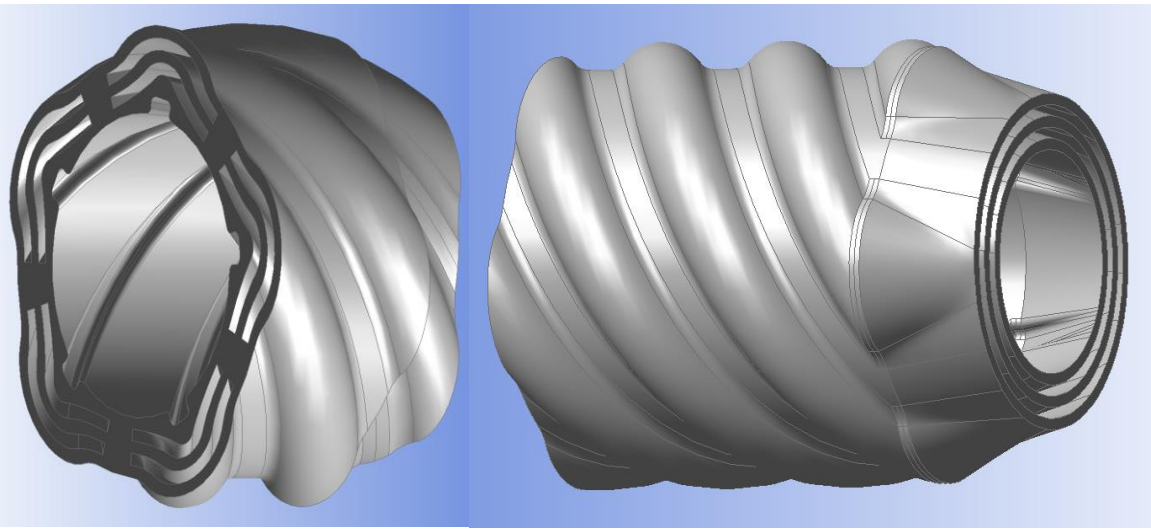

(a) ***(b)***

Figure 3.44 Complete outer section of the Leak Resistant Screw for the Counterflow Helical Heat Exchanger (a) the male screw connection and (b) the female screw connection including the core screw design

Chapter 4

Finite Volume discretisation and boundary conditions

4.1 Ansys Fluent

The design of the recuperative heat exchanger model with ANSYS Design Modeller transitioned smoothy to the use of ANSYS ® Fluent. Fluent was used for the finite volume discretisation and analysis of the various heat exchanger models designed as part of this work. The finite volume discretisation was the initial step within Fluent and shown selected within Fig 4.1. This window also allowed for the configuration of double decision as well as the computational resources available for the mesh and solving processes. The heat exchanger model was then defined as a watertight geometry and forming a linear sequence for the generation of the mesh represented in Fig 4.2. The import geometry function was used directly to import the model designed within ANSYS Design Modeller, with local sizing defined in mm, and configure the model within Fluent.

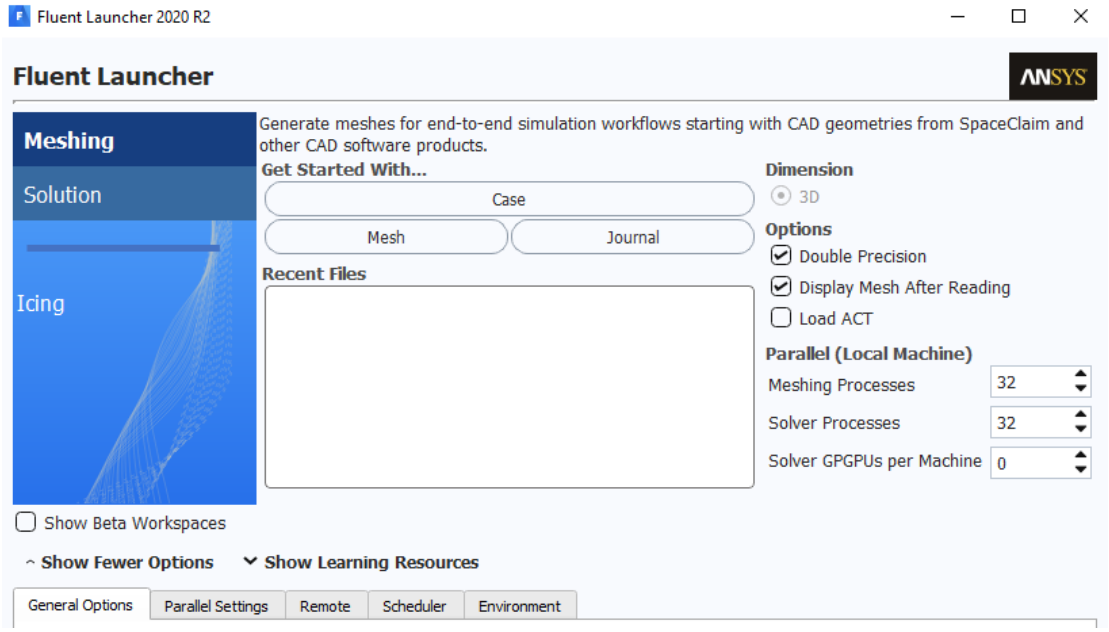

Figure 4.1 ANSYS Fluent Configuration Window

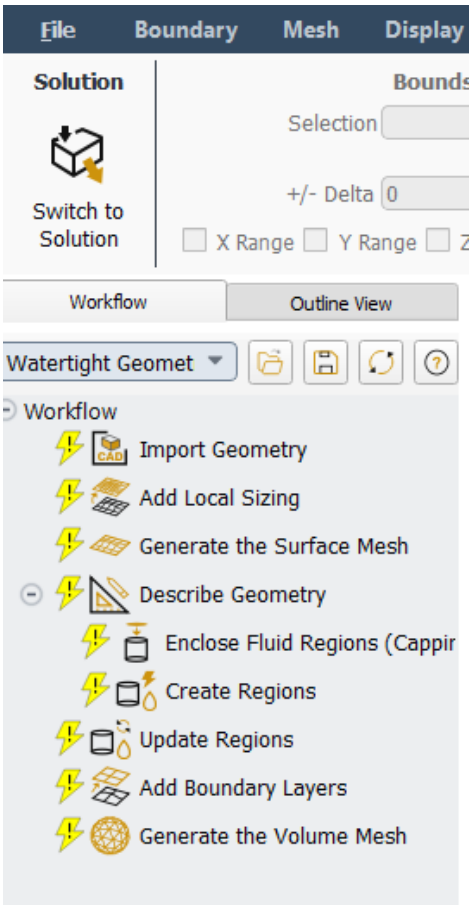

Figure 4.2 ANSYS Fluent Watertight Geometry Configuration

4.2 Volumetric Mesh

The first step was to generate a surface mesh for the model. The mesh parameters were set to utilise both curvature and proximity size functions and the resulting FE mesh as presented in Fig 4.3 (a) had 267,558 boundary nodes and 480,305 boundary faces. The key challenge was to identify and discretise the fluid regions. Two options were available to identify the two- inlet and outlet fluid domains: either singular or annular. This however was further limited by the ability of the generated surface mesh to segregate these regions into separate surfaces which can be individually selected. To achieve this, multiple design iterations were required to specify the fluid inlet and outlet regions. Key requirements included aligning both inlet and outlet along a single 2D plane to select the annular regions together with defining separate solid surfaces for each of the fluid boundaries. The successfully defined and selected boundaries for each of the fluid domains are depicted in Fig 4.2 (b).

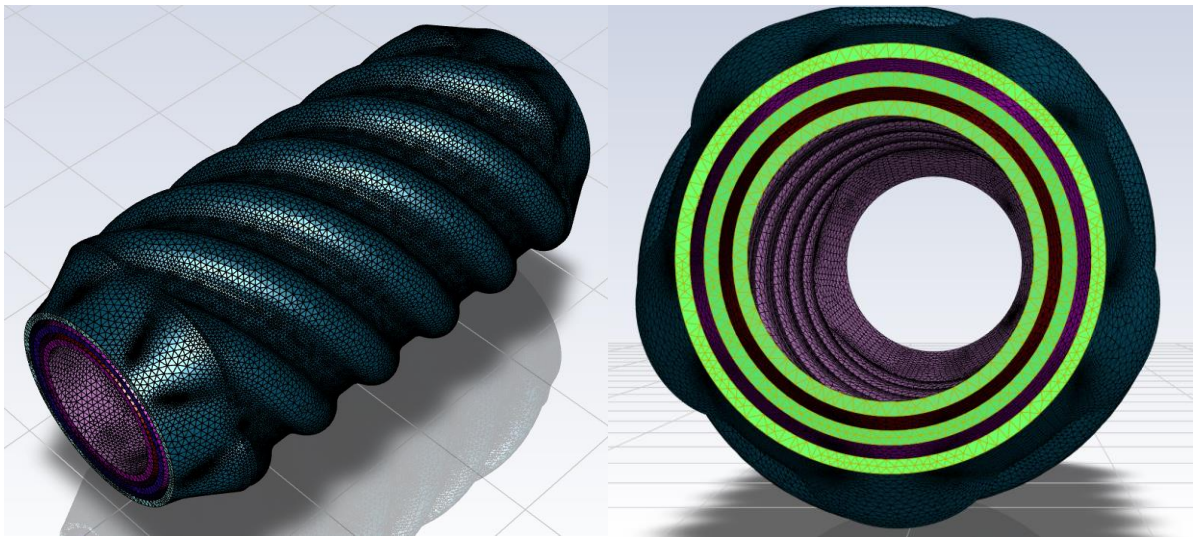

(a) ***(b)***

Figure 4.3 Finite Volume discretisation of the Helical Heat Exchanger (a) the solid structure and (b) the separate fluid boundary region

The later simulations utilise a second domain surrounding the helical counter flow pathways to define a fluid region around the heat exchanger and simulate losses to the environment. The next step was to discretise both the 3D solid and fluid domains of the heat exchanger with volume elements. The fluid regions were defined with a counter flow configuration with velocity inlet and pressures outlet conditions, using the four inlet and outlet surfaces and the solid body to define the fluid domain boundaries. Fig. 4.4 presents the two counterflow fluid regions, showing the five separate helical fluid pathways for each region.

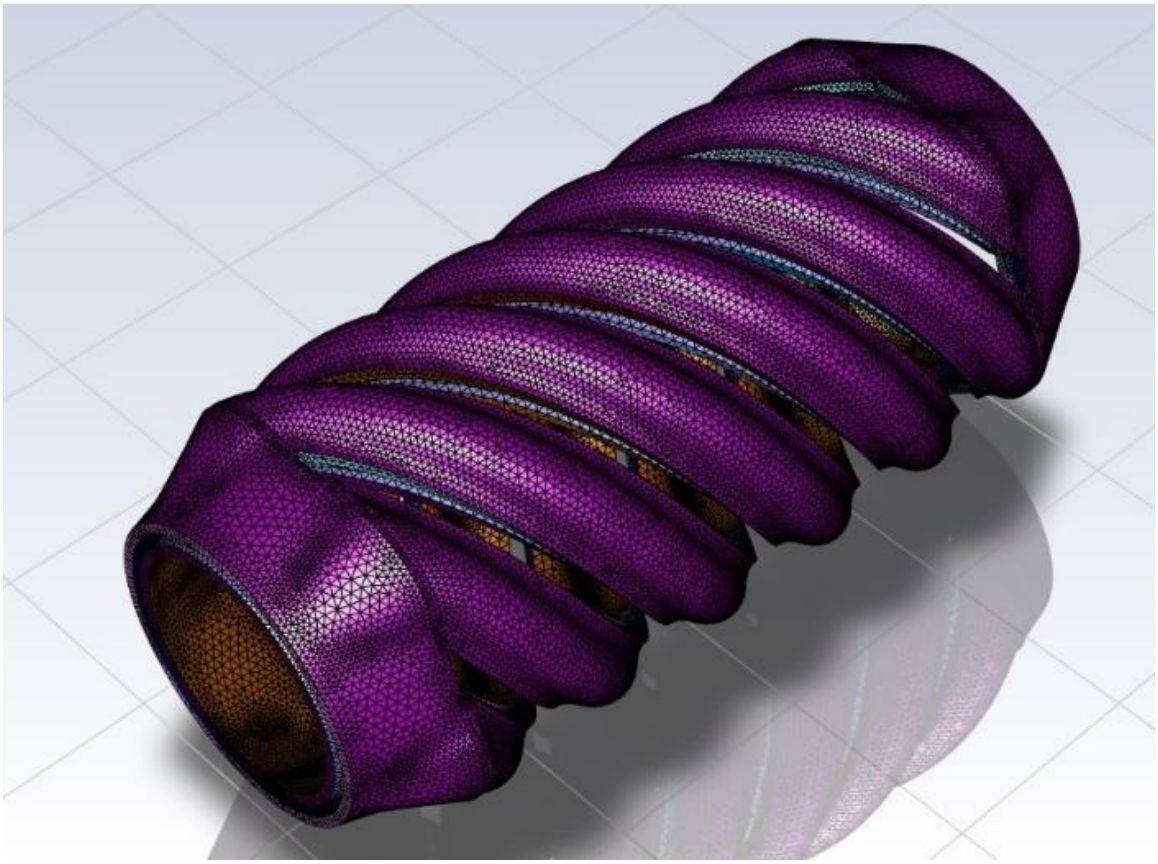

Figure 4.4 Finite Volume discretisation of the fluid flow pathways

4.3 Boundary Layers

Three boundary layers were added between the solid and fluid regions applying the smooth transition offset method, marked by the rectangular element regions presented in Figure 4.5 (a) alongside the generated polhedra for the solid and fluid regions. Finally, the volumes mesh was generated and filled wi70olyhedraldra as seen in Figure 4.5 (b), generating the two fluid and one solid domains, with a total cell count of 690,708. For comparative evaluation, a variation of mesh for the fluid domain was considered by removing the boundary layers and filling the whole region with tetrahedral elements as depicted in Figure 4.5 (c), with a modified maximum cell length limit of 0.25 and 1 for the fluid and solid regions respectively. The growth rate was

increased to 2 to further increase the accuracy of the mesh. A close-up view of the discretisation with the boundary layer is presented in Figure 4.5 (d) which uses the same maximum cell length and growth rate settings. The total number of elements in these two meshes were 1444476 and 1110771 respectively. For the sake of clarity, the fluid which is cooled is flowing in the inner channel and the other fluid which is used to cool is flowing in the outer channel. The key temperatures will be identified as the inlet and outlet temperatures of the inner and outer fluid channels in the subsequent discussions.

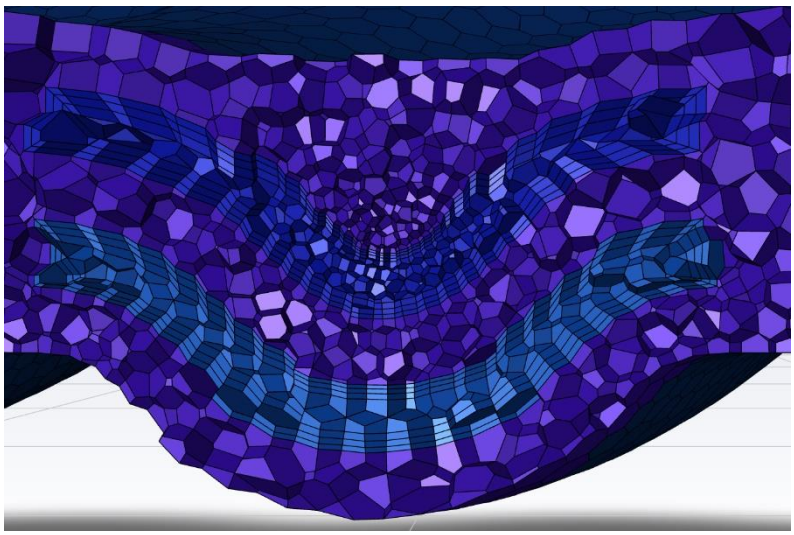

(a)

(b)

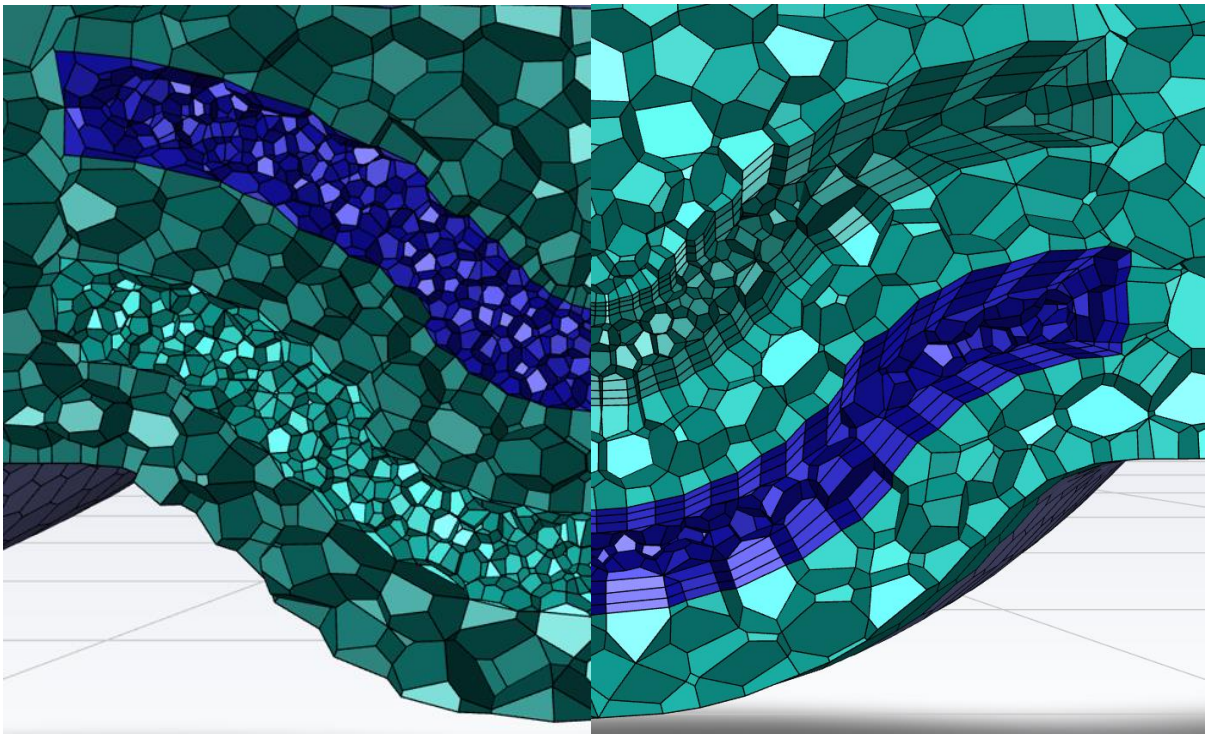

(c) ***(d)***

Figure 4.5 Volume Mesh for the Spiral Heat Exchanger (a) view of a single counterflow fluid region and (b) the sectioned view of the generate volume mesh and (c) Refined Mesh without Boundary Layers and (d) Refined Mesh with 3 Boundary Layers

4.4 Boundary Conditions

Two critical requirements were set for this model for achieving an effective cryogenic heat exchanger configuration. First, for the efficient exchange of heat between the two fluids, heat must be lost evenly across the length of the heat exchanger. If the heat transfer rate is too high, the temperatures of both fluids quickly converge into a mean temperature at which the fluids in both channels will stabilise. It has been a known fact that materials like Stainless steels exhibit very low thermal conductivities at low temperatures. In order to avoid drastic heat flow across the fluid and solid boundaries, a very low thermal conductivity value, almost representative of an insulating material has been used for the solid domain in this study. To meet the cryogenic temperatures within a single phase, helium was chosen as the fluid medium. Constant values

presented in the Fluid Database were used to run the simulations with density set at 0.1625 kg/m^3, thermal conductivity as 0.152 W/mK and viscosity at 1.99 * 10^{-5} kg/ms. The hot inlet temperature was taken to be 300 K and for the best efficiency of the heat exchanger, this should drop to 20 K at the cold outlet, which is the cold inlet temperature of the fluid in the other column of the counterflow heat exchanger. To accommodate this, a slight volume reduction at 12.6% was provided to the inner fluid channel which resulted in total fluid volumes 8.265 * 10^{-6} m^2 and 7.226 * 10^{-6} m^2 respectively for the outer and the inner fluid columns. With these base boundary conditions set, the simulations under various model configuration were conducted.

The SST K-Omega Viscous model was chosen for the analysis combining both the Wilcox k-omega and the k-epsilon models. To ensure the appropriate model is used, blending function is used which activates either the Wilcox or k-epsilon model depending on proximity to a wall or free stream respectively. Figure 4.6 shows the spiral heat exchanger model with arrows for inlets and outlets plus the wall boundaries surrounding the fluid flow paths. As shown in Figure 4.6, the two flow channels had opposing inlet and outlet boundaries following a counterflow heat exchanger design. The inlets were set to constant velocity and temperature, with the outlets at a constant pressure. The end walls of the solid were set to the end temperatures of 20K and 300K and the side walls were adiabatic to simulate vacuum insulation. With the second case being a simulated with an air domain outside the heat exchanger. Water was used rather than helium for the ambient case with the two inlets being set to 290K and 370K respectively. The air domain’s boundary walls were 300K to simulate ambient.

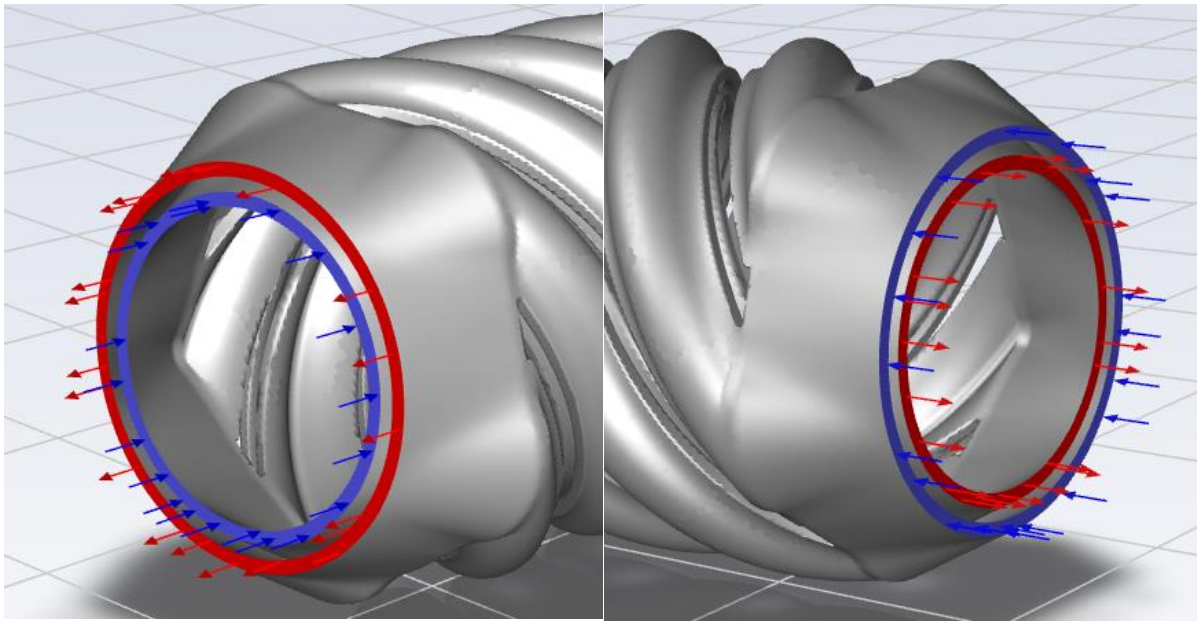

(a) ***(b)***

Fig. 4.6 The Inlets and Outlets to the Spiral Heat Exchanger with (a) showing the outer outlet (red) and inner inlet (blue) and (b) showing the outer inlet (blue) and inner inlet (red))

4.5 Justification for the selection of key parameters for the CFD analyses

The base volumetric mesh density was set to the recommended defaults provided by ANSYS ® Fluent. Once the geometry was successfully meshed, the cross section was inspected to review the density of the polyhedral that were generated. The mesh was correctly generating a higher density mesh in the critical regions while maintaining a reasonable number of overall elements to maintain computationally viable with the hardware that was available. To match the element sizing in the fluid regions of the three-boundary layer variant, shown in Fig 4.5 (d), with the 0-boundary layer mesh variant, shown in Fig 4.5 (c), the mesh density of the fluid regions in the 0-boundary layer mesh was increased. The number of elements in the fluid region were roughly doubled to produce approximately double the number of elements within the fluid

regions. The comparison between the use of boundary layers was the first analysis that was conducted in the subsequent section in combination with the inlet velocities used for the fluid regions.

4.6 Low Thermal Conductivity Material

The key requirement for the recuperative cryogenic heat exchanger design was to equalise the temperatures at either end of the heat exchanger. The inlet temperature of one liquid would ideally be identical to the outlet temperature of the other liquid at the same end of the heat exchanger. This was due to the loop of transformation from a cryogenic fluid to a room temperature fluid, through a warm pump and then back to a cryogenic fluid. The means of achieving this transformations loop set the requirement for controlled heat flow from the inlet to the outlet. Rather than a pure focus on heat loss, as is typical with many heat exchanger designs, the focus was concentrated on efficient and controlled thermal management. Following this, a high thermally conductive material would lead to a heat transfer that is too high where both fluids would quickly converge into a mean temperature. This would achieve neither a cryogenic nor room temperature outlet as both outlets would be in the middle. Instead, the use of a low thermally conductive material was proposed, which would control the heat flow from the inlet to the outlet. This would enable both ends of the heat exchanger to achieve the inlet temperatures at either ends of the heat exchanger. This would enable the two outlets to achieve the desired cryogenic and room temperatures.

Chapter 5

Results and Discussion

5.1 The velocity of flow

The flow rate of the fluid is a critical parameter that needed to be defined as a base line for the simulations presented. The role of velocity of the fluids was estimated by means of a repeated simulation runs with the velocity varied over a range from 0.01 to 1 m/s. Fig. 5.1 is a depiction of the role of the velocity of the fluid flow on the temperature at the cold outlet end. The simulations showed a significant variation in the outlet temperatures as the fluid flow velocity was increased from 0.01 to 1 m/s. Both with and without boundary layer cases showed similar results where the mean cold outlet temperature gradually decreased with increasing velocity, attaining a minimum at around 0.025 m/s and then increasing subsequently. The convective and conductive heat flow conditions across the fluid and the solid media were affected by the fluid flow velocity, with better heat exchange at lower velocities due to the more time available for the radial heat transfer. This combined with a slightly reduced inner channel volume while maintaining equal fluid inlet velocities enabled the 300 K fluid inlet to be reduced to 25 K at an ideal velocity of 0.25 m/s, where the efficiency of the heat exchanger reached 98%. The peak efficiencies occurring at 0.25 m/s can be

primarily attributed to a maximum being found between the time for heat transfer to occur and the temperature equalisation of both fluids at very low velocities. The model with no boundary layers predicted slightly lower temperatures at all the velocity levels, perhaps due to the reduced fluid volume within each channel. Considering that both the models predicted similar temperature results, the three-boundary layer approach as recommended by ANSYS ® Fluent was used for all subsequent simulations. Additionally, the 0.25 m/s though proved to be an optimum velocity, the 1 m/s condition was employed in subsequent simulations so as to clearly capture the thermal responses to the design variables of the heat exchanger.

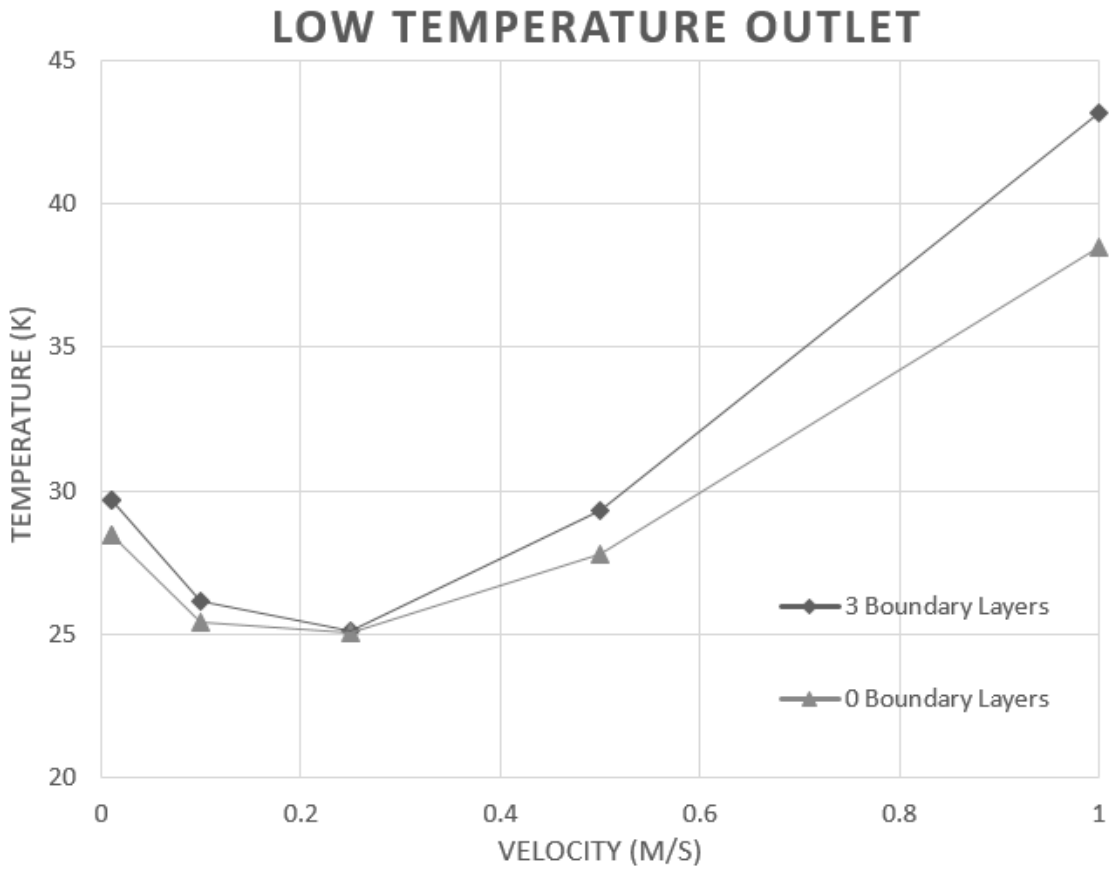

Figure. 5.1 The role of the velocity of fluid flow on the average temperature of the cold outlet end.

5.2 Thermal Short-Circuits

Concerns regarding the potential for thermal short circuiting to occur and negatively influence the heat exchanger performance led to the design of a second model shown in Fig. 5.2 (a), including a 1 mm gap along the helical path to ensure no conduction directly along the direction of the longitudinal axis. Fig 5.2 (b) highlights the original cross section of the two fluid regions, while Fig 5.2 (c) is representing the new cross section geometry. The inlet and outlet conditions are kept the same as with the original model. A comparative evaluation of the two models is done considering both insulating and highly conducting material options for the solid body domains of the structures. With the thermal and fluid velocity boundary conditions remaining the same as discussed above, the steady state temperature distributions obtained with the two models, considering an insulating solid medium are presented in Fig. 5.3 (a) to (d). The thermal distribution along the cross section of the heat exchanger shown in Fig 5.3 (a) and (b) highlight a indicate that the temperature distribution is very similar in both models. The comparison between the hot fluid outlets, marked in red in Fig 5.3 (c) and (d) reinforces this conclusion with a similar distribution and a near identical mean temperature. The same distribution is also present for the cold fluid outlets, marked in green in Fig 5.3 (c) and (d). The ‘bot’, and ‘top’ labels refer to either ends of the heat exchanger while the inner and outer descriptor refers to the location of the fluid volume in proximity to the centre of the heat exchanger. The x position represents the diameter of the heat exchanger inlet and outlets, highlighting the slight diameter increase for the outer fluid regions compared to the inner fluid region.

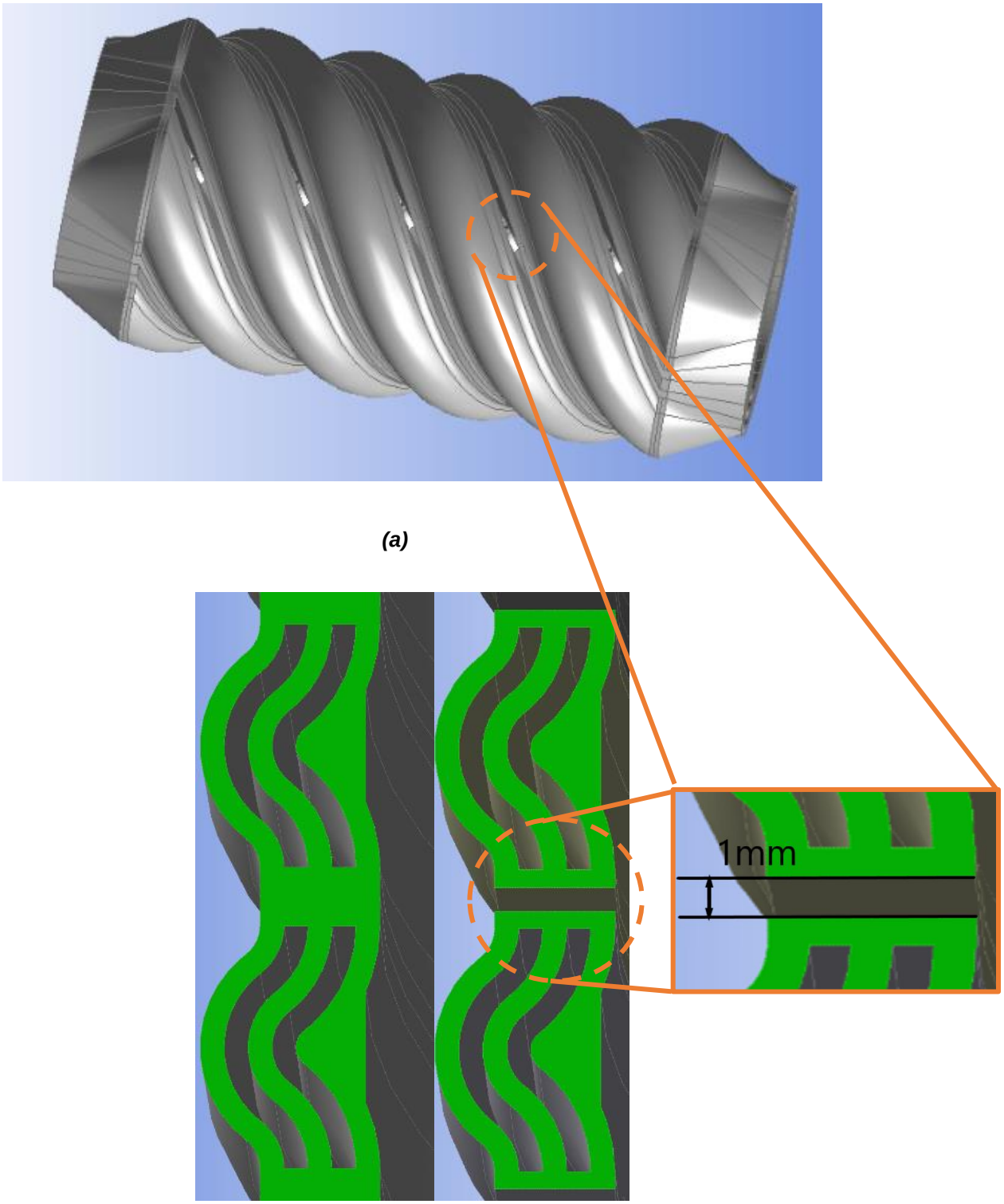

(a)

(b) *(c)*

Figure 5.2 The second model concept with a 1 mm gap, designed to reduce the potential for thermal short circuits with (a) representing the complete model and (b) two fluid regions of the original geometry and (c) two fluid regions of the new non-thermal short-circuited model

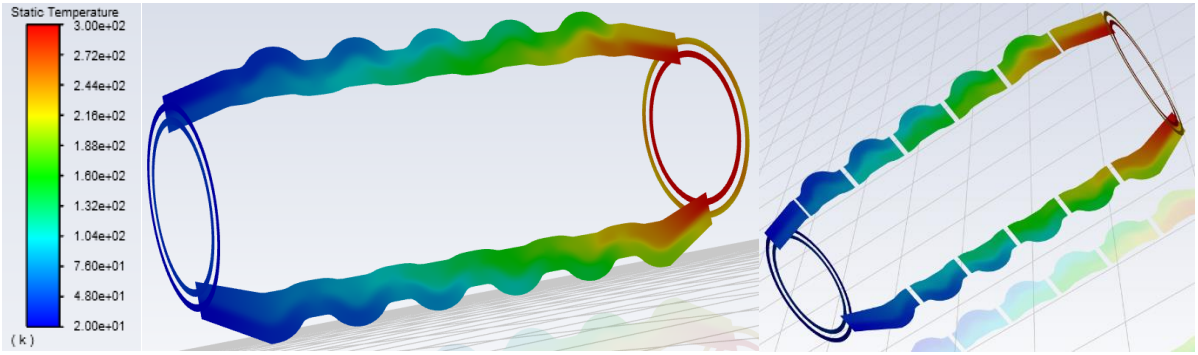

(a) *(b)*

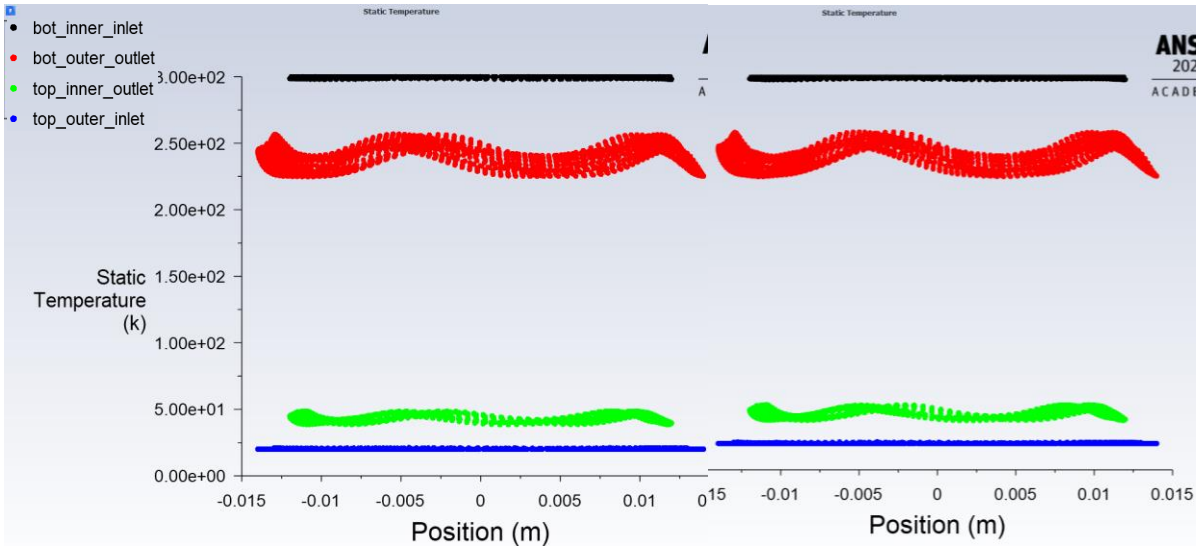

(c) *(d)*

Figure 5.3 Effects of thermal short-circuiting temperature distribution at the mid-sections of (a) the standard short-circuited heat exchanger and (b) the reduced short-circuit model, and (c) and (d) temperature distribution at the inlet and outlet for the two models in the same order

Next, the possibility of thermal short-circuiting along the axial direction of the original model was evaluated against the same two models but using a highly conducting material for the solid medium. Aluminium alloy with thermal conductivity at 202.4 W/mK was used as the material option for the solid structure of the heat exchanger and the analyses was conducted with the two models with exactly the same conditions as discussed above. The use of a high thermal conductivity material would amplify the

effects of thermal short circuits, which would make a temperature difference between the outlets of the two models distinct. The temperature distribution results at different locations, as obtained with the original and modified models, are presented in Fig. 5.4 (a) and (b) respectively. A wide variation may be noted in these results as compared to the results in Fig 5.2.2, as the highly conducting inter-fluid solid walls lead to rapid heat exchange between the two streams and homogenising of the temperature profiles at the average levels. However, a comparison of the temperature profiles in Fig 5.4 (a) and (b), specifically the cold outlet temperature, marked in green, indicate some variation in the temperature profiles of the two fluids at their respective outlets. The difference between the hot outlets, marked in red is also visible, although smaller compared the cold outlet. To further elucidate the effects of thermal short circuiting, the same analyses were repeated with water as the flowing medium in the channels and the hot and cold entry temperatures at 360 K and 300 K respectively. The results as presented in Fig. 5.5 (a) and (b) show a large variation in the temperature along the two outlets of 20 degrees between the maximum and minimum temperatures of both the hot and cold outlets. This effect is amplified as the overall temperature difference between the two inlets was only 60 degrees, which shows the variation at a third of the overall temperature delta. However, comparing the two cold outlet distributions, marked in red and the two hot outlet distributions, marked in green, show no significant differences between the two models. From the results of Fig 5.3 and 5.2.4, it may be clearly stated that the thermal short-circuiting effects were present with some specific conditions but were negligible in most cases. Hence, the original model, with no gaps between the helical pathways, was used in the subsequent analyses as it further reduces the additive manufacturing complications.

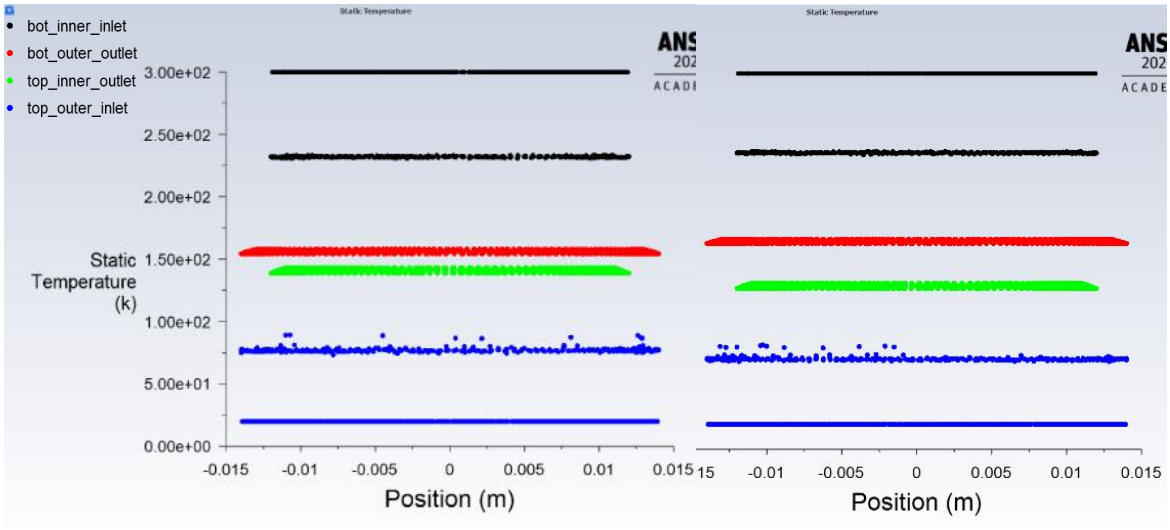

(a) ***(b)***

Figure 5.4 Temperature distribution at different locations in (a) the original short-circuited model and (b) the modified model with no short-circuiting using a highly conducting metal for the solid support structures of the spiral heat exchanger

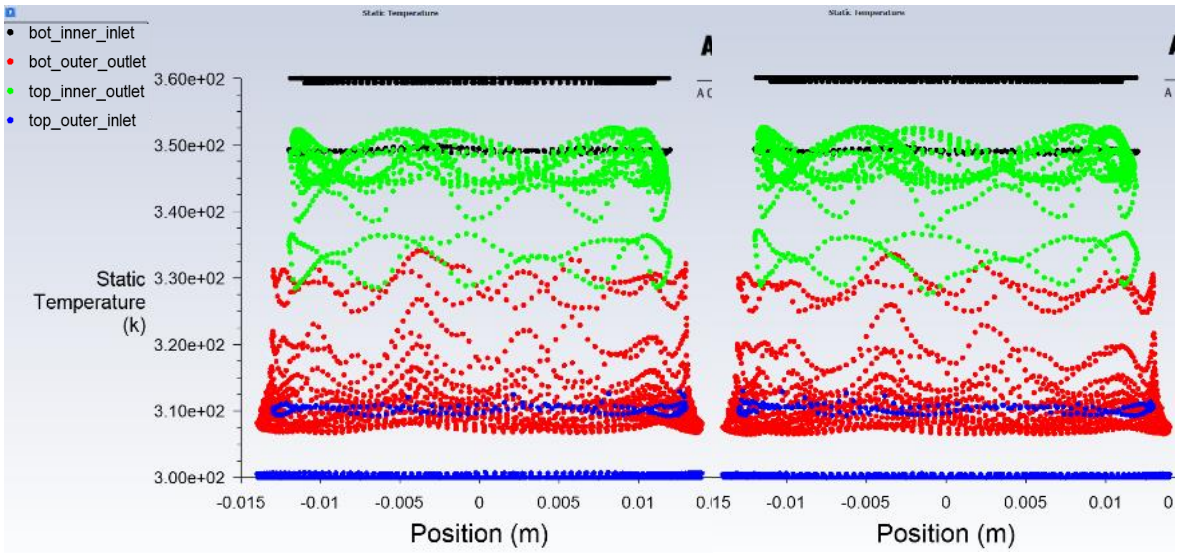

(a) ***(b)***

Figure 5.5 Temperature distribution at different locations in (a) the original short-circuited model and (b) the modified model with no short-circuiting using a highly conducting metal for the solid support structures of the spiral heat exchanger and with water as the fluid at 360 ^{0}K and 300 ^{0}K at the entry points of the two flow channels

5.3 Ambient Conditions

Now some attention is paid to evaluate the effect of the surrounding medium on the performance of the spiral helical heat exchanger. For these simulations, an exterior cylinder was added around the model as shown in Fig 5.6 (a), within which the atmospheric conditions surrounding the heat exchanger could be included. Three separate sets of conditions as listed in Table 5.1 were used to simulate different scenarios relevant to the application of the heat exchanger. The thermal simulation results for the case with the conditions in the first column of Table 2, as presented in Fig 15 (b), represents the minimal effect with the presence of the surrounding vacuum. This is to be expected, with negligible heat transfer seen to the exterior of the recuperative heat exchanger.

Table 5.1 Parameters for numerical simulation with the ambient conditions

	Cryogenic heat exchange in atmospheric air	**Hot water cooling in atmospheric air**
Solid structural material	Insulator	Stainless Steel
Fluid medium	Helium	Water
Temperature Range	20-300 K	290 – 370 K
Surrounding medium	Vacuum at 300 K	Air at 300 K

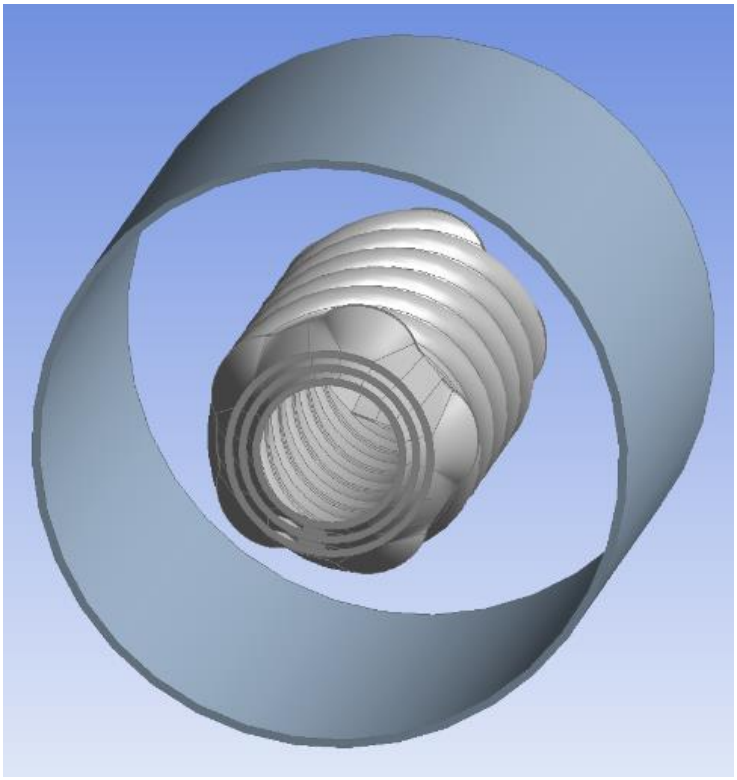

(a)

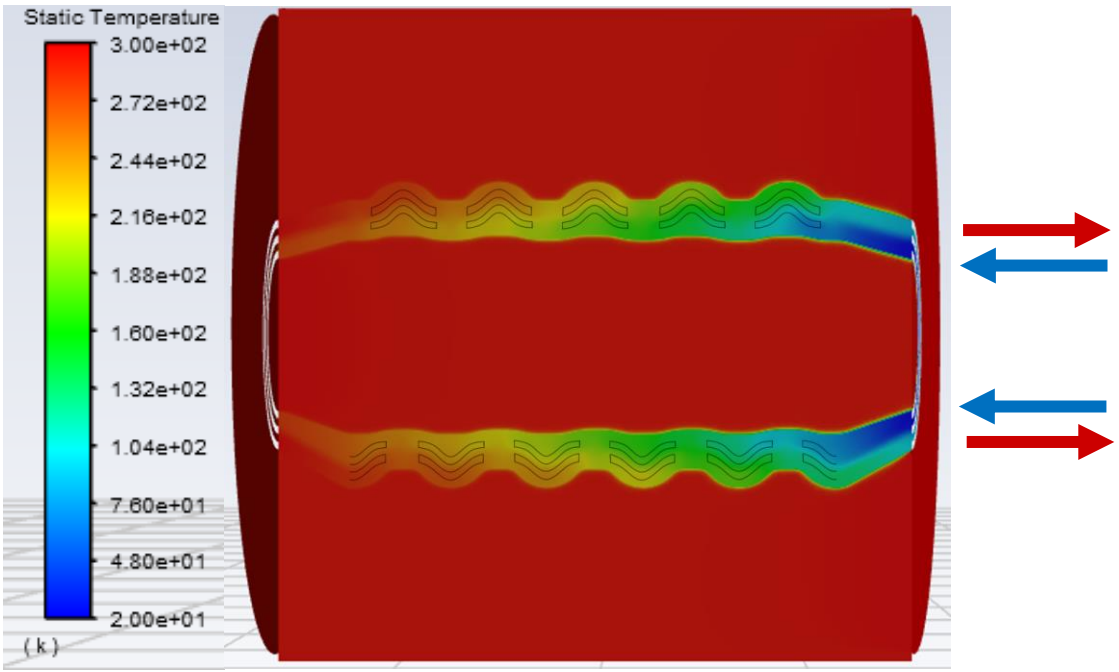

(b)

Figure 5.6 Simulation of the ambient conditions (a) the cylindrical enclosure and temperature profiles for the cryogenic cooling in (b) vacuum as surrounding media

5.4 Simulations for later experimental validation

The experimental validation of the results presented based on the numerical simulation could not be completed as yet and will be undertaken as the continuation of this work in the next stages. However, the numerical simulation trials were undertaken with the virtual models and the conditions suitable for such an experimental validation. Stainless steel 316L as the laser melted material for the solid phase structure and water as the fluid medium at inlet temperatures 290 K and 360 K and air at 290 K as the surrounding medium within the cylindrical enclosure are the critical conditions for the numerical experiments. Considering the limitations on the maximum height of samples that can be produced efficiently using the selective laser melting process, it was decided that the spiral heat exchangers are constructed with a maximum length of 62.83 mm. However, the heat transfer processes may not be achieved fully within this short span of interactions between the two fluids. Modelling natural convection with a steady-state calculation requires a constant density to be specified. As there are large temperature differences in the domain, this approach is not valid. For this case a transient approach would need to be considered to accurately model natural convection. Due to this, the steady-state calculations depicted in the results below do not consider convection.

The temperature distribution profiles presented in Fig. 5.7 (a) for the spiral heat exchanger of one unit length clearly demonstrate this as the heat transfer across the two fluid zones is results in a homogenised temperature levels in both zones along the short axial distance. Also, a substantial heat loss into the surrounding air may be

noticed in the temperature profiles of the case in Fig 5.7 (a). For the temperature differences between the two fluids at their respective inlets and the velocity of flow condition used the length of the heat exchanger needs to be increased so as to provide sufficient time for the heat exchange to take place and achieve the objective of cooling the hot liquid down to the room temperature level at the exit at the other end. This is evaluated by considering the numerical simulation tests with longer heat exchangers with two (Fig 5.4.1(b)) and four (Fig 5.7 (c)) units. While the temperature loss along the axial length of the hot fluid significantly improved in Fig 5.4.1(b) as compared to Fig 5.4.1(a), the model with four units joined together has achieved almost 90% of the objective of heating the water at 360 K down to 290 K. The heat loss to the surrounding air is still considerable, but manageable and more importantly, another fluid zone around the current two-fluid model will avoid this heat loss altogether, if necessary. The spiral heat exchanger model of four units is the most ideal within the three cases analysed, to fabricate and conduct experimental validation of the current numerical results using water as the medium, entering the heat exchanger zones at two different temperatures at the two inlets.

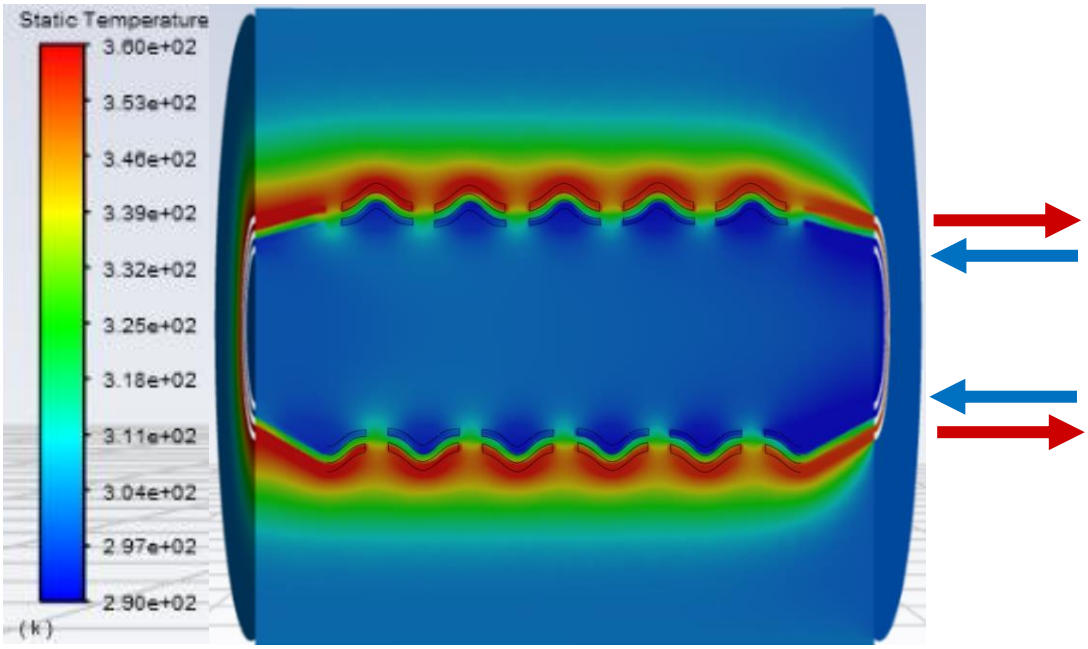

(a)

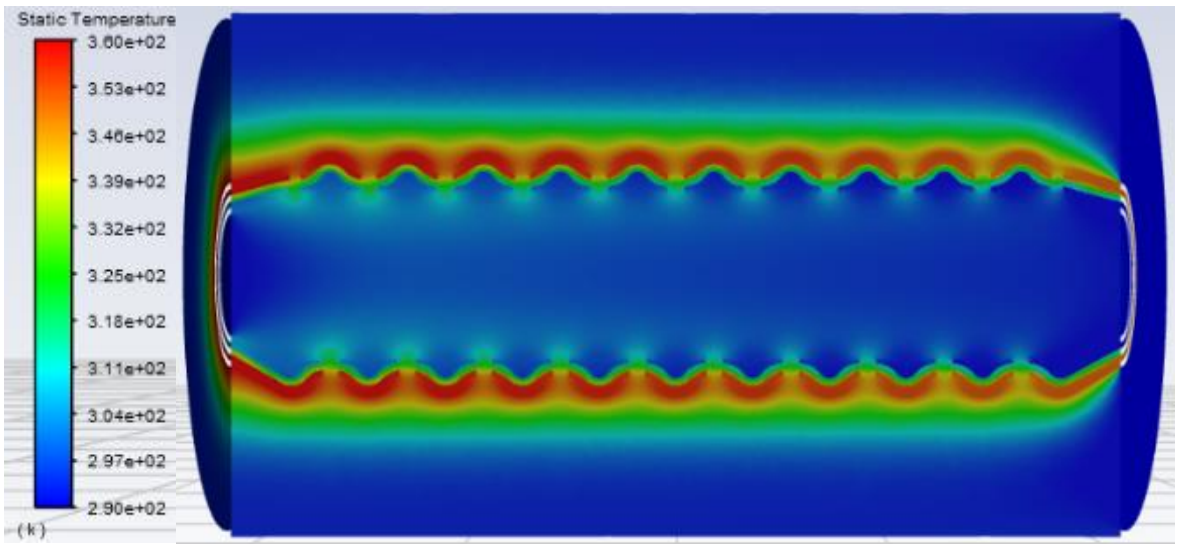

(b)

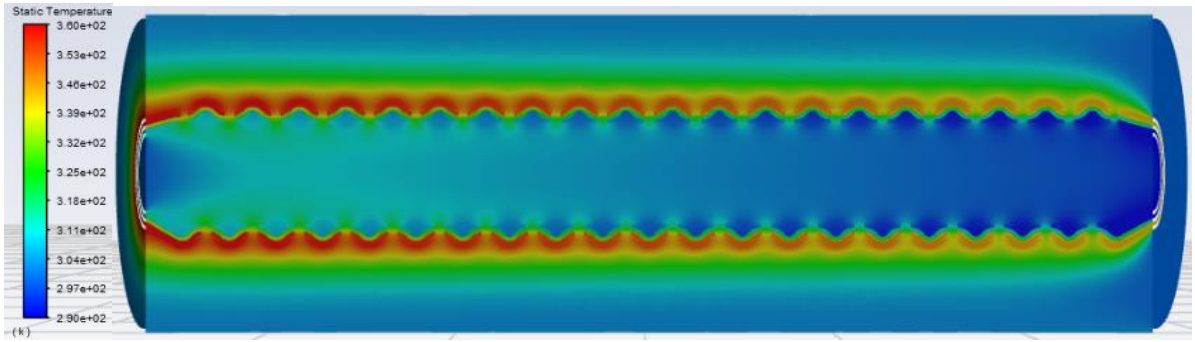

(c)

Figure 5.7 Heat Exchanger models using conditions set for the practical experiment with stainless steel 316L as the solid phase and water as the fluid medium at 360K and 290 K inlet temperatures considering (a) one, (b) two, and (c) three-unit lengths

Figure 5.8 (a) and (b) are depictions of temperature profiles in the heat exchanger with two- and four-units long models considering an insulating solid medium and helium at 300 K and 20 K at the two inlets of the two fluids, respectively. Compared to the results of Fig. 5.6 (c), which is the one-unit model, the heat transfer conditions have improved significantly with both the models, under the same vacuum at 20 K conditions for the envelope zones. Further, the temperature distribution plots at the two inlet and two outlet surfaces of the two- and four-unit models as presented in Fig. 5.8 clearly indicate 95% and 98% efficiencies respectively deride following Eq. 5.1, indicating the successful achievement of the design objectives.

$$Q_{max} = C_{min}(T_{hot,in} - T_{cold,in})$$

$$\varepsilon = \frac{Q_{actual}}{Q_{max}}$$

$$Q_{actual} = C\left(T_{cold,out} - T_{cold,in}\right) = C\left(T_{hot,in} - T_{hot,out}\right)$$

$$\varepsilon = \frac{(T_{hot,in} - T_{hot,out})}{(T_{hot,in} - T_{cold,in})} = \frac{(T_{cold,out} - T_{cold,in})}{(T_{hot,in} - T_{cold,in})}$$

Equation 5.1 Effectiveness of the Heat Exchanger

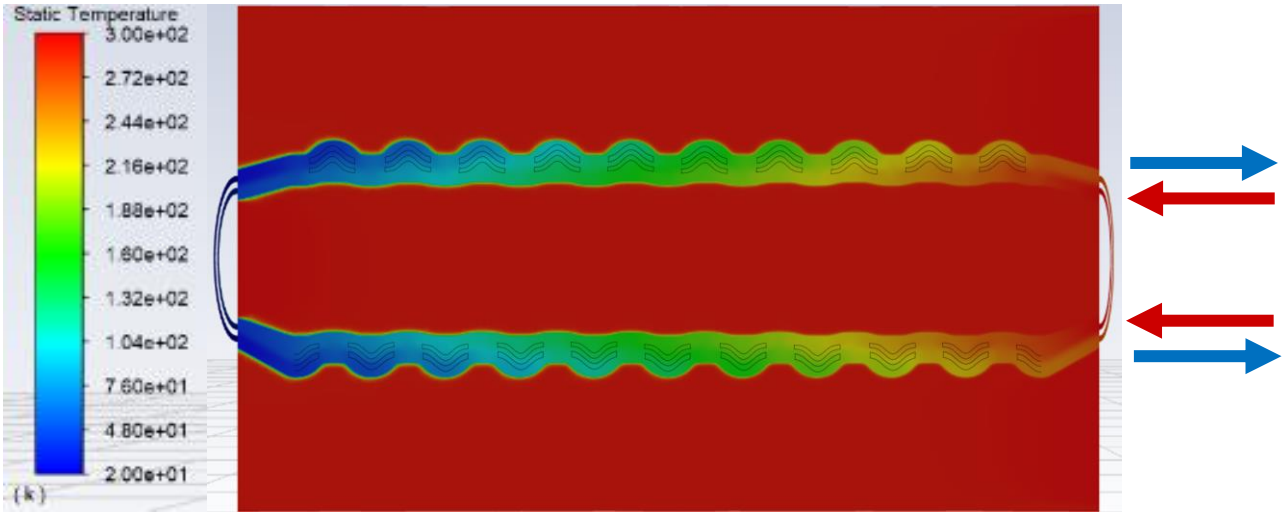

(a)

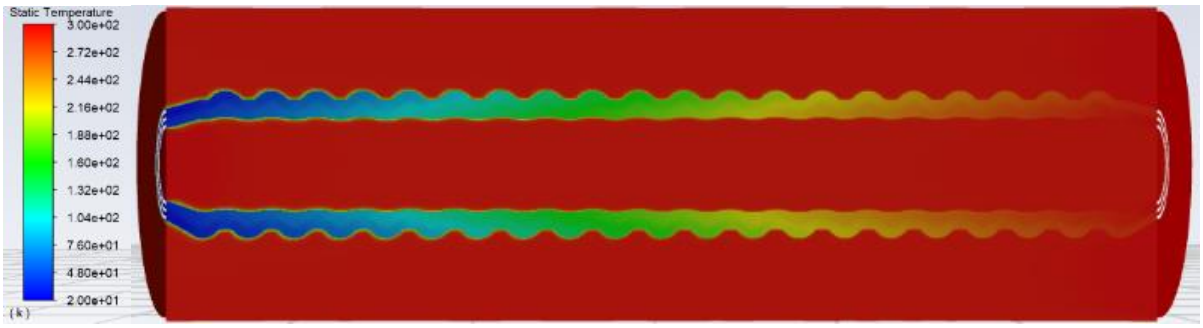

(b)

Figure 5.8 Influence of varying length of heat exchanger with the insulating structural material and helium at 300 K and 20 K at the hot and cold inlets in (a) two and (b) four units long spiral heat exchanger in vacuum surroundings at 300 K

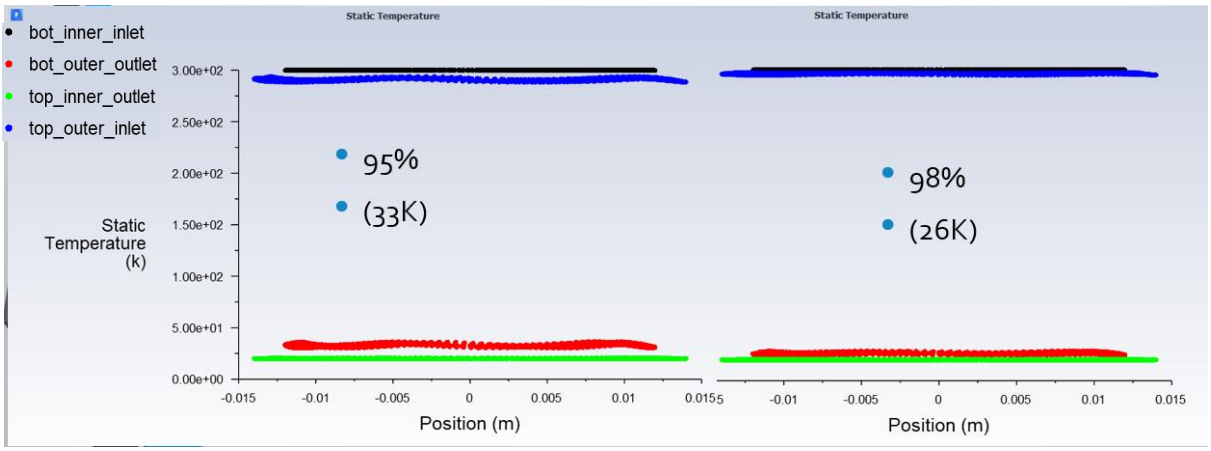

Figure 5.8 Temperature distribution profiles in the two (left) and four (right) units long models with insulating solid structures, helium at 300K and 20K inlet temperatures and in vacuum at 20 K

5.5 Simulations with Realistic Material Properties

With a baseline for the potential efficiencies for a counterflow recuperative heat exchanger set, the next step was to incorporate realistic material properties into the simulation. The key influencing factor in the efficiency of the heat exchanger geometry was the thermal conductivity of the both the fluid medium and solid material. The fluid was fixed to helium, however there was more flexibility with the selection of the solid material. The standard material used to additively manufacture the counterflow heat exchanger was 316 stainless-steel. Due to this, realistic thermal conductivity properties for 316 stainless-steel were used in the subsequent simulations to determine the viability of the material within the heat exchanger geometry. The thermal conductivity for stainless steel 316 under cryogenic condition is presented in Fig 5.9 and a 5^{th} order polynomial approximation following Eq. 5.2. The coefficients of the 5^{th} order polynomial are given in Table 5.2. Fig 5.10 depicts the stainless-steel thermal conductivity properties represented within ANSYS Fluent. The successful application of the thermal conductivity variation can be seen in the results from Fig 5.11 where the thermal conductivity gradient can be seen between the upper maximum and minimum temperatures of the heat exchanger.

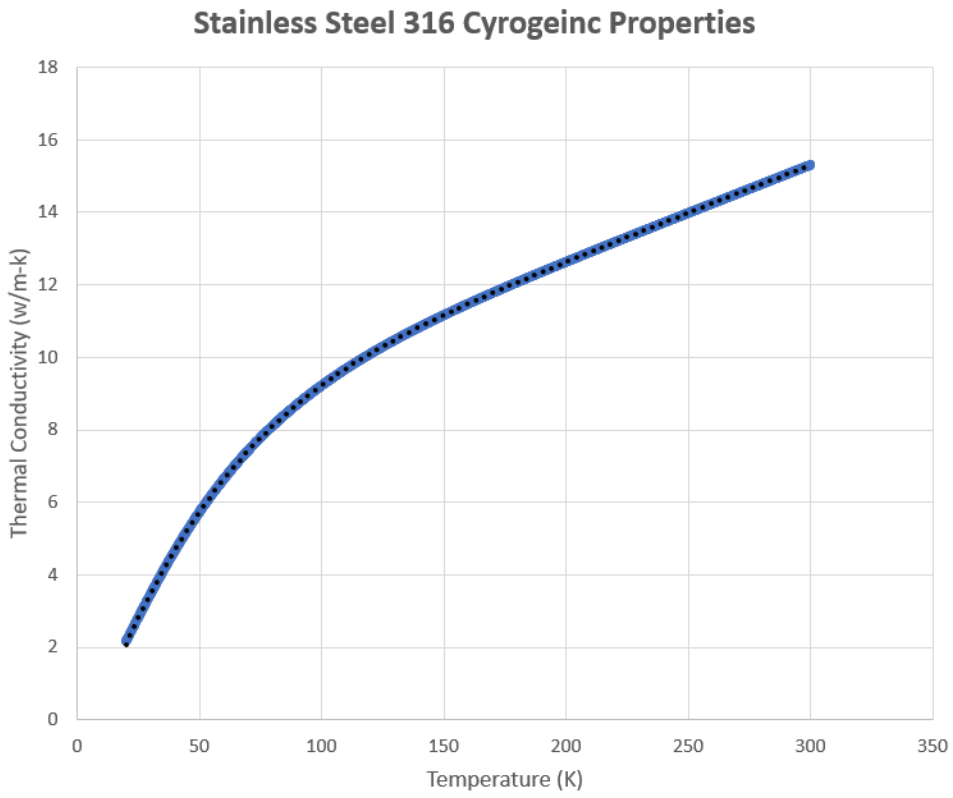

Figure 5.9 Stainless Steel 316 Cryogenic Properties for Thermal Conductivity

$$Thermal\ Conductivity\ = ax^5 + bx^4 + cx^3 + dx^2 + ex + f$$

Equation 5.2 5th Order Polynomial for the Stainless Steel 316 Cryogenic Properties for Thermal Conductivity

Table 5.2 Coefficients for 5th Polynomial Approximation of the Thermal Conductivity of Stainless Steel 316

	Coefficients
a	$9.558 * 10^{-12}$
b	$-1.163 * 10^{-8}$
c	$5.667 * 10^{-6}$
d	$-1.389 * 10^{-3}$
e	$1.988 * 10^{-1}$
f	$-1.371 * 10^{0}$

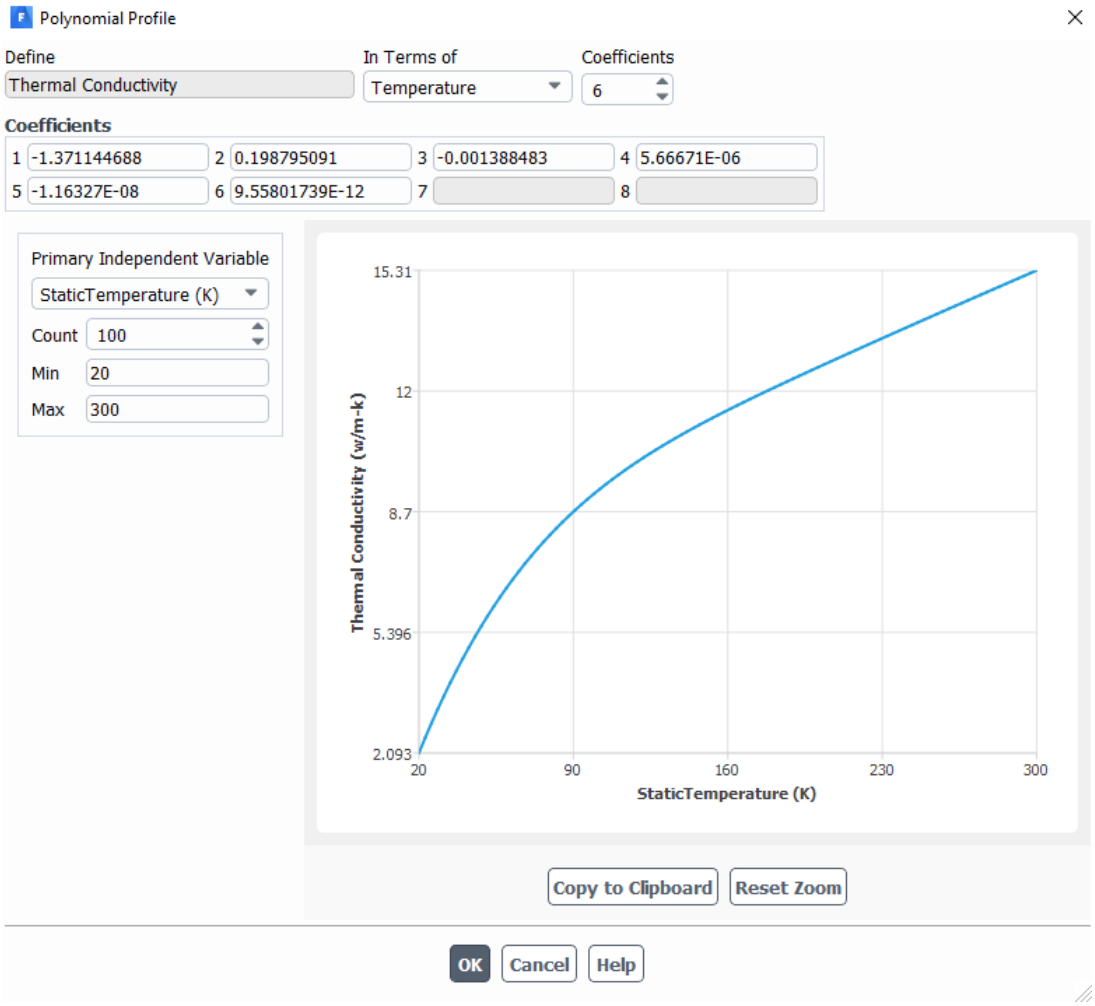

Figure 5.10 Stainless Steel 316 Cryogenic Properties for Thermal Conductivity depicted with ANSYS Fluent

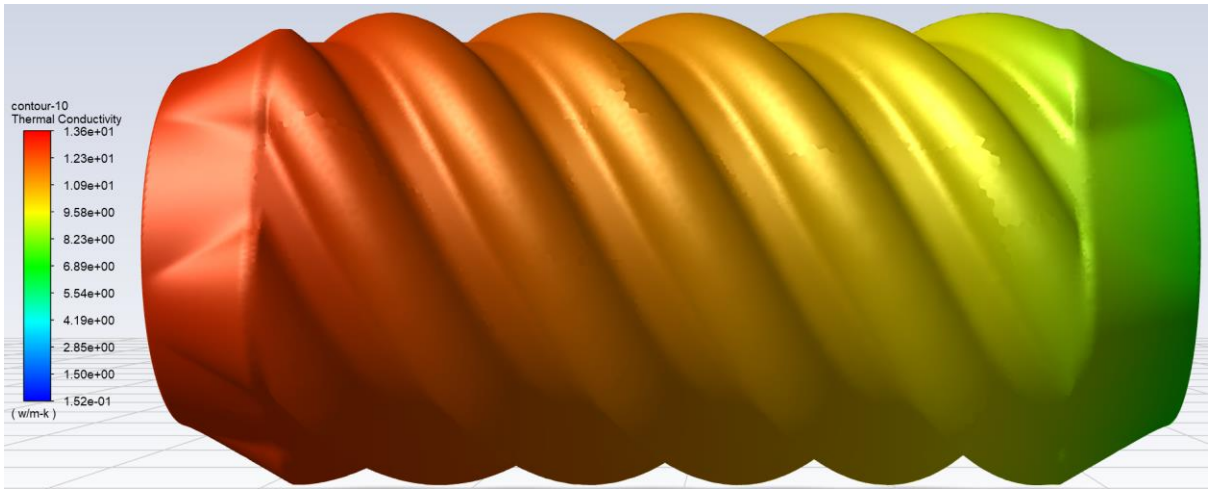

Figure 5.11 Thermal conductivity along the cross-section of the recuperative heat exchanger using the 5th order polynomial approximation

To analyse the impact of the variation of thermal conductivity with temperature of stainless-steel 316, three distinct points were simulated. The first included a constant thermal conductivity of stainless steel 316 at room temperature of 16w/m-k, with a second being the thermal conductivity close to 20k at 3w/m-k. The third simulation involved utilising the 5^{th} order polynomial equation to establish a realistic use case of stainless-steel 316. Following the results from the simulations with an ideal extremely low conductivity solid material, it was expected that a 3w/m-k thermal conductivity would perform significantly better than the 16w/m-k thermal conductivity. The thermal distributions of both the inner and outer fluids for a constant 16w/m-k thermal conductivity can be seen in Fig 5.12 (a) and 5.12 (b) respectively. Through the minimal colour variation between the two sides of the recuperative heat exchanger it is clear that the efficiency of the heat exchanger has been reduced significantly. Following the same simulation except for the application of a constant thermal conductivity of 3 w/m-k the thermal distributions of the outer in inner fluids in Fig 5.13 (a) and Fig 5.13 (b) respectively are produced. These highlight the significant thermal improvement between the inlet and outlet temperatures approach a similar value. The third simulation involved the 5^{th} order polynomial being used as a realistic thermal conductivity of stainless steel. The results depicted in Fig 5.14 (a) and Fig 5.14 (b) representing both the outer and inner fluids respectively mark close resemblance to the 16w/m-k constant simulation. Further emphasising this, Fig 5.5.7, presents the cross-section of the heat exchanger for the three cases. Fig 5.15 (a) shows the temperature distribution with a constant thermal conductivity of 16 w/m-k while Fig 5.15 (b) depicts the constant thermal conductivity of 3 w/m-k. The cross-section is Fig 5.15 (c) from the use of the polynomial thermal conductivity highlights the resemblance to the 16 w/m-k case.

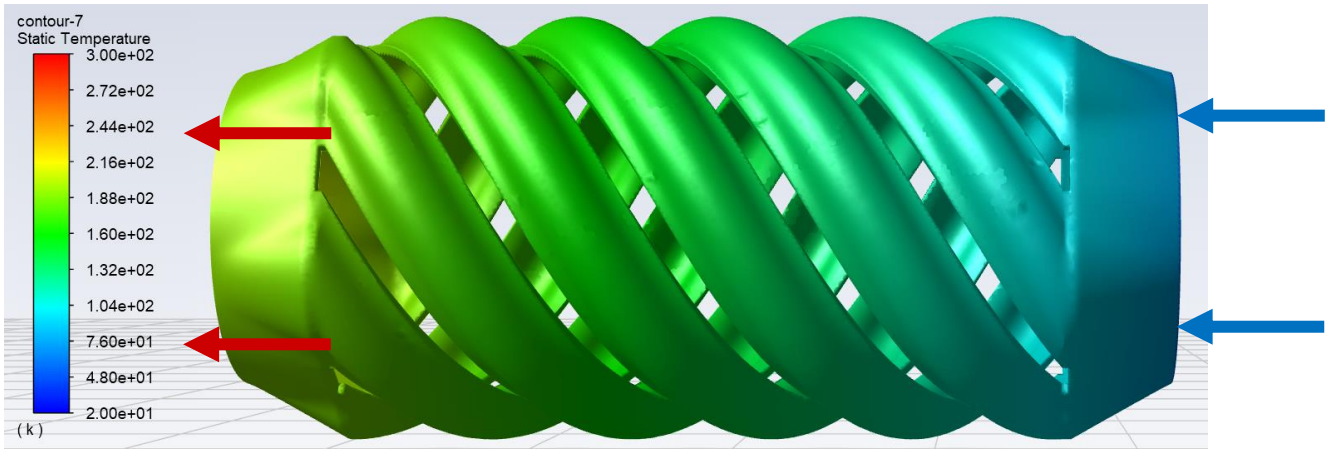

(a)

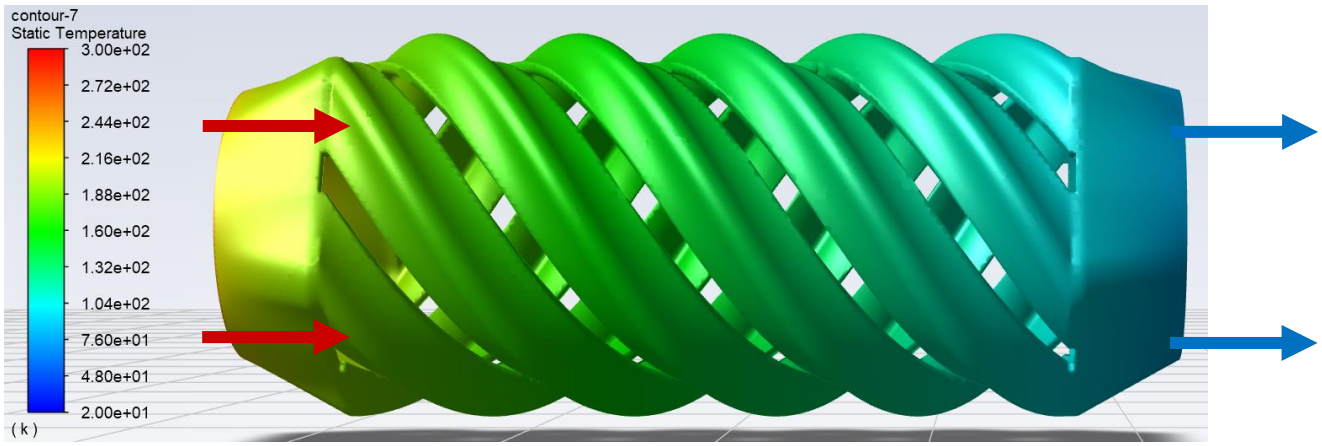

(b)

Figure 5.12 Constant 16w/m-k Thermal Conductivity along the cross section of the recuperative heat exchanger (a) depicting the outer fluid volume and (b) the inner fluid volume

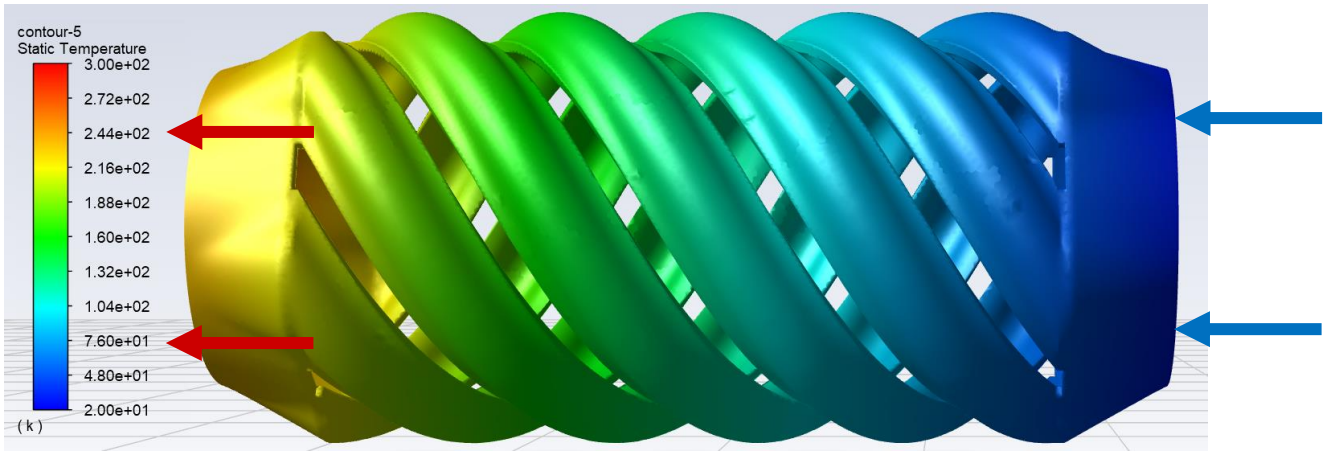

(a)

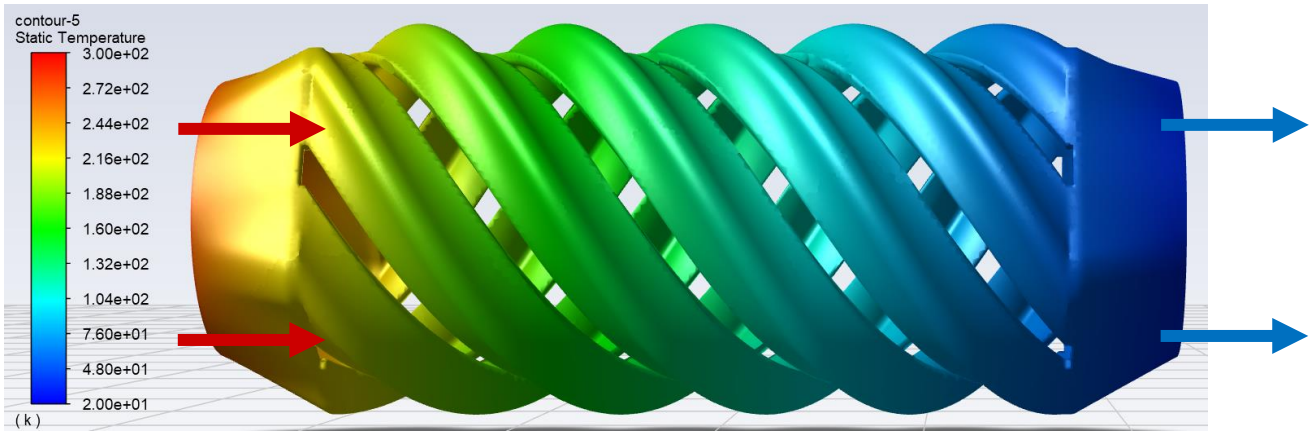

(b)

Figure 5.13 Constant 3w/m-k Thermal Conductivity along the cross section of the recuperative heat exchanger (a) depicting the outer fluid volume and (b) the inner fluid volume

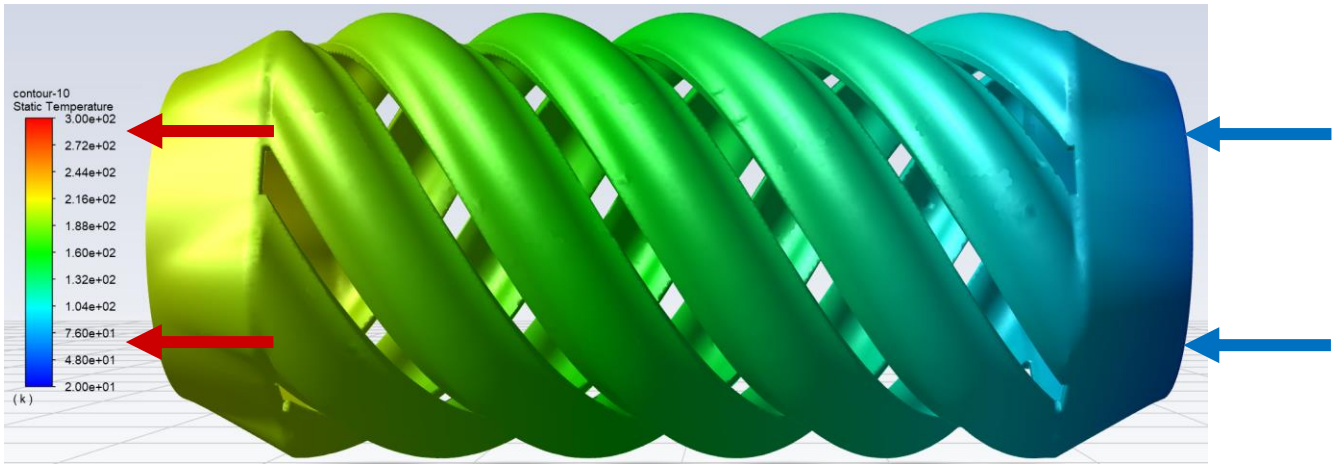

(a)

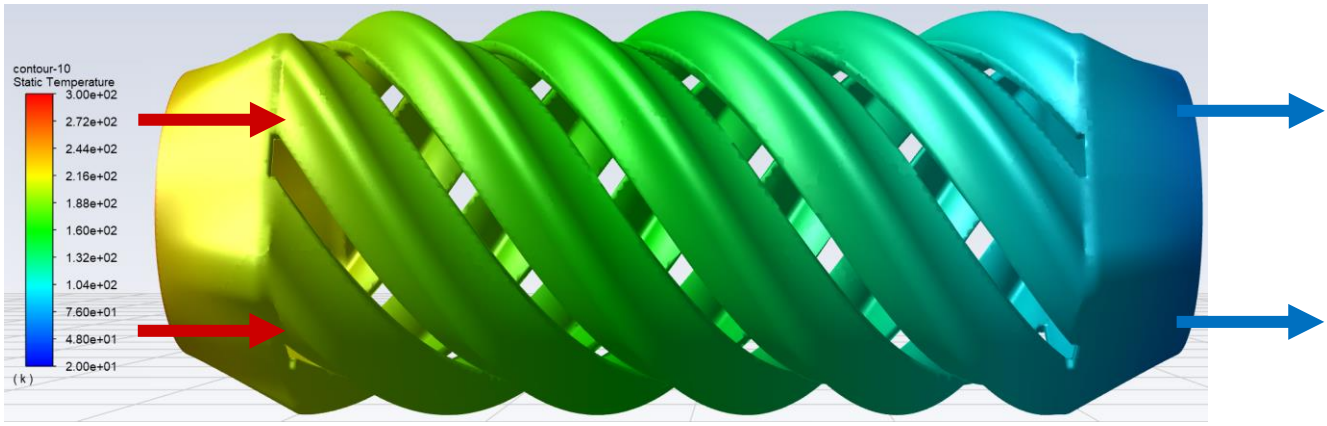

(b)

Figure 5.14 5th order Polynomial approximation for Thermal Conductivity along the cross section of the recuperative heat exchanger (a) depicting the outer fluid volume and (b) the inner fluid volume

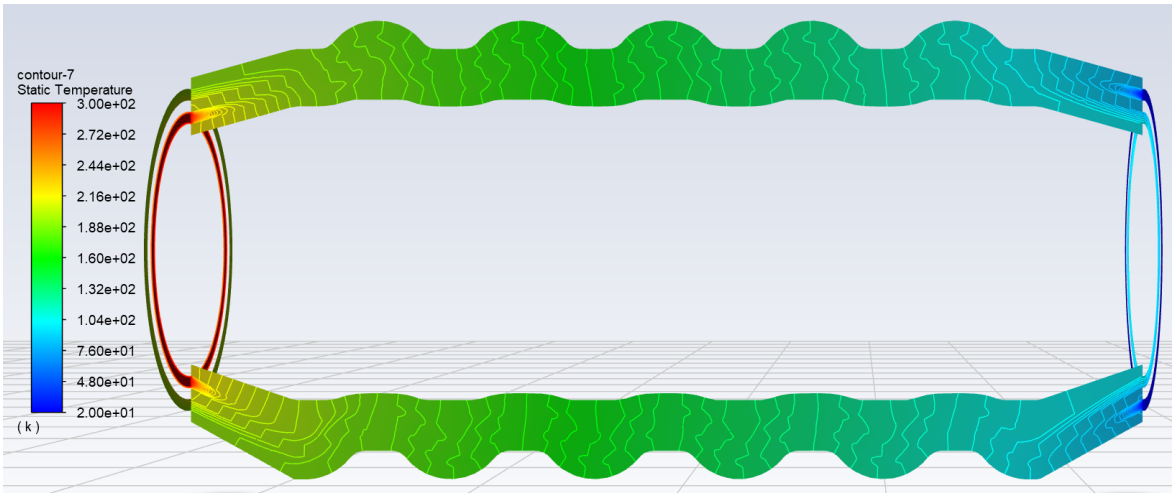

(a)

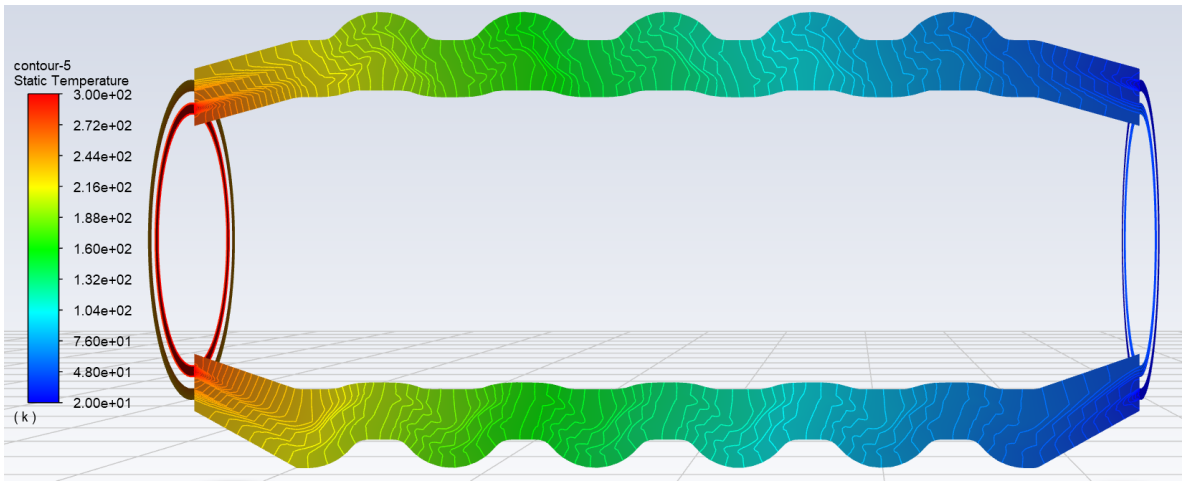

(b)

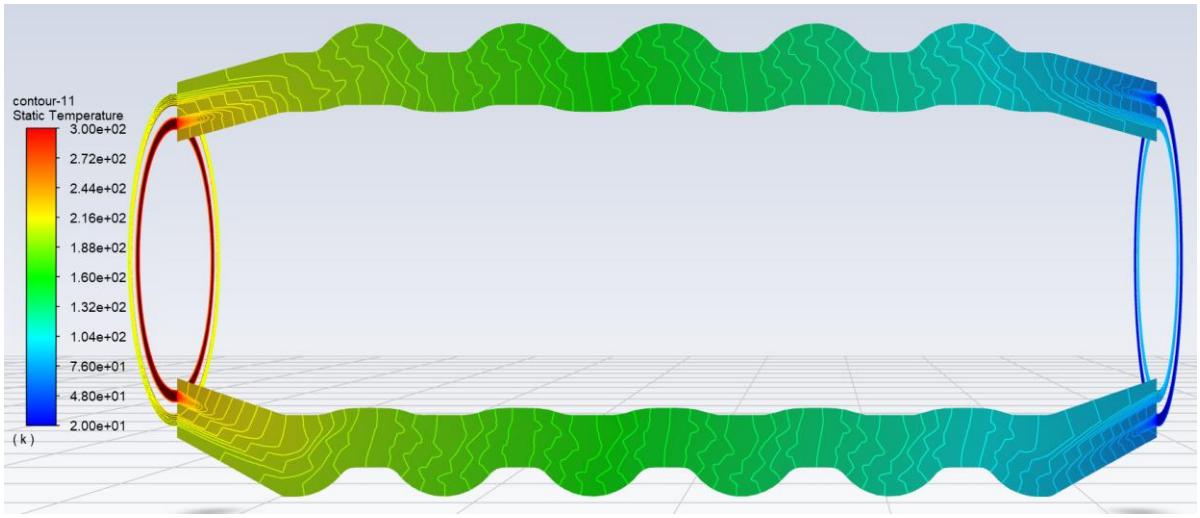

(c)

Figure 5.15 Thermal Gradient along the cross-section of the recuperative heat exchanger with (a) applying a constant 16 w/m-k and (b) applying a constant 3 w/m-k with (c) applying the 5th order polynomial thermal conductivity.

The drop in thermal performance for the third case can be partially attributed to the average thermal value of the polynomial being significantly closer to 16w/m-k compared to the 3w/m-k case. On average the 5^{th} order polynomial results in a thermal conductivity of 10.8 w/m-k. However, this alone does not account for the significant reduction in heat exchanger performance. The dramatic reduction in performance can be primarily attributed to a cyclic performance reduction of the heat exchanger. Fundamentally any reduction in heat exchanger performance increases the minimum temperature of the heat exchanger. With a constant thermal conductivity this can be the sole influencing factor. However, as the polynomial approximation for thermal conductivity is included, as the minimum temperature of the heat exchanger increases, so does the average thermal conductivity. The performance of the heat exchanger has been shown to peak at low thermal conductivities. This highlights the significance of any reduction of heat exchanger performance to itself cause a reduction in heat exchanger performance due to the reduction of performance at higher thermal conductivities. The minimum temperature of the simulation using the polynomial approximation for thermal conductivity is 66.7K, with a maximum temperature of 270.6K. Using these limits within the polynomial approximation increase the average thermal conductivity to 11.5 w/m-k and results in the minimum thermal conductivity increasing from 2.1 w/m-k to 7.3 w/m-k. This significant reduction in the minimum thermal conductivity as well as the maximum conductivity only decreasing from 15.6w/m-k to 14.3 w/m-k clearly contributions significantly to the stark reduction in heat exchanger performance. Fig 5.16 shows the temperature distribution along the cross-section of the heat exchanger of the outer fluid. This clearly highlights the similar performance of the third, polynomial, case and the 16 w/m-k, second case. Fig 5.17 represents the maximum and minimum temperatures at the outlets of the heat

exchanger. The 3 w/m-k case approaches 36K on the cold fluid outlet with both the polynomial and 16 w/m-k case being above 65K. A similar trend is visible for the hot fluid outlet with the 3w/m-k reaching 290k and the other two case not rising above 270K. The low thermal performance of Stainless steel 316 make it difficult to be used effectively within the current heat exchanger geometry. The limitations of an insufficiently low thermally conductive material are complex to overcome due to the inability to increase the wall thickness beyond 1mm.

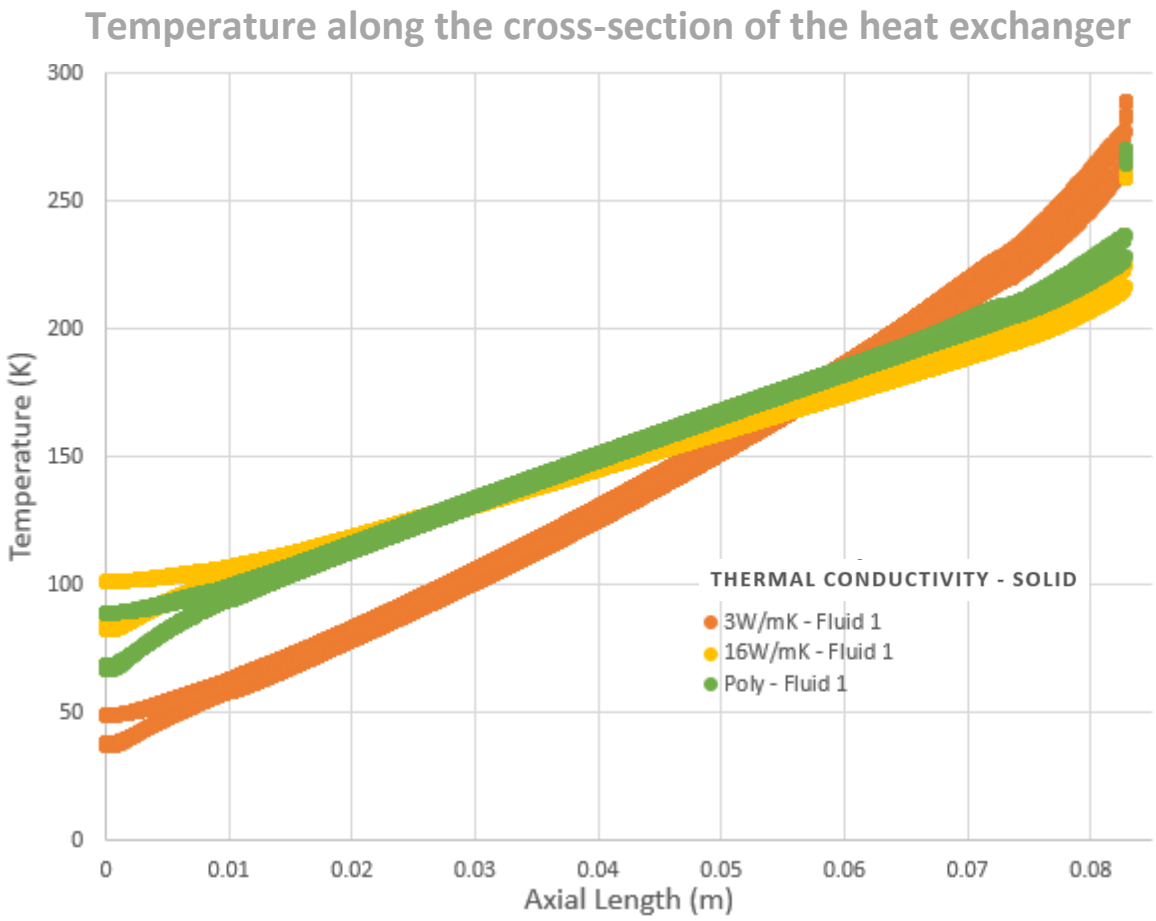

Figure 5.16 Temperature distribution of the outer fluid along the cross section of the recuperative heat exchanger for three thermal conductivity cases

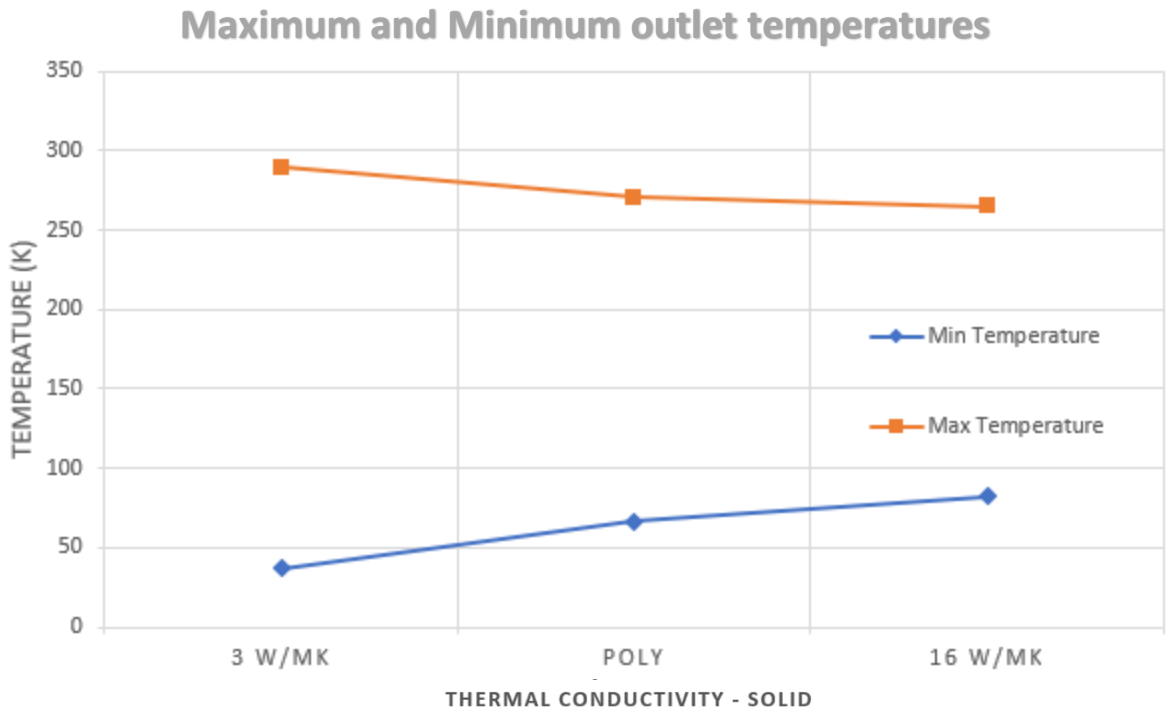

Figure 5.17 Maximum and Minimum outlet temperatures of the recuperative heat exchanger for three thermal conductivity cases

To determine the improvement in effectiveness of the helical recuperative heat exchanger provide, a standard tube in tube cylindrical design was modelled. The geometry followed the same parameters set in the recuperative heat exchanger design with a 40mm maximum diameter for the cross section of the tube and 1mm fluid flow channels with corresponding 1mm walls surrounding the fluid flow channels. The inlet and outlets for the tube in tube heat exchanger were also matched to the helical heat exchanger design. The generated mesh for the tube in tube heat exchanger design in depicted in Fig 5.18. The tube in tube heat exchanger was lengthened to 1.5 times the spiral section of the helical heat exchanger design to match the length of the fluid flow channels in helical heat exchanger design. Simulations of the standard tube in tube design across the thermal conductivity range between 3 and 16 w/m-k we conducted

to compare the two designs. An identical inlet and outlet configuration was used as well as the same boundary conditions. The results presented in Fig 5.19 show a near identical minimum outlet temperature between the two heat exchangers with a consistent 2–4-degree variation for the three thermal conductivities cases. The presented results show that the helical recuperative heat exchanger is comparable to a standard tube in tube design that is 50% longer.

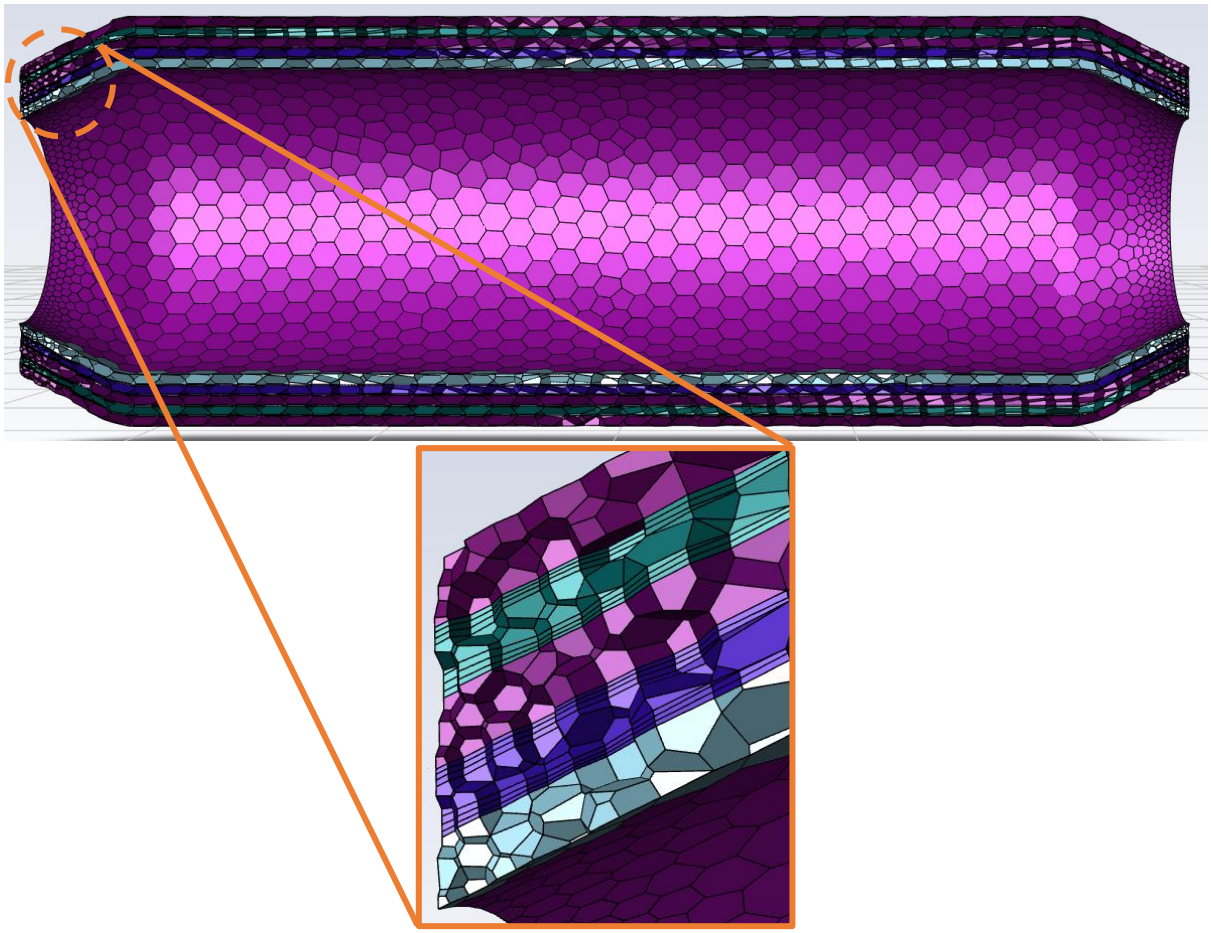

Figure 5.18 Tube in Tube Recuperative heat exchanger design

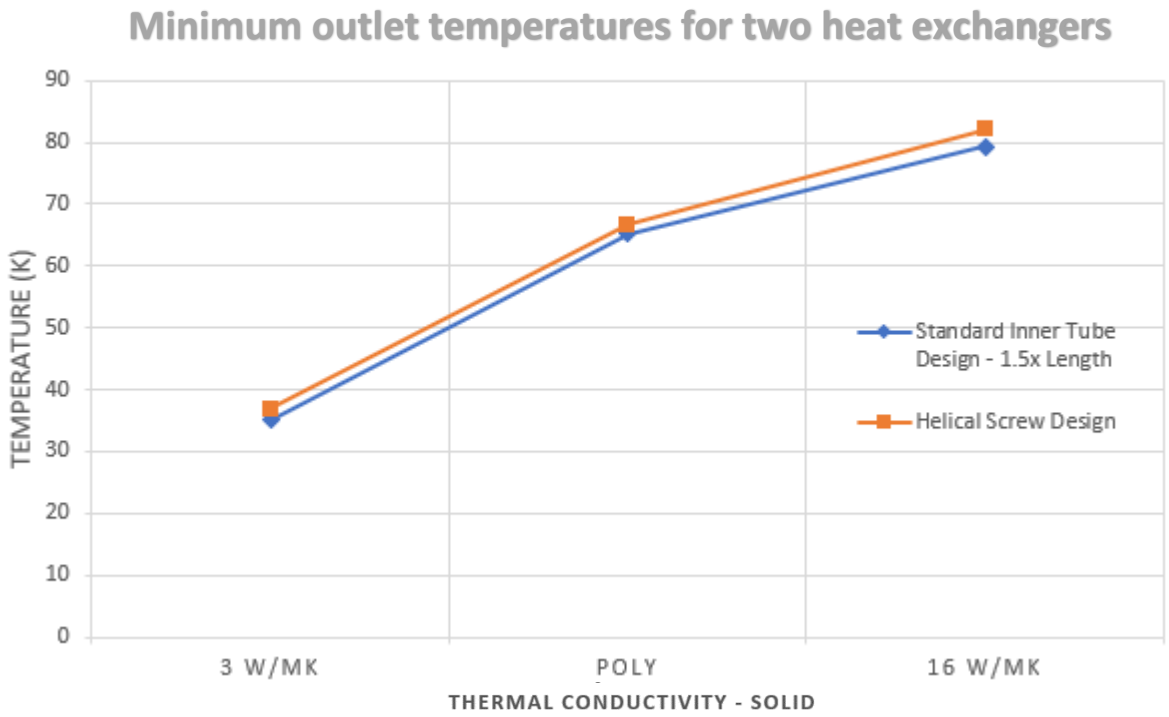

Figure 5.19 Minimum outlet temperatures of the tube in tube heat exchanger design compared to the recuperative heat exchanger for three thermal conductivity cases

The decision to use a low thermally conductive material to control the heat flow from the inlets to the outlets was justified by the results present in Fig 5.4 (a) and (b). These highlighted the anticipated effect, that when the heat transfer is too high both fluids quickly converge to a mean temperature, failing both the requirement for a hot outlet at room temperature as well as a cold outlet at cryogenic temperatures. The use of a low thermally conductive material shows promise to control the heat flow and achieve high efficiencies for the recuperative counterflow heat exchanger. These simulations showed the ability to achieve the desired outlet temperatures at both ends of the heat exchanger, without altering any other aspect of the design.

The comparison between the helical heat exchanger and a design following traditional manufacturing techniques, centralised around the heat exchanger using a similar volume for the heat exchanger. A key factor for the effectiveness of the heat exchanger is the space that is required to achieve the performance. A more compact heat exchanger with the same performance as a larger heat exchanger would be much more valuable. Due to this, the cross-sectional area of the two heat exchangers were kept closely related, with the diameter and wide of the fluid regions constant. This would compare the performance shown in the simulations between two exchangers with a similar total volume that was occupied.

5.6 Additive manufacturing of the helical spiral heat exchanger

5.6.1 Additive manufacturing equipment

The additive manufacturing approached using to evaluate the processing of selected metal-matrix composites was selective laser melting. Selective laser melting utilises metals, such as stainless steel, as well as manufacturing with a small layer thickness between 20 and 50 micrometres, both of which are essential for the manufacturing of the heat exchanger prototype. Geometries imported directed from computer aided design sources are able to be printed in metal for application specific complex parts. The build plate of the laser melting system utilising the same material as the metal powders that are spread layer over layer during the print. The high energy laser follows a predefined scan path lines and selectively melts the metal particles. The process is repeated layer-by-layer, until the part is fully made. A schematic diagram of the

selective laser melting process is depicted in Fig. 5.20. The selective laser melting technique is compatible with various metals and metal composites and provides height structural integrity. The Renishaw AM400 laser melting system presented in Fig. 5.21 is available at the 3D printing laboratory of Auckland University of Technology was employed for all the printing tasks. The AM400 system is equipped with a solid-state Nd: YAG laser (wavelength = 1070 nm) of 75 µm spot size. The thermally complex laser melting process is influenced by multiple experimental, which include the base metal powder, the laser power, scan speed and the spacing and thickness of the powder layer.

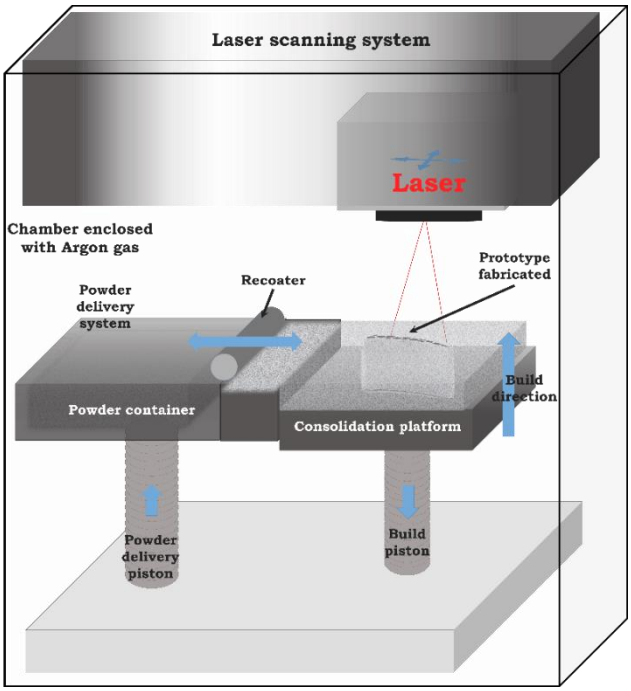

Figure 5.20 Schematic diagram of selective laser melting process

Figure 5.21 The Renishaw selective laser melting system

5.6.2 Selective laser melted prototypes

The Renishaw AM400 selective laser melting system was used for the physical production of the prototype designs and evaluate the feasibility of achieving the complex helical structures in reality. Stainless steel 316L was the powder material used as supplied by Renishaw and the default process parameters as included in the material data file were used. The 45˚-helix angle was carefully chosen at the start to facilitate the direct production of the complex profiles in a vertical build orientation without the need for any internal support structures. The design of the structures applies a 1 mm minimum wall thickness for the solid structures of the models. With metal 3D printing a series of initial trials are often necessary with each new product printed. In this case also a few trials were made to ascertain the correct and complete

consolidation of all the layers and the first set of prototypes produced of the two models with and without thermal short circuiting as removed from the build chamber are shown in Fig. 5.22 (a) and (b). Once the print conditions, the layer consolidation outcomes and confirmation of the geometrical features of the physical prototypes were ascertained, attention was paid to design the appropriate joining and locking mechanisms for producing several individual units of the models so that they could be printed comfortably (the height of the build above the bottom plate is a critical factor in SLM) and joined together to form the two, -three-, and four- units long heat exchanger arrangements. Again, after a few trial-and-error attempts, the design as shown in Fig 5.23 was finalised and printed with the same process and build orientation conditions. The final parts printed, and bead blasted are shown in Fig 5.23 (a) and (b) and the turning screw joint was found to work perfectly with very close tolerances presented in Fig 5.23 (c). A suitable thermally resistive glue or enclosing the assembly under a compressive clamping would eliminate leakages if any from the joints.

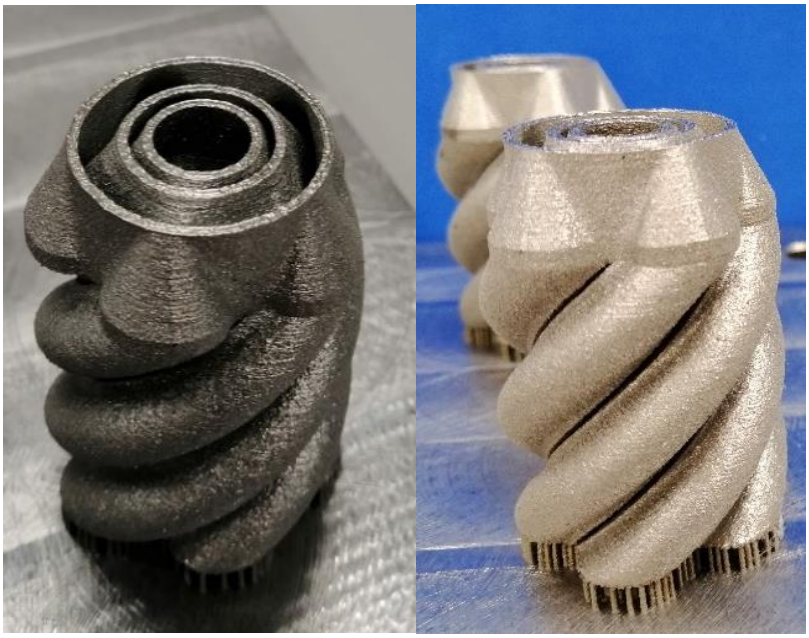

(a) *(b)*

Figure 5.22 The first prototypes of the models (a) without and (b) with thermal insulation as printed using the Renishaw AM400 elective laser melting system. The models in (b) are subjected to a certain amount of bead blasting

(a) *(b)* *(c)*

Figure 5.23 Additively manufactured counterflow helical sequential heat exchanger prototypes (a) male connection and (b) female connection and (c) combined configuration

Chapter 6

Conclusion

The hypothesis that additive manufacturing allows for the design of better heat exchanger systems through the freedom to generate more complex forms is evaluated in this work. A counterflow helical heat exchanger design is developed and numerically tested for a cryogenic coolant circulation system with a warm circulation pump and a heat exchanger that takes the coolant at around 30 K up to the ambient temperature. The energy losses and expenses with the cryogenic pump and the pressure drop and temperature differences within the heat exchanger are critical competing attributes. The ANSYS ® DesignModeller module is used to create the CAD models of the counterflow helical heat exchanger and ANSYS ® Fluent is used for the finite volume discretisation and numerical analyses. The roles of the velocity of flow, thermal short-circuiting across the counterflow channels, and the ambient conditions are given due consideration in the numerical experiments. Physical realisation of the complex form of the counterflow heat exchanger is demonstrated by successfully fabricating the final form based on additive manufacturing by selective laser melting of 316L stainless steel. The overall design of the counterflow helical heat exchanger is effective, the numerical results are satisfactory, and the physical prototype produced further reinstated the possibilities to stretch the limits of the complexity of forms that can be considered for better heat exchanger solutions with additive manufacturing.

And the following quantitative observations could be made based on the results of the numerical experiments conducted as part of this research:

- Complex geometries can be successfully additively manufactured through the metal selective laser melting process
- Complex geometries can be manufactured without internal support structure, while the geometries maintain a greater than 45-degree incline on any angled surface
- An insulator between two adjacent fluids can be used effectively to achieve high efficiencies of between 95 and 98% for a recuperative heat exchanger design
- Thermal short circuits can be avoided through both the use of an insulator and separating axial conduction surfaces
- A cryogenic recuperative heat exchanger design is most effective with the use of a very low conductive material which can yield up to a 20K drop in outlet temperature compared to stainless steel.
- The 45-degree helical geometry yields efficiencies matching an equivalent tube in tube design 50% longer than the helical geometry.

References

[1] Davim, J. P., Pou, J., & Riveiro, A. (2021). *Additive manufacturing*. Elsevier.

[2] J.-P. Kruth, B. Vandenbroucke, J. Van Vaerenbergh, P. Mercelis, Benchmarking of different SLS/SLM processes as rapid manufacturing techniques, in: Proceedings of the International Conference Polymers & Moulds Innovations PMI 2005 (April 2023, 2005, Gent, Belgium), 2005. *Additive Manufacturing*, edited by Juan Pou, et al., Elsevier, 2021. *ProQuest Ebook Central*, http://ebookcentral.proquest.com/lib/aut/detail.action?docID=6630989.
Created from aut on 2022-10-26 22:59:54.

[3] Boxleitner, J., & Nellis, G. F. (2018). Additive Manufacturing of Heat Exchangers.

[4] Arie, M. A., Shooshtari, A. H., Rao, V. V., Dessiatoun, S. V., & Ohadi, M. M. (2017). Air-side heat transfer enhancement utilizing design optimization and an additive manufacturing technique. Journal of Heat Transfer, 139(3).

[5] Chekurov, S., Kajaste, J., Saari, K., Kauranne, H., Pietola, M., & Partanen, J. (2019). Additively manufactured high-performance counterflow heat exchanger. Progress in Additive Manufacturing, 4(1), 55-61.

[6] Keramati, H., Battaglia, F., Arie, M. A., Singer, F., & Ohadi, M. M. (2019, May). Additive Manufacturing of Compact Manifold-Microchannel Heat Exchangers Utilizing Direct Metal Laser Sintering. In 2019 18th IEEE Intersociety Conference on Thermal and Thermomechanical Phenomena in Electronic Systems (ITherm) (pp. 423-429). IEEE.

[7] Haertel, J. H., & Nellis, G. F. (2017). A fully developed flow thermofluid model for topology optimization of 3D-printed air-cooled heat exchangers. Applied thermal engineering, 119, 10-24.

[8] Ho, J. Y., Wong, K. K., Leong, K. C., & Wong, T. N. (2017). Convective heat transfer performance of airfoil heat sinks fabricated by selective laser melting. International Journal of Thermal Sciences, 114, 213-228.

[9] Bacellar, D., Aute, V., Huang, Z., & Radermacher, R. (2017). Design optimization and validation of high-performance heat exchangers using approximation assisted optimization and additive manufacturing. Science and Technology for the Built Environment, 23(6), 896-911.

[10] Zeng, S., Kanargi, B., & Lee, P. S. (2018). Experimental and numerical investigation of a mini channel forced air heat sink designed by topology optimization. International Journal of Heat and Mass Transfer, 121, 663-679.

[11] Nidal H. Abu-Hamdeh, R. A. (2021). A detailed hydrothermal investigation of a helical micro double-tube heat exchanger for a wide range of helix pitch length. *Case Studies in Thermal Engineering*.

[12] Hossein Javadi, S. S. (2019). Thermal analysis of a triple helix ground heat exchanger using numerical simulation and multiple linear regression. *Geothermics, Volume 81*, 53-73.

[13] Jewad, M. A. (1977). 'Thermal design of a compact recuperative heat exchanger for a stirling engine'

[14] Gužela,Š. & Dzianik,F.(2018).Some Facts Resulting from the Key Variables Used in the Description of the Recuperative Heat Exchangers. Strojnícky časopis - Journal of Mechanical Engineering,68(3) 249-260. https://doi.org/10.2478/scjme-2018-0038

[15] Štefan,G. & František,D.(2021).Countercurrent Index Determination for the Recuperative Heat Exchangers. Strojnícky časopis - Journal of Mechanical Engineering,71(1) 51-60. https://doi.org/10.2478/scjme-2021-0005

[16] Stević, D., Debeljković, D., & Simeunović, G. (2017). Modelling, simulation and geometric optimization of cross flow recuperative heat exchanger based on controllability condition number. *Tehnika*, *72*(2), 221-228. https://doi.org/10.5937/tehnika1702221S

[17] Štefan,G. & František,D.(2020).The Recuperative Heat Exchangers – The Mean Temperature Difference in the Special Cases of Heat Transfer. Strojnícky časopis - Journal of Mechanical Engineering,70(1) 47-56. https://doi.org/10.2478/scjme-2020-0005

[18] Gyuwan Hwang, Sangkwon Jeong. (2010) Pressure loss effect on recuperative heat exchanger and its thermal performance. Cryogenics, Volume 50, Issue 1, Pages 13-17. https://doi.org/10.1016/j.cryogenics.2009.10.002.

[19] Kyoung Joong Kim, Junhyuk Bae, Lingxue Jin, Sangkwon Jeong, Yeon Suk Choi. (2021). Experimental and numerical investigations on continuous pressure drop characteristic of tube-in-tube recuperative heat exchanger for 1.8 K cooler. Cryogenics, Volume 118. https://doi.org/10.1016/j.cryogenics.2021.103345.

[20] Omar, H., Kuz'michev, V. S., & Tkachenko, A. Y. (2020). Improving the efficiency of aviation turbofan engines by using an intercooler and a recuperative heat exchanger. *VESTNIK Of Samara University. Aerospace And Mechanical Engineering, 19*(3), 85-99. doi: 10.18287/2541-7533-2020-19-3-85-99

[21] Hoseyn Sayyaadi, Hamid Reza Aminian. (2010) Design and optimization of a non-TEMA type tubular recuperative heat exchanger used in a regenerative gas turbine cycle. Energy, Volume 35, Issue 4, Pages 1647-1657. https://doi.org/10.1016/j.energy.2009.12.011.

[22] R.M. Damle, P.M. Ardhapurkar, M.D. Atrey. (2016) Numerical investigation of transient behaviour of the recuperative heat exchanger in a MR J–T cryocooler using different heat transfer correlations. Cryogenics,Volume 80, Part 1,Pages 52-62. https://doi.org/10.1016/j.cryogenics.2016.09.003.

[23] Yingwen Liu, Liu Liu, Lili Liang, Xin Liu, Jiapeng Li. (2015) Thermodynamic optimization of the recuperative heat exchanger for Joule–Thomson cryocoolers using response surface methodology. International Journal of Refrigeration, Volume 60, Pages 155-165. https://doi.org/10.1016/j.ijrefrig.2015.07.034.

[24] Ezhov, V. S., Evgenievna, S. N., Nikolaevich, T. D., Petrovich, B. A., & Sergeevich, P. N. (2021). VERSION OF A MATHEMATICAL MODEL OF PURGE VENTILATION SYSTEM WITH A COMPLEX

RECUPERATIVE HEAT EXCHANGER. *Istrazivanja i projektovanja za privredu*, *19*(1), 1–6. doi:10.5937/jaes0-30068

[25] Ngoctan Tran, Jane-Sunn Liaw, Chi-Chuan Wang. (2021). Performance of thermofluidic characteristics of recuperative wavy-plate heat exchangers. International Journal of Heat and Mass Transfer, Volume 170. https://doi.org/10.1016/j.ijheatmasstransfer.2021.121027.

[26] Debeljković, D. L., & Simeunović, G. V. (2016). Modelling, simulation and dynamic analysis of the time delay model of the recuperative heat exchanger. *Tehnika*, *71*(3), 407-413. https://doi.org/10.5937/tehnika1603407D

[27] KOCA T, C. A. (2021). Design and Analysis of Double-Pipe Heat Exchanger Using Both Helical and Rotating Inner Pipe. *Thermal Science, 25(2B)*, 1545–1559.

[28] Tendulkar, P. S. (2017). Modeling and analysis of shell & tube type heat exchanger for optimized performance. *Advances in Computing, Communication and Control (ICAC3)*.

[29] Bhattacharjee, A. A. (2018). Influence of Helix Angle on the Performance of Shell-and-Tube Heat Exchanger with Continuous Helical Baffle. *AIP Conference Proceedings*, (pp. Vol. 1980 Issue 1, p1-9).

[30] Khan, A. (. (2020). Experimental investigations on the effect of the spiral helical fins & flow channel routing inside flowing water stream on the heat exchanger performance in tropical environment. *Australian Journal of Mechanical Engineering*.

[31] Ngoctan Tran, C.-C. W. (2019). Effects of tube shapes on the performance of recuperative and regenerative heat exchangers. Energy, Volume 169, 1-17.